2009

Numerical Study of Effects of High Exhaust Gas Recirculation and Energy Recovery System on Diesel Engine Performance

Brian James Kalina
Iowa State University

Numerical study of effects of high exhaust gas recirculation and energy recovery system on diesel engine performance

by

Brian James Kalina

A thesis submitted to the graduate faculty

in partial fulfillment of the requirements for the degree of

MASTER OF SCIENCE

Major: Mechanical Engineering

Program of Study Committee:
Song-Charng Kong, Major Professor
J. Adin Mann III
Terrence R. Meyer

Iowa State University

Ames, Iowa

2009

TABLE OF CONTENTS

LIST OF TABLES

LIST OF ABBREVIATIONS FOR VARIABLES

$BSFC$	brake specific fuel consumption
Cp	heat capacity
M	molar mass
$mdot$	mass flow rate
P	pressure
Q	thermal energy
V	volume
$Vdot_{exhaust}$	volumetric flow rate for exhaust gas
$Wdot$	power
γ	specific heat ratio
η_{system}	efficiency of exhaust energy recovery system
θ	engine crank angle position
$\Delta T_{exhaust-gas}$	change in temperature for exhaust gas across heat exchanger

ACKNOWLEGEMENT

I extend utmost gratitude to my advisor, Dr. Song-Charng Kong, for his significant contribution to this study. I owe to him much thanks for guiding me through my research, and for helping me prepare this thesis. Indeed, I have greatly enjoyed being his student, fondly learning multitudes from him as I sought to better understand the engines in which I so greatly delight.

Thanks to my committee members Dr. Adin Mann and Dr. Terry Meyer for their expertise, for being a pleasure to know. Thanks to Dr. Kong's research group for helping me seek out answers to many of the 'little' questions which came up during the course of my research.

Thanks to my family and friends. To my grandpa for being the first to teach me about engines back on the farm, like those powering his 2-cylinder John Deere 630 and International Harvester 856 diesel tractors. To Dustin for being such a valued brother in Christ; thank you for coming alongside me during the tough times.

I would like to dedicate this thesis to God, my Lord and savior, the author and perfecter of love, He who transcends time, bestows precedence to all which is, yet touches lives on a personal level. Awe envelops my mind and heart as I amazedly consider the wonder He has woven into creation, internal combustion engines and the thermal sciences included.

ABSTRACT

This study investigates how high levels of exhaust gas recirculation (EGR) combined with certain fuel injection strategies and energy recovery systems affect diesel engine emissions and fuel economy. The key test apparatus was a John Deere 4.5L diesel engine which was modeled using the computer-based engine simulation tool GT-Power.

The conclusion was made that utilization of high EGR levels (30% and above) can enable a diesel engine operating at low-load/low-speed conditions to meet Tier 4 emissions regulations without the use of NOx after-treatment, but that employment of such EGR levels will likely make necessary the use of soot after-treatment. Results found that using a single, late injection produced the lowest brake specific fuel consumption (BSFC) for high EGR operation conditions. Results also found that, among varying EGR levels and injection strategies tested, the combination of 30% or more EGR with a double injection produced the lowest levels for NOx and soot emissions combined, but at the cost of increased BSFC.

This study also performed a numerical analysis on certain designs of energy recovery systems used to generate mechanical power from exhaust gas heat. Two Brayton cycle systems were tested, but a Rankine cycle system, also tested, proved to generate more power. A numerical study was performed on this Rankine cycle energy recovery system integrated into the John Deere engine, in which this engine was operated with 30% EGR,

varying load/speed conditions, and either a low or high pressure EGR loop. It was found that for low-load/low-speed and high-load/low-speed operation conditions the Rankine cycle recovery system could decrease engine BSFC by 4% to 5%.

CHAPTER 1. INTRODUCTION

1.1 Background

Enactment of more stringent diesel engine emissions regulations has required industry to develop and employ new technologies which curb diesel engine emissions. These regulations, formulated by the United States Environmental Protection Agency (EPA), are aimed at reducing the extent to which diesel engine exhaust emissions adversely impact the environment and public health. The first set of federal standards for non-road diesel engines was adopted in 1994 and only applied to engines producing 37 kW or more. Since the establishment of this initial Tier 1 standard, which at first only applied to engines with power ratings of 37 kW or more, the EPA has also introduced Tier 1 standards for engines producing under 37 kW, and has successively unveiled Tier 2, Tier 3, and currently, Tier 4 emissions standards for all power levels of engines, each standard being more stringent than its predecessor.

Diesel engine emissions regulations primarily consider nitrogen oxides (NOx) and soot. The final stage of the two-stage Tier 4 regulation will go into

effect January 2014 and require that non-road diesel engines rated at power levels of 56 kW and above emit no more than 0.40 g/kWh NOx, and no more than 0.02 g/kWh soot. This represents a 90% reduction over preceding Tier 3 standards.

Technologies aimed at modifying diesel engines to comply with Tier 4 standards may be classified into two categories: in-cylinder and after-treatment. For soot reduction, proven in-cylinder technologies include utilization of unique fuel injector geometries, multiple fuel injections, and alteration of injection timing. After-treatment consists predominantly of diesel particulate filtration (DPF).

For NOx reduction, in-cylinder technologies include late injection timing, compression ratio reduction, and implementation of cooled exhaust gas recirculation (EGR). NOx after-treatment consists of selective catalytic reduction (SCR) using urea injection and various lean NOx traps. Yet another, but more novel, method of reducing NOx emissions is the utilization of stoichiometric diesel combustion, as this could enable use of a three-way catalyst.

Adapting engines to meet the Tier 4 emissions standard presently accounts for most diesel engine manufacturers' chief concern. Nonetheless, minimizing engine fuel consumption still matters a good deal, reasons for which include minimization of engine operation costs, conservation of dwindling non-renewable fuel resources, and concern over excessive release

into the atmosphere of the greenhouse gas carbon dioxide. Even though in-cylinder and after-treatment emissions control can theoretically decrease diesel engine emissions of NOx, soot, carbon monoxide (CO), and unburned hydrocarbons (HC) to zero, carbon dioxide emissions may only be decreased by either using a fuel which contains less carbon, or by more efficiently consuming presently used carbon containing fuels such as No. 2 diesel fuel oil.

Complicating matters is the tendency of in-cylinder emissions controls to increase brake specific fuel consumption (BSFC). For the last few decades agricultural engine manufacturers have made efforts to progressively lower BSFC with the unveiling of new engine models, but this trend has experienced a degree of stagnation since the introduction of Tiers 1 through 4 emissions regulations. In fact, it is suspected that in adapting present Tier 3 certified engines to meet Tier 4, some engines may regress to producing increased BSFC levels over their immediate predecessors.

1.2 Objective

One objective of this study is to investigate how high EGR combined with certain fuel injection strategies affects both emissions and engine fuel economy. Application of EGR is commonly known to reduce engine fuel efficiency, but it is suspected that for some cases, high EGR may actually raise efficiency. Moreover, this study makes its second objective to

investigate how significantly engine fuel economy can be improved by recovering exhaust heat otherwise rejected by EGR coolers or discharged through the tailpipe, and using it to generate mechanical power.

CHAPTER 2. LITERATURE REVIEW

2.1 Diesel Emissions Standards

Tier 4 emissions standards, formulated by the United States EPA and made law by the United States government, will impose new restrictions on how much NOx, soot, and other emissions a newly manufactured diesel engine may legally release into the atmosphere. In the case of agricultural and other non-road engines producing from 56 to 560 kW, Tier 4 emissions regulations will mandate that any new engine emit no more than 0.40 g/kWh NOx, 0.02 g/kWh soot, and 0.19 g/kWh non-methane hydrocarbons (NMHC), with CO limits remaining unchanged from the Tier 3 stage [1, 2].

The phasing-in of Tier 4 emissions standards for non-road diesel engines producing from 56 to 560 kW is divided into two sub-stages. The first of which, Tier 4A (also referred to as interim Tier 4), requires that the Tier 4 soot emissions regulation be met by 2011 for 130 to 560 kW engines and by 2012 for 56 to 129 kW engines. The second of which, Tier 4B (also referred to as final Tier 4), requires the Tier 4 NOx emissions regulation be met by 2014.

Even though non-road diesel engines will require more intensive preparation measures than their on-road counterparts to meet Tier 4 regulations, the EPA, as well as published professional opinion, maintains these regulations as important for safeguarding both public health and the environment [3, 4].

2.2 Exhaust Gas Recirculation (EGR)

Among in-cylinder NOx reduction technologies, cooled EGR has proven itself one of the most popular since it does not necessitate significant modification to the engine and, when employed correctly, does not adversely affect engine performance by any significant degree. Moreover, since EGR decreases the formation of NOx from within the cylinder [5], the equipment it requires (piping network from the exhaust stream to intake stream, EGR valve, and EGR cooler) occupies a good deal less space than after-treatment equipment such as urea injection [6].

Exhaust gas recirculation works by mixing exhaust gases into the fresh air intake stream. This increases the amount of carbon dioxide and water vapor present in the cylinder before and during combustion, and since each of these species possesses a greater heat capacity (C_p) than air, in-cylinder gas temperatures are reduced for a given amount of energy released, thereby reducing NOx formation [7, 8]. To further reduce NOx emissions, many EGR systems utilize a cooler to decrease the temperature of EGR gases

being recirculated, thereby further lowering in-cylinder temperatures before and during combustion [9].

For non-road diesel engines, utilization of 15% EGR is presently a common means to meet Tier 3 NOx regulations [10]. However, if a manufacturer wishes to forgo NOx after-treatment to meet Tier 4 standards, EGR will likely need to be increased to levels of around 30% or perhaps more.

While the use of EGR significantly reduces NOx emissions, it has been shown to generally achieve this at the cost of increasing soot and CO emissions, one of the primary reasons being that an increased EGR rate leads to displacement of oxygen gas by exhaust gases, thereby lowering the extent to which soot and CO may be oxidized after being formed. One method to combat this is to employ higher turbocharger boost pressures to increase oxygen delivery to the combustion chamber while maintaining the same EGR level [11].

For certain operation conditions, however, EGR has conversely been shown to reduce soot emissions since increased EGR further delays start of combustion (SOC). Increased time between start of injection (SOI) and SOC allows for more mixing of air and fuel, thereby enabling a greater fraction of premixed instead of diffusion combustion [12]. All the while, care must be taken not to allow this premixed fraction achieve too high a level: a greater degree of premixed combustion will result in increased heat release rate, and

this can partially offset the NOx reduction for which EGR use is chiefly meant.

Beyond reducing NOx emissions, using EGR can provide slight effects advantageous to reduction of fuel consumption. For one, since EGR lowers peak in-cylinder temperatures, the resulting decrease in temperature gradient between the combustion chamber gases and the cylinder wall reduces heat transfer from the combustion chamber [13]; the net effect is an increase in indicated mean effective pressure (IMEP). Additionally, EGR can increase total combustion efficiency by reintroducing into the intake stream products of incomplete combustion [14].

In other ways, however, use of EGR increases engine fuel consumption, and usually these increases outweigh the aforementioned reductions. Specifically, EGR reduces the specific heat ratio of the in-cylinder working fluid, and this means less thermal energy can be extracted to perform work during expansion. Additionally, even though EGR reintroduces species of incomplete combustion, its provision of lower in-cylinder temperatures can intensify the mechanisms which cause incomplete combustion [15].

2.3 Novel Fuel Injection Strategies

Characteristics of in-cylinder combustion processes can be changed by adjusting injection timing, and also, by partitioning a single injection into

multiple smaller injections. These modifications to fuel injection strategy can decrease formation of NOx, soot, and other emissions.

Start of injection (SOI) may be varied from -20 crank angle degrees (CAD) after top dead center (ATDC) and sooner, to 5 CAD ATDC and later, though use of around -10 to 0 CAD ATDC had been most common for engines (rated at 56 kW to 560 kW) before the advent of Tiers 1 through 4 diesel emissions standards. When injecting later in the power cycle (slightly after top dead center), usually ignition delay is shorter. This leads to less premixed combustion and a lowered heat release rate, thereby lowering NOx formation [16, 17]. However, too late of an injection timing will deteriorate the combustion process and increase BSFC.

Utilization of multiple injections has proven able to reduce in-cylinder formation of soot emissions [18], in part due to the increased homogeneity it imputes to the mixing of fuel and air. However, this increase in homogeneity does not necessarily lead to an increase in NOx emissions as would usually be the case with a single injection. Multiple small injections can result in multiple small premix heat releases, whereas one large injection results in one large premix heat release, and in consequence, a higher peak heat release rate and NOx emissions. While conducive to lowing NOx, the partitioning of fuel injections tends to increase BSFC since it increases the diesel cycle's cut-off ratio [19].

Use of EGR delays onset of combustion, in effect requiring advancement of SOI. As such, care must be taken not to advance SOI excessively since any combustion occurring during the compression stroke will perform negative work on the power cycle, thereby increasing BSFC. Moreover, heat release rate will be increased for any premixed combustion which occurs during the compression as opposed to power stroke, and the tendency of higher heat release rate to increase NOx can partially offset NOx reduction achieved through employment of EGR.

2.4 Exhaust Energy Recovery

Since its invention the internal combustion engine has achieved steady gains in how much of the chemical energy in its fuel it converts to useful mechanical power. However, many presently manufactured designs of diesel engines still reject to the exhaust stream approximately 30% to 40% of the energy supplied by fuel, thereby restricting some of the more efficient direct injection 4-stroke diesel engines to presently achieve no better than 46% thermal efficiency [20]. As efforts persist to further lower engine BSFC, it is anticipated that more interest will be paid toward recovering some of this exhaust gas energy, for which the following technological solutions presently exist: turbocompounding, bottoming cycles (Rankine- or Brayton-based with various working media), and thermoelectric generators [21].

Among these three solutions, exhaust turbocompounding has presently seen the most usage. All the while, it has been shown that employment of an exhaust energy recovery system based on a Rankine cycle can produce about three times as much improvement in fuel economy as turbocompounding [22]. If Rankine-based exhaust energy recovery is combined with turbocharging and turbocompounding, drive cycle performance for a diesel engine could be increased by as much as 20%, and by as much as 40% for an adiabatic diesel engine.

Furthermore, exhaust energy recovery can facilitate the present industry trend of engine downsizing: replacing large displacement engines with equally powerful but smaller engines to reduce engine friction mean effective pressure (FMEP) while maintaining IMEP levels [23].

2.5 Trends in Fuel Economy Improvement

Ever since the diesel engine first began to widely replace gasoline engines as the power generation device of choice for agriculture, construction, industry, and heavy transportation applications, manufacturers have made persistent strides to decrease diesel engine fuel consumption for each new engine model [24, 25]. While the goal of reducing operation costs served as the initial motivation for decreasing fuel consumption, more recent impetus has come from desire to minimize emissions released per unit of shaft power developed.

Deere & Company, a leading manufacturer of agricultural equipment, has offered a diesel engine in its most powerful row-crop tractor since 1949. Since the introduction of its first inline 6-cylinder diesel-powered row-crop tractor in 1960, John Deere has achieved for its most powerful gear-drive row-crop tractor an average reduction in BSFC (taken at rated engine speed) of around 3% for every 8 years, or 1 g/kWh per year (Figure 2.1) [25].

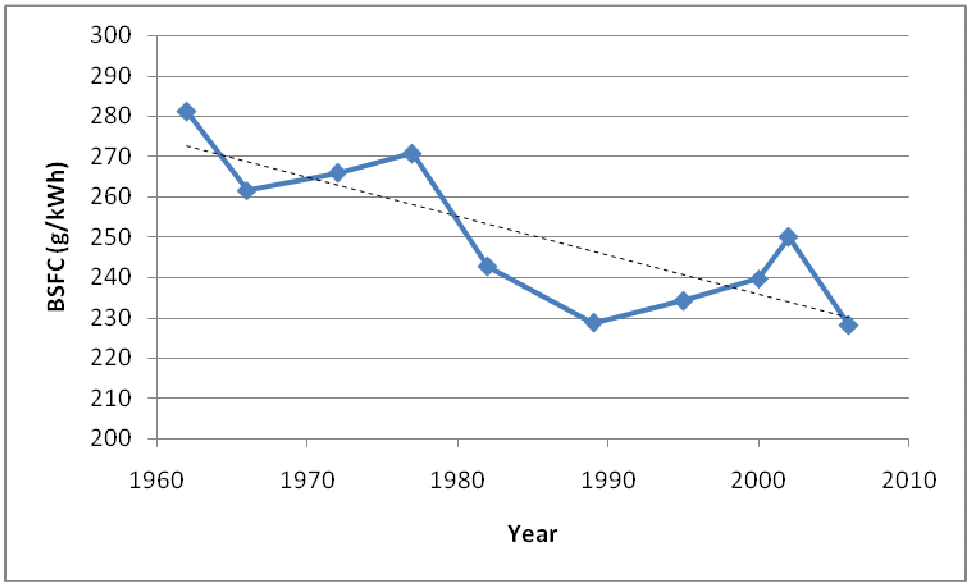

Figure 2.1: BSFC (at rated engine speed) achieved by diesel engine in most powerful John Deere gear-drive row-crop tractor versus tractor model year (solid line); linear trend in average BSFC reduction versus model year (dashed line)

During the 1980s fine-tuning of diesel engine technology such as turbocharging and intercooling contributed to reduction in BSFC from 1960s levels when neither technology was employed (Table 2.1). The 1990s and 2000s saw an increase in BSFC due in part to John Deere's incorporation of

certain emissions control equipment needed to meet Tier 1 and subsequent stages of emissions regulations.

Table 2.1: Engine specifications and performance for most powerful John Deere gear-drive row-crop tractor for model year; power take-off (PTO) power shows PTO power at engine rated speed; rated BSFC shows minimum BSFC achieved at this engine speed; PTO power and rated BSFC were measured by the Nebraska Tractor Test Laboratory

Tractor Model Year	Tractor Model	Displacement (L)	Compression Ratio	Aspiration	Tier Emissions Rating	PTO Power (kW)	Rated BSFC (g/kWh)
1962	5010	8.7	16.0:1	natural	N/A	90.3	281
1966	5020	8.7	16.5:1	natural	N/A	99.4	262
1972	6030	8.7	15.4:1	turbocharged, intercooled	N/A	131.2	266
1977	4840	7.6	15.5:1	turbocharged, intercooled	N/A	134.7	271
1982	4850	7.6	15.0:1	turbocharged, intercooled	N/A	143.9	243
1989	4955	7.6	16.0:1	turbocharged, intercooled	N/A	151.2	229
1995	8400	8.1	15.8:1	turbocharged, intercooled	Tier 1	170.2	234
2000	8410	8.1	16.5:1	turbocharged, intercooled	Tier 1	176.6	240
2002	8520	8.1	16.5:1	turbocharged, intercooled	Tier 2	191.3	250
2006	8430	9.0	16.3:1	turbocharged, intercooled	Tier 3	188.7	228

CHAPTER 3. METHOLOGY

3.1 Test Engine

A John Deere PowerTech 4.5L inline-4 diesel engine (model number: 4045HF475, serial number: PE4045H516927) was selected to be modeled using a GT-Power computer-based simulation. The engine featured 4-valves per cylinder and a Schwitzer S2A fixed geometry turbocharger (model number: RE509818) which utilizes a John Deere turbine housing. The engine was set up in the Iowa State University Department of Mechanical Engineering engines laboratory for experimental use, and is shown in Figures 3.1 through 3.3 as follow. Figure 3.4 shows this same model of engine, but not the particular unit used in this study.

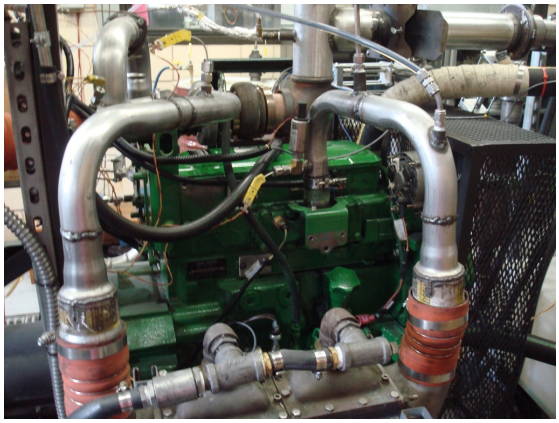

Figure 3.1: John Deere 4.5L diesel engine

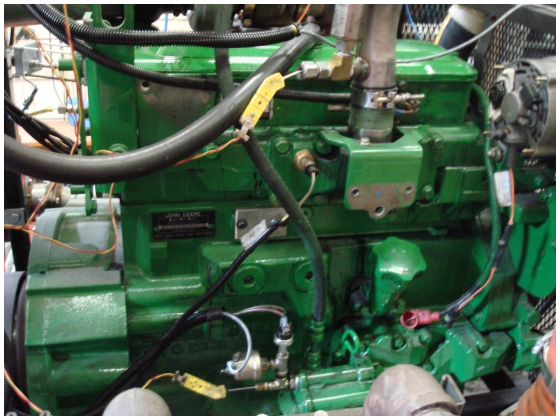

Figure 3.2: John Deere 4.5L diesel engine, close-up

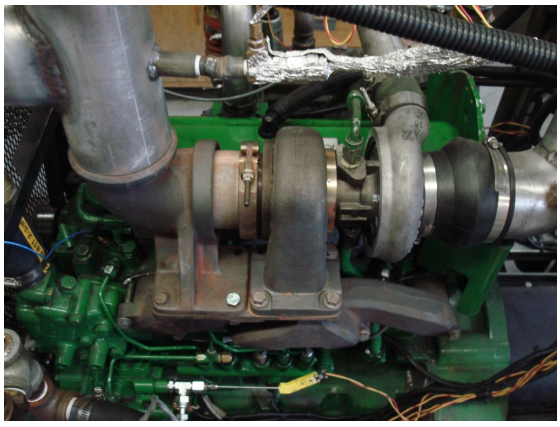

Figure 3.3: John Deere 4.5L diesel engine, top view; note turbocharger

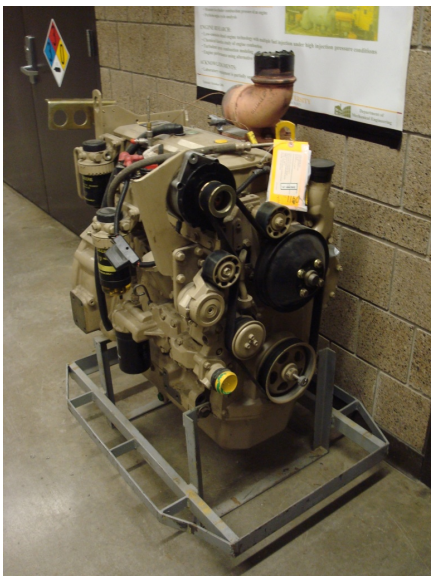

Figure 3.4: Front-right view of another John Deere 4045HF475 diesel engine

Specifications for the John Deere 4045HF475 diesel engine are given in the following table [26].

Table 3.1: Specifications of the present John Deere diesel engine

Model	4045HF475
Application	Industrial, Intermittent
Configuration of Cylinders	Inline-4
Bore and Stroke -- mm $(in.)$	106 x 127 (4.19 x 5.00)
Displacement -- L $(in.^3)$	4.5 (275)
Compression Ratio	17.0:1
Valves per Cylinder -- Intake/Exhaust	2 / 2
Firing Order	1-3-4-2
Combustion System	Direct Injection
Aspiration	Turbocharged and Intercooled
Engine Crankcase Vent System	Open
Maximum Crankcase Pressure -- kPa $(in.\ H_2O)$	0.5 (2)
Emissions Certification	EPA Tier 2

In factory trim, the engine was rated at producing maximum power of 129 kW (173 hp) at 2400 rpm, which is peak operation speed. Peak torque was 645 N-m (476 lb-ft) at 1400 rpm. Minimum BSFC was 203 g/kWh (0.333 lb/hp-hr) at 1600 rpm.

The particular engine in the laboratory did not, however, produce these exact performance numbers since it was modified to incorporate equipment and utilize operation conditions other than how it was factory-equipped and manufacturer-specified.

Among the new equipment incorporated, a marine air-to-water intercooler was used to replace the factory air-to-air intercooler. This marine intercooler used tap water as its cooling medium and could cool compressed air exiting the compressor to as low as 18ºC. Also, the engine was fitted with a low pressure EGR loop and a single EGR cooler from a Tier 3 John Deere 13.5L PowerTech diesel engine, the EGR cooler using tap water as its laboratory setup cooling medium. The inlet to the compressor used by the 4.5L engine's turbocharger was fit with a 4" O.D. aluminum pipe. The compressor's outlet was fit with a 2" O.D. aluminum pipe which was used to feed air into the intercooler. The intercooler's outlet was connected to the factory intake manifold with a 2" O.D. aluminum pipe. Factory design which directly coupled the engine's exhaust manifold outlet to the inlet of the turbocharger's turbine was retained in the laboratory. However, the outlet of the turbine was fit with a 4" O.D. aluminum pipe.

Among the operation condition changes, the engine's electronically controlled common-rail fuel injection system was operated with a pressure varying from 120 to 240 MPa; this study only collected data from and modeled the engine at 150 MPa injector operation pressure. Moreover, the electronic controls were programmed to deliver either single or double injections. Start of injection (SOI) timing for single injections was varied among -20, -15, -10, -5, 0, and 5 crank angle degrees (CAD) after top dead center (ATDC). Double injections were programmed to consist of both a pilot

injection and a subsequent main injection. This study utilized programming which specified that the pilot amount to 15% of the total mass of fuel injected, and commence at SOI timing varying among -40, -30, -20, and -15 CAD ATDC. The SOI of the main injection for all double injections was fixed at 5 degrees ATDC.

The laboratory engine was coupled to a General Electric motoring dynamometer (Figure 3.5) rated at 150 horsepower (112 kW). The engine was brought to steady-state operation conditions via the following ordered procedure:

1) Bring the dynamometer from a standstill to 1000 rpm, and motor the engine at this speed for 5 to 10 minutes.
2) Gradually increase the amount of fuel delivered per injection to desired fueling, 50 mg per injection in the case of this study.
3) Once engine is sustaining a coolant temperature of 90°C, increase dynamometer speed to desired level, 1400 rpm in the case of this study.

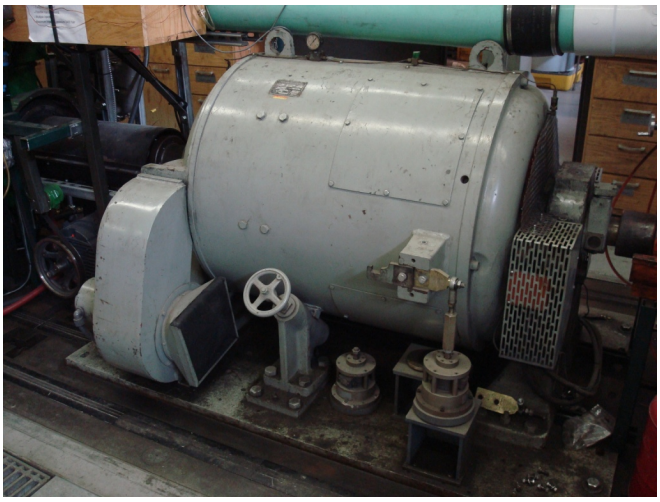

Figure 3.5: General Electric 112 kW dynamometer

3.2 Computer Model

The John Deere 4045HF475 engine in study was modeled using GT-Power, a computer-based engine-simulation tool which utilizes one-dimensional computational fluid dynamics (CFD) analysis and is designed by Gamma Technologies. GT-Power may be used to perform a variety of steady-state and transient analyses and may consider torque curve, fuel consumption, combustion/emissions, turbocharger response, EGR system design, and heat transfer [27]. Industry has shown a good deal of favor toward GT-Power, what with many major engine manufacturers presently using this tool to test and validate new designs.

Construction of a GT-Power model of the John Deere 4.5L engine first entailed inputting into GT-Power the engine's aforementioned cylinder configuration, bore, stroke, and compression ratio. Moreover, connecting rod

length and top dead center (TDC) clearance height were specified as 203 mm and 0.77 mm, respectively. Next temperatures for the head, piston, and cylinder surfaces adjacent to the combustion chamber were inputted as 550 K, 525 K, and 473 K, respectively. These temperatures were obtained directly from the John Deere Product Engineering Center in Waterloo, IA. Initial swirl at intake valve close (IVC) was inputted as 0.6, and the dimensions for the piston bowl were specified as follows in Table 3.2.

Table 3.2: Specifications of engine combustion chamber

Piston Cup Diameter (*mm*)	78.5
Maximum Piston Cup Depth (*mm*)	16.6
Piston Cup Center Depth (*mm*)	4.5

Engine friction constants, also obtained from John Deere Product Engineering Center, were then inputted into the model's cranktrain specifications, and are listed in Table 3.3 as follows.

Table 3.3: Specifications of engine friction constants

Constant Part of FMEP (bar)	0.4
Peak Cylinder Pressure Factor	0.005
Mean Piston Speed Factor $(bar/(m/s))$	0.09
Mean Piston Speed Squared Factor $\left(bar/(m/s)^2\right)$	0.0009

Next, GT-Power was given instructions to utilize the Woschni heat transfer predictor [19]. The head/bore area ratio of the engine was specified as 1.0, and the piston/bore area ratio was specified as 1.3.

At this point, a suitable combustion predictor was researched for selection. To glean insight into the nature of computer simulated combustion predictors such as those used by GT-Power, a very simple predictor was first selected for study, namely GT-Power's Direct Injection Wiebe combustion predictor. Using a three-term Wiebe function which considers ignition delay, premixed fraction, tail fraction, premixed duration, main duration, and tail duration, this predictor imposes the combustion burn rate for direct injection, compression-ignition engines To estimate what terms should be inputted into the three-term Wiebe function, in-cylinder pressure measurement was taken from the laboratory John Deere 4.5L engine, and then Engineering Equation Solver (EES) was used to calculate heat release rate (HRR) using the following equation [19].

$$\frac{dQ}{d\theta} = \frac{\gamma}{\gamma - 1} P \frac{dV}{d\theta} + \frac{1}{\gamma - 1} V \frac{dP}{d\theta} + \frac{dQ_{to-cylinder-wall}}{d\theta} \tag{3.1}$$

The plot of one such in-cylinder pressure measurements and the plot of its corresponding HRR calculation is shown as follows.

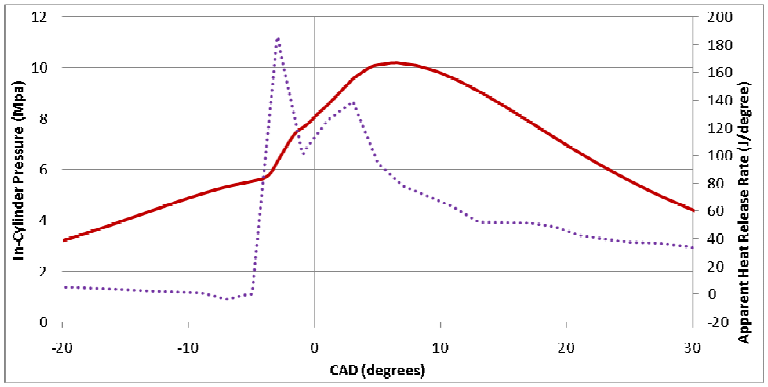

Figure 3.6: In-cylinder pressure (solid line) and apparent heat release rate (dotted line) versus crank angle degrees for 0% EGR, single injection at -10 degrees ATDC

All HRR calculations were based on in-cylinder pressure measurements taken from the laboratory engine operating at conditions which would later be inputted into the model, i.e., 1400 rpm engine speed and 50 mg per injection fueling. Moreover, these pressure measurements were taken for both single and double injection conditions for which SOI was varied, and for both 0% and 30% EGR conditions.

Upon initial completion of the GT-Power model, the Direct Injection Wiebe combustion predictor was employed, and once it was observed that the GT-Power model of the engine could be used to predict engine performance

with reasonable accuracy, the Wiebe combustion predictor was replaced with GT-Power's Direct Injection Jet combustion predictor, which fully predicted combustion rate and associated emissions. The Wiebe combustion predictor proved only semi-predicative and, unlike the Jet combustion predictor, required adjustment for different SOI and EGR operation conditions.

Next, fuel injector parameters were entered into the GT-Power model. These included such parameters as mass per injection, SOI, and injected fluid temperature and properties. Among fixed parameters, nozzle hole diameter was entered as 0.148 mm, number of nozzle holes as 6, and nozzle discharge coefficient as 0.675. Lastly, a profile of rate of injected mass versus crank angle degrees was entered. Figure 3.7 as follows shows the profile used for the fueling rate of 50 mg per injection. This profile was determined by using an injection rate test bench that was developed in-house.

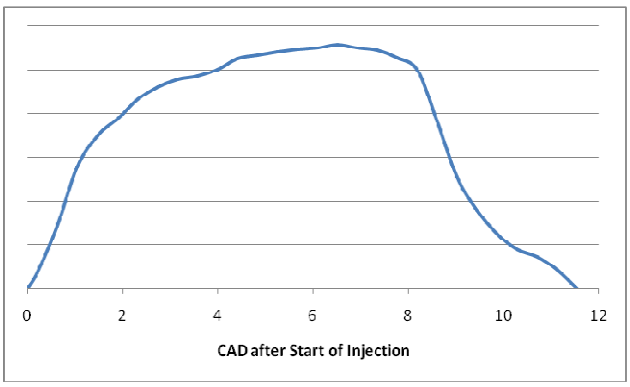

Figure 3.7: Typical shape of 50 mg injection profile

Later, a 95 mg injection profile was loaded into GT-Power when time came to model the engine at higher load conditions. This profile had similar

shape to the 50 mg profile, except fuel was injected for longer crank angle duration.

All diesel engines presently designed and manufactured by John Deere employ fixed cam timing. Deere designs most of its engines for specific applications, and most applications anticipate fairly set load conditions (usually high), so utilization of a variable-timing and/or variable-lift camshaft would not provide much benefit considering the added expense. As such, the present 4.5L engine's camshaft lift profile was inputted as a non-varying array of lift versus crank angle degrees. Additionally, for both intake and exhaust valves, forward and reverse flow coefficients were inputted as arrays versus crank angle degrees.

The next step was to model intake and exhaust piping for the engine. GT-Power enables the user to model individual piping parts, i.e., cylindrical pipes (both straight and bent) and Y-fittings, in which all parts are then joined together in desired order. Every time a piping part is created in GT-Power, the program places an icon onto a part assembly page. Once many piping parts are created (Figure 3.8), parts may be connected using GT-Power's connection tool which works by first selecting a part, and then selecting the part desired to be placed directly downstream. GT-Power then draws a solid line connecting each icon with an arrow to represent the direction of flow (Figure 3.9). Additionally, GT-Power automatically places a connector icon ● between each part which is connected. If a pipe's outlet is

connected to another pipe with an inlet of different diameter, GT-Power instead uses a bellmouth icon .

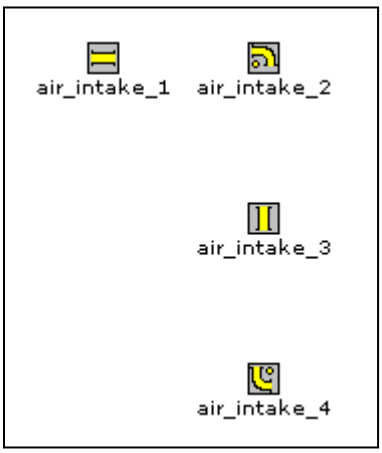

Figure 3.8: Example of GT-Power piping parts, unconnected

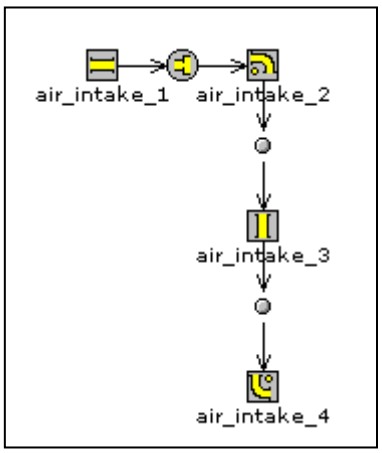

Figure 3.9: Example of GT-Power piping parts, connected

A network of intake and exhaust piping for the 4.5L engine was created in this manner. Dimensions for the laboratory engine's intake and exhaust piping parts were taken and then inputted into GT-Power whereby each pipe or Y-fitting was given specifications of length and diameter. In addition, each pipe was also given specifications of surface roughness, wall temperature, and wall heat conduction properties. Next each piping part was connected in the manner prior depicted, and Figure 3.11, later on in this chapter, shows the resulting assembly, complete with icons which represent other engine components such as cylinders, valves, etc.

For each segment of piping, as well as for each of the four engine cylinders, GT-Power required specification of initial conditions of temperature, pressure, and fluid composition. Since GT-Power is essentially a CFD program, it requires inputs of both initial and boundary conditions to solve governing differential equations.

Selection of a turbine and compressor for the engine's turbocharger was undertaken next. The item of key interest for modeling both turbine and compressor was each component's respective map. Since no manufacturer specified maps were available, it was decided to estimate each map's required inputs of speed, mass flow rate, pressure ratio, and efficiency. Next, an intercooler was created and fitted into the GT-Power network of intake and exhaust pipes represented on the piping part assembly page (Figure 3.11). This was done by bundling in parallel 936 straight cylindrical pipes, each with very narrow cross-section and a constant wall temperature 17°C.

As one of the last steps taken to finish the GT-Power model, the low pressure, cooled EGR loop built into the laboratory engine was modeled from a collection of both straight and bent cylindrical pipes, some of which were used to model the EGR cooler. The inlet to this EGR loop was then attached via Y-fitting (termed the EGR-split) to the engine's exhaust ducting, 45 mm downstream of the turbine. The part of the EGR-split which diverted exhaust to the EGR loop protruded into the exhaust stream at a 25 degree

angle (Figure 3.10) so as to force moving exhaust gases to stagnate inside this inlet to the EGR loop and drive EGR gas through the loop.

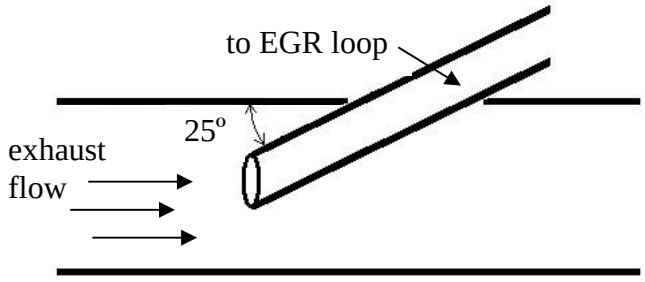

Figure 3.10: EGR-split showing inlet to EGR loop

To guard against exhaust gas within the EGR loop from flowing in the reverse direction, that is, away from the air intake piping, a check valve was placed within the modeled EGR loop.

The EGR cooler was modeled using a parallel bundle of 4 straight cylindrical pipes, each with a specified wall temperature of 27ºC, a wall temperature which later proved effective at cooling the EGR gas to a laboratory observed 130ºC for the 50 mg fuel per injection, 1400 rpm engine speed, 30% EGR operation condition.

Upon loading specifications for the engine's cylinders, valves, injectors, turbocharger, and cranktrain into the model, GT-Power automatically placed a representative icon for each of these engine components onto the part assembly page. As the final step for finishing the model, GT-Power's connection tool was used to connect each of these component's icons to each other and/or icons representing the piping part network already created,

effectually telling GT-Power the sequential order in which fluid and mechanical power are to flow through the engine system, thereby providing sufficient specification for GT-Power to run its one-dimensional CFD simulation. The following figure shows the completed part assembly page representing the 4.5L John Deere engine.

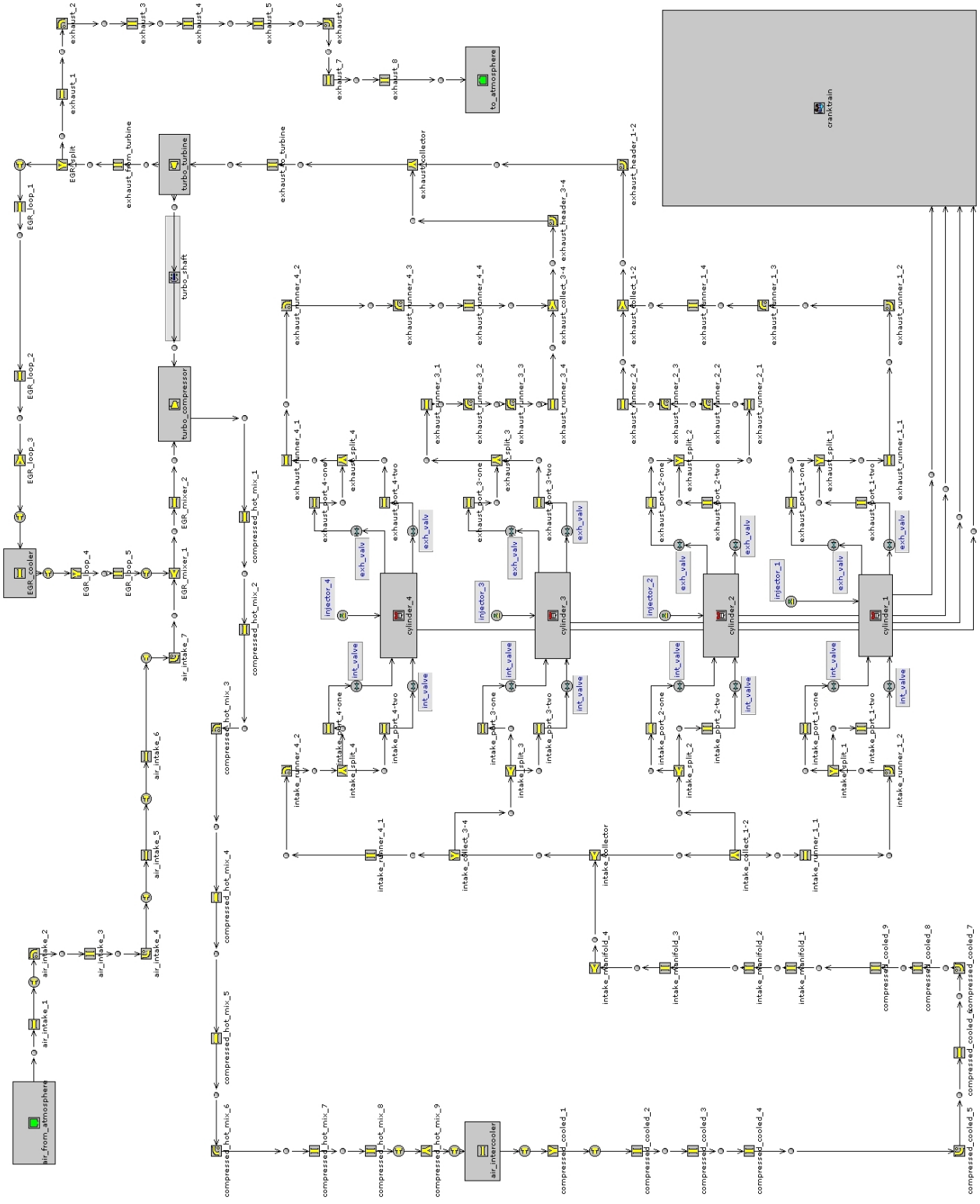

Figure 3.11: GT-Power part assembly page; arrows show direction of fluid or mechanical power flow

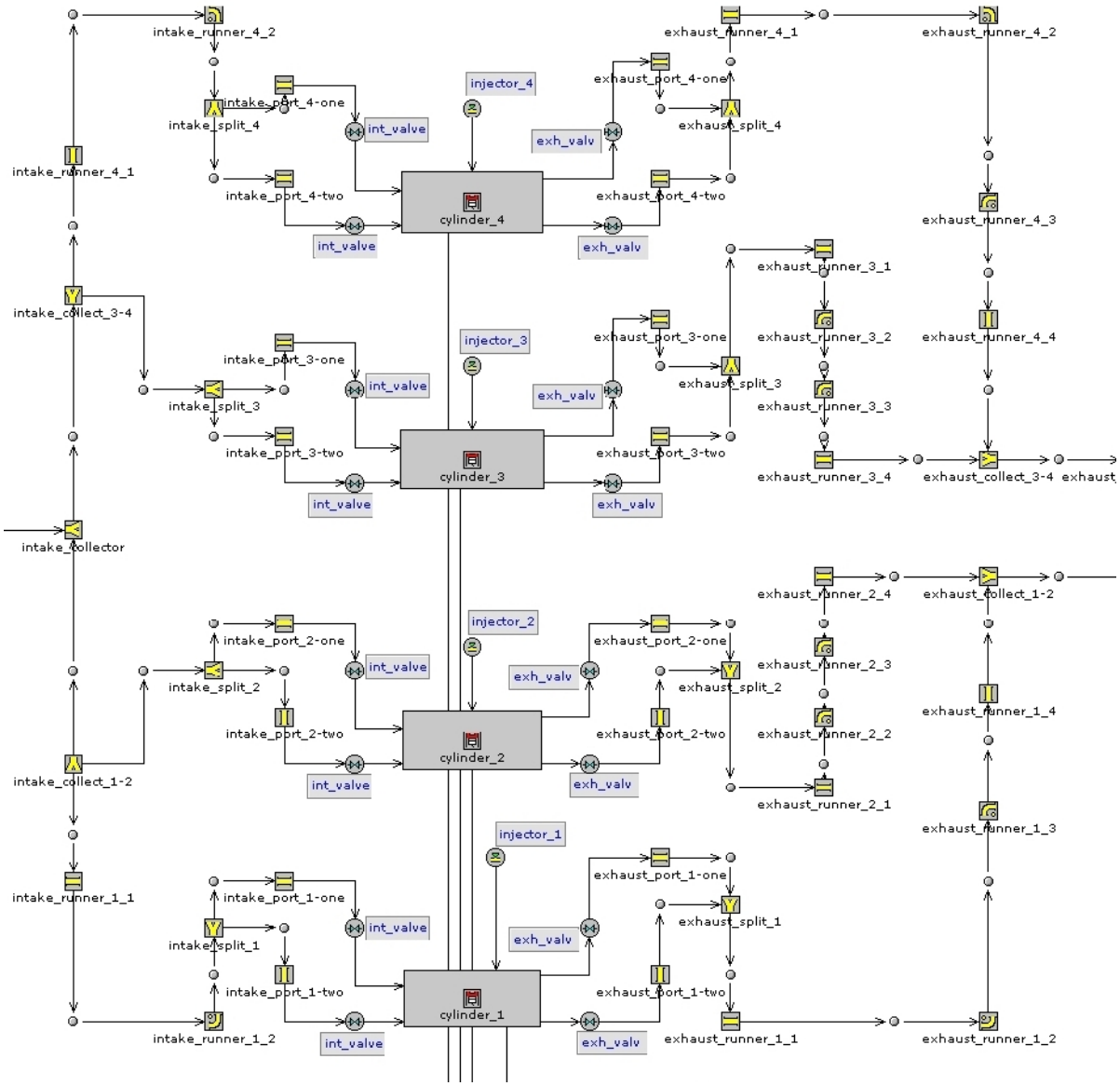

Figure 3.12: GT-Power part assembly page, close-up of engine cylinders and adjacent intake and exhaust piping

To run the GT-Power model, maximum simulation run time was specified, and then the model's "Start Simulation" command was selected. Once the simulation ran through the maximum specified run time, it saved a post-processing file which contained all simulation results, specifically engine

performance predictions. From here, this post-processing file was opened with GT-Power's dedicated program for post-processing, GT-Post. Among the engine performance predictions recorded in the post-processing file, only those made at the end of the simulation were considered for this study since these predictions, unlike those made early in the simulation, best approximated steady-state operation. If end-of-simulation engine operation appeared to still be in transient, the model's maximum specified run time was increased, and the model was run again until steady-state conditions were observed.

CHAPTER 4. FUEL ECONOMY AND EMISSIONS RESULTS

4.1 Model Validation

To verify that the GT-Power model of the present laboratory John Deere 4045HF475 could accurately predict this engine's performance, both the model and laboratory engine were run using the same operation conditions. The model's predictions for engine performance were then compared to the laboratory engine's performance recorded at steady-state, and the model was modified accordingly.

4.1.1 Operation Conditions

For the model validation process, both the GT-Power model and laboratory engine were run with identical operation conditions among 20 cases of varying EGR and SOI. Single injection cases accounted for 12 of these 20. They included operation with SOI at -20, -15, -10, -5, 0, and 5 CAD ATDC, each conducted with 0% and then 30% EGR. Double injection cases accounted for 8, and included operation with pilot injection at SOI of -40, -30, -20, and -15 CAD ATDC, each conducted with 0% and then 30% EGR.

Before the model was run to predict torque, fuel consumption, emissions, and in-cylinder pressure, the laboratory engine was run with all 20 cases, and its four dependent steady-state operation conditions of intake manifold pressure, intake manifold temperature, EGR rate, and air-to-fuel ratio were recorded during each case's run. What distinctly characterizes these four operation conditions is that, like independent operation conditions, they affect the performance results of torque, fuel consumption, emissions, and in-cylinder pressure, yet each of the four is dependent upon other, purely independent, operation conditions. Specifically, as far as the workings of the GT-Power model were concerned, intake manifold pressure depended largely on turbocharger compressor and turbine map inputs; intake manifold temperature depended largely on compressed air intercooler specifications, and also, EGR rate; EGR rate depended largely on EGR valve position; and air-to-fuel ratio, like intake manifold pressure, depended largely on turbocharger compressor and turbine map inputs.

For laboratory runs, the engine's intake manifold temperature and pressure were measured using a thermocouple and pressure transducer, respectively, both attached to the intake manifold via T-fitting (Figure 4.1), so as to place both downstream of the compressed air intercooler, and upstream of the cylinder head's intake valves.

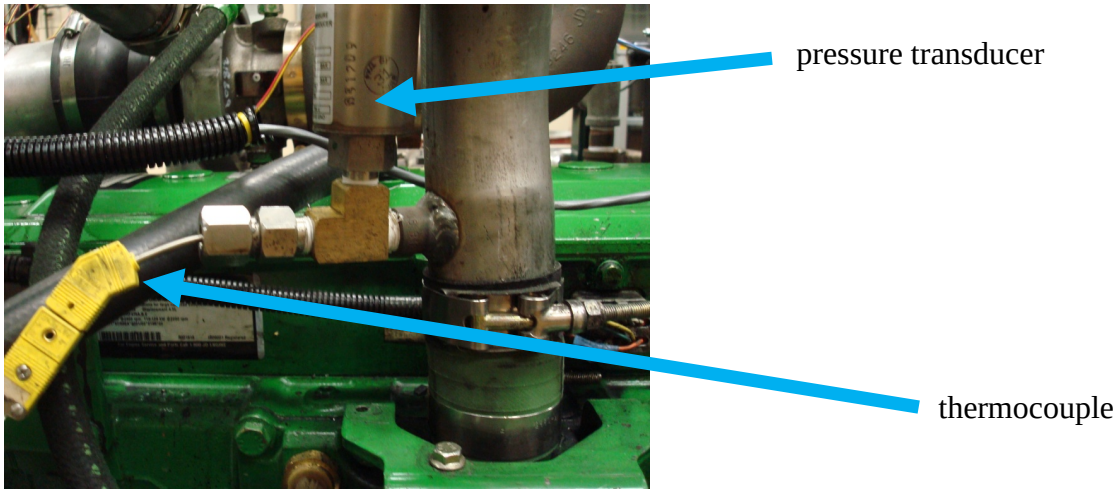

Figure 4.1: Thermocouple and pressure transducer attached to intake manifold via T-fitting

The laboratory engine's EGR rate was regulated via adjustment of an EGR valve (Figure 4.2), which, like the intake and exhaust piping, was fabricated in-house. A Horiba exhaust gas analyzer, model MEXA-7100DEGR (Figure 4.3) was used to measure the EGR rate, sampling both intake manifold and exhaust manifold gases for carbon dioxide mole fraction; this analyzer was also used to measure air-to-fuel ratio.

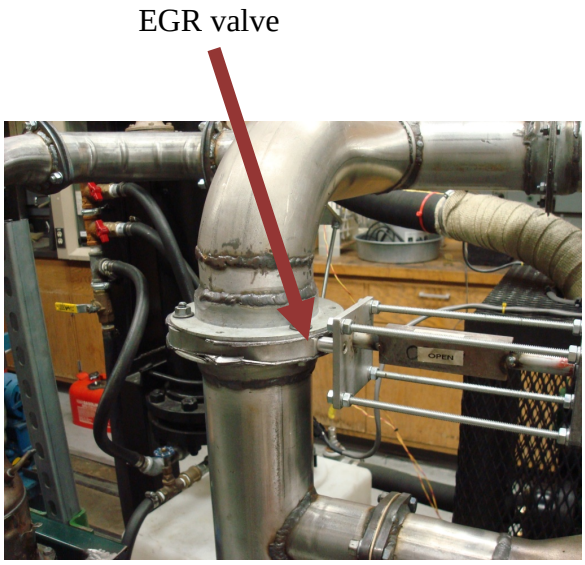

Figure 4.2: Laboratory engine EGR valve, directly upstream of EGR cooler

Figure 4.3: Horiba exhaust gas analyzer

Next the GT-Power model was run for all 20 aforementioned cases, and the dependent operation conditions of intake manifold pressure and temperature, EGR rate, and air-to-fuel ratio were compared to those indicated by GT-Power. If the GT-Power model's results showed its dependent operation conditions to not match that of the laboratory engine, the GT-Power model's inputted independent operation conditions were changed until model's results showed dependent operation conditions agreeing with laboratory results.

Upon the initial run of all 20 cases with the GT-Power model, it was discovered that two 30% EGR cases produced significant misfiring, specifically, that with single injection SOI at 5 CAD ATDC, and double injection with pilot SOI at -40 CAD ATDC. In both cases, misfiring was

evidenced by model indications of in-cylinder pressures near motoring levels, and also, a large percentage (15% to 100%) of each injection's fuel mass leaving the exhaust port unburned. In the case of the single injection at 5 CAD ATDC, it was suspected that the tendency of high EGR to retard SOC timing delayed SOC sufficiently late in the piston's descent to hinder onset of combustion.

While intake manifold pressure and temperature, and air-to-fuel ratio were directly outputted by GT-Power, the simulation's predicted EGR rate needed to be calculated by dividing GT-Power's prediction for intake carbon dioxide mole fraction by its prediction for exhaust carbon dioxide mole fraction. As with all engine performance predictions made by the GT-Power model, only mole fractions predicted at the end of the simulation were considered since the model was run until performance steadied. The following figure illustrates how each mole fraction varied during the course of the simulation, and then steadied near the end of the simulation. It also shows EGR rate.

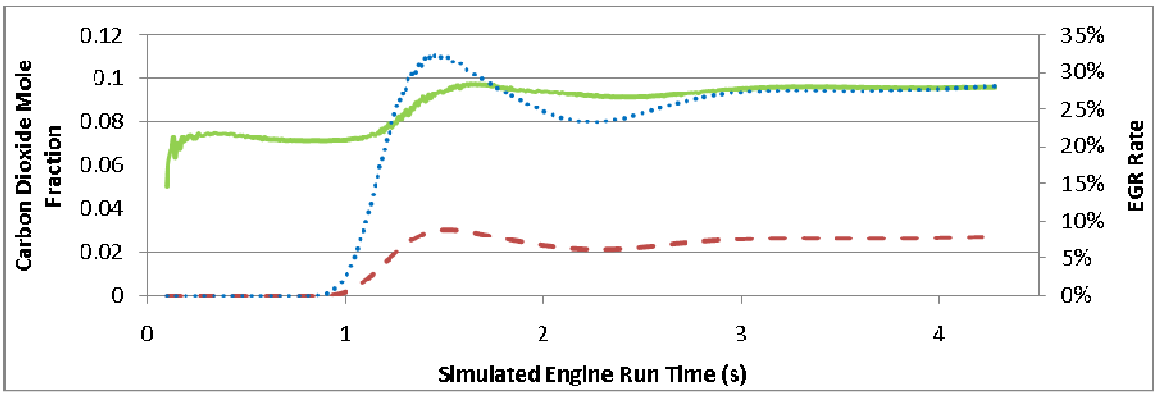

Figure 4.4: Intake carbon dioxide mole fraction (dashed line), exhaust carbon dioxide mole fraction (solid line), and EGR rate (dotted line) versus simulated engine run time for 30% EGR, single injection at 0 CAD ATDC

The EGR level as calculated from each carbon dioxide mole fraction was then used to adjust the effective flow area of the model's EGR valve, so as to achieve 0% EGR for 10 cases, and then 30% EGR for the other cases. For 0% EGR, the effective flow area of the EGR valve was set to zero.

After sufficient analysis of the values predicted by GT-Power for the four dependent operation conditions, and after subsequent adjustment of corresponding independent operation conditions, the GT-Power model eventually predicted values for these four dependent operation conditions within desired proximity to those measured on the laboratory engine.

Figures 4.5 and 4.6 show how intake manifold temperatures compare among 0% EGR cases, for single and double injection cases, respectively.

**Note that GT-Power predictions are represented by a solid line with square markers, and corresponding laboratory results are represented by a dashed line with diamond-shaped markers; this labeling convention is used

for all following figures up through Figure 4.16 which compare GT-Power predictions to laboratory results for the dependent operation conditions intake manifold temperature, intake manifold pressure, and air-to-fuel ratio. SOI for double injections refers to pilot injection SOI, since main is fixed.

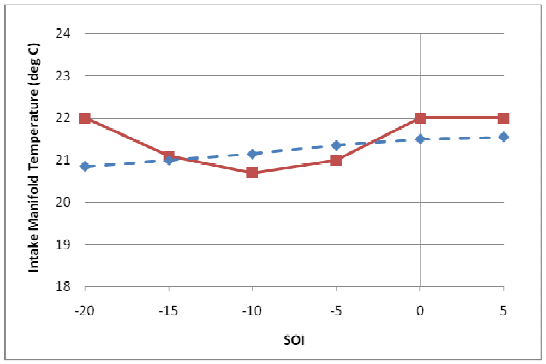

Figure 4.5: Intake manifold temperature versus SOI for 0% EGR, single injection

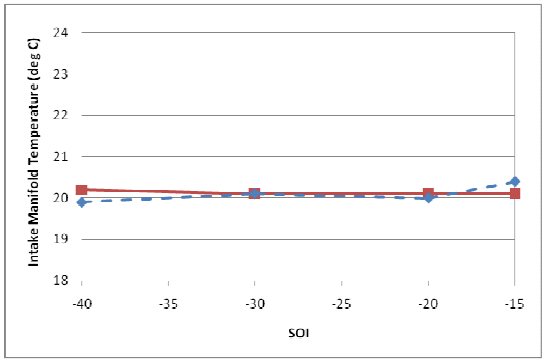

Figure 4.6: Intake manifold temperature versus SOI for 0% EGR, double injection

Figures 4.7 and 4.8 show how intake manifold temperatures compare among 30% EGR cases, for single and double injection cases, respectively.

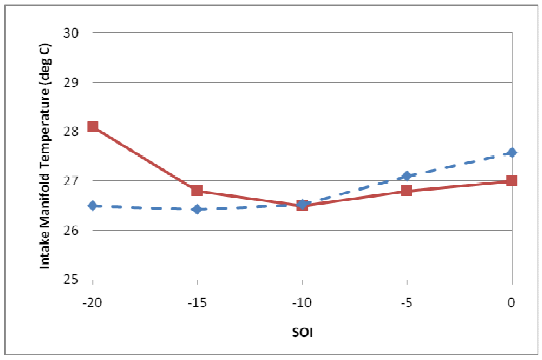

Figure 4.7: Intake manifold temperature versus SOI for 30% EGR, single injection

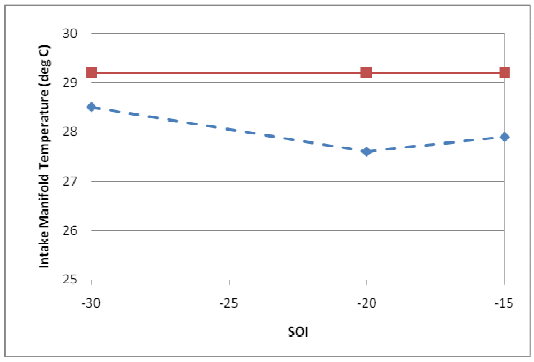

Figure 4.8: Intake manifold temperature versus SOI for 30% EGR, double injection

Figures 4.5 through 4.8 show decently good agreement between laboratory and model results for intake manifold temperature. This would indicate that the GT-Power model's air intercooler was predictiong cooling levels near that of the laboratory engine's.

Figures 4.9 and 4.10 show how intake manifold pressures compared among 0% EGR cases, for single and double injection cases, respectively.

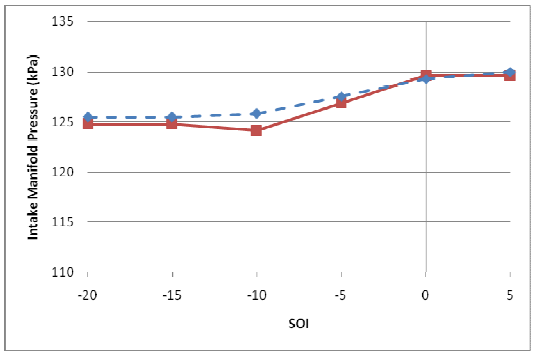

Figure 4.9: Intake manifold pressure versus SOI for 0% EGR, single injection

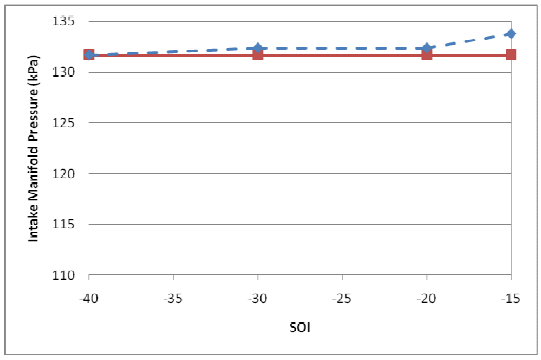

Figure 4.10: Intake manifold pressure versus SOI for 0% EGR, double injection

Figures 4.11 and 4.12 show how intake manifold pressures compare among 30% EGR cases, for single and double injection cases, respectively.

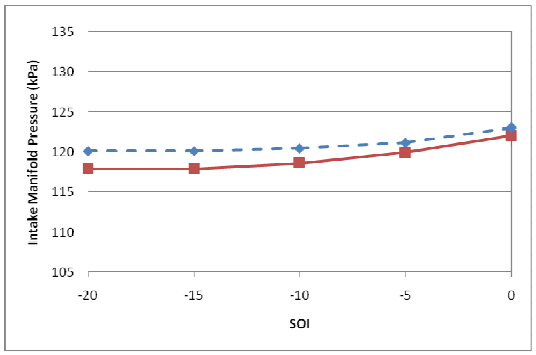

Figure 4.11: Intake manifold pressure versus SOI for 30% EGR, single injection

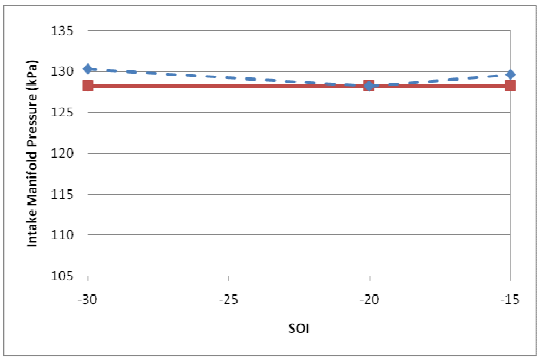

Figure 4.12: Intake manifold pressure versus SOI for 30% EGR, double injection

By-and-large Figures 4.9 through 4.12 show a good level of agreement between GT-Power results for intake manifold pressure and those recorded in the laboratory, even better than the agreement Figures 4.5 through 4.8 show for temperature.

Figure 4.11, however, shows that the model slightly under-predicted intake manifold pressure, especially for early injection timings. While only a hypothesis, this trend could perhaps be attributed to the model possibly over-predicting heat transfer from the combustion chamber, especially near TDC, as this would result in under-prediction of enthalpy flow rate leaving the exhaust valves and, in turn, that delivered to the turbocharger turbine. Early injection timing would lengthen time between combustion and expulsion of exhaust gases, thereby causing this over-prediction of heat transfer to more greatly decrease exhaust manifold gas temperature for cases employing early injection timing. As such, reduction of enthalpy flow rate to

the turbine would reduce compressor power and, in effect, compressor pressure ratio.

Figures 4.13 and 4.14 show how air-to-fuel ratios compare among 0% EGR cases, for single and double injection cases, respectively.

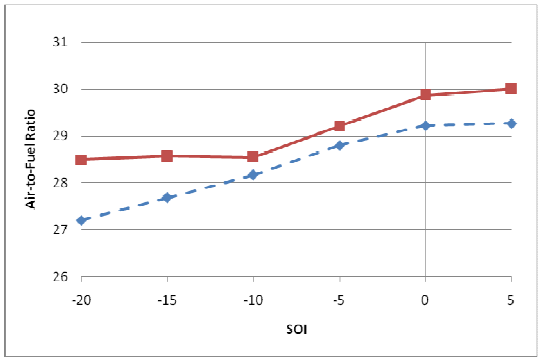

Figure 4.13: Air-to-fuel ratio versus SOI for 0% EGR, single injection

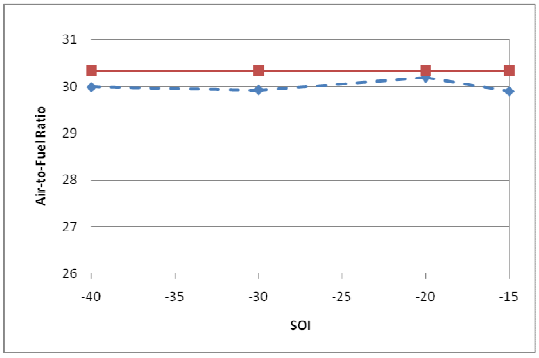

Figure 4.14: Air-to-fuel ratio versus SOI for 0% EGR, double injection

Figures 4.15 and 4.16 show how air-to-fuel ratios compare among 30% EGR cases, for single and double injection cases, respectively.

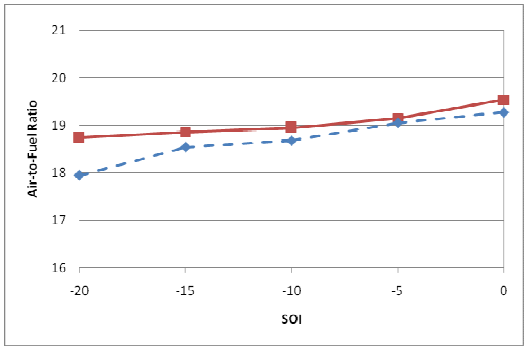

Figure 4.15: Air-to-fuel ratio versus SOI for 30% EGR, single injection

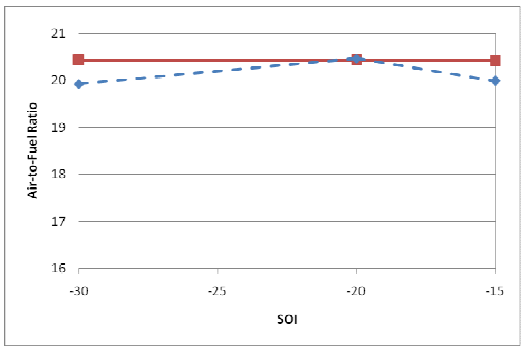

Figure 4.16: Air-to-fuel ratio versus SOI for 30% EGR, double injection

Here, GT-Power model results tended to slightly over-predict air-to-fuel ratio, especially for early injection timings. Granted, inputs to the GT-Power model could have been modified to decrease air-to-fuel ratio, but this measure was decided against because doing so would likely have decreased intake manifold pressure, which was already lower than in laboratory results. Since GT-Power over-predicted air-to-fuel ratio by about the same amount it under-predicted intake manifold pressure, it was decided to not make model input changes to adjust either.

Slight discrepancies aside, Figures 4.5 though 4.16 show that the GT-Power model could accurately simulate the dependent operation conditions of intake manifold pressure, intake manifold temperature, and air-to-fuel ratio, and in doing so, predict values no more than 10% different from those measured in the laboratory.

4.1.2 Performance Results

Next, the model was run again, and the performance predictions of torque, fuel consumption, emissions, and in-cylinder pressure were compared to data measured on the laboratory engine. Any observed discrepancies were corrected by adjusting the GT-Power model, making sure to not alter the already validated simulation of the dependent operation conditions discussed in subsection 4.1.1.

Among the performance results of interest, engine torque was measured in the laboratory via readout displayed on the dynamometer control panel shown below.

Figure 4.17: Dynamometer control panel

In laboratory, engine torque was recorded for the primary purpose of later reporting fuel consumption and emissions on a brake power specific basis, so no plots depicting torque are shown in this chapter.

As for the GT-Power model, it directly outputted numerical results for brake torque. Trends in discrepancy between brake torque predicted by the model and that recorded in laboratory proved nearly identical to trends in discrepancies for BSFC: when the model under-predicted brake torque, it over-predicted BSFC by about the same percentage. These trends in discrepancy are portrayed later on in this subsection by Figures 4.19 through 4.22 which show BSFC versus SOI.

Granted, the pressure ratio specified in the turbocharger's compressor map could have been raised or lowered to respectively raise or lower brake torque predicted by GT-Power, but this would in turn alter GT-Power's already validated predictions for the dependent operation condition of intake manifold pressure, so it was decided to not adjust inputs to GT-Power in attempt to correct its brake torque predictions, almost all of which proved no more than 10% different from laboratory measured results.

Laboratory engine fuel consumption was found by taking the difference in fuel tank weight between the beginning and end of a timed duration and dividing this difference by elapsed time. Laboratory measured torque was then multiplied by engine speed 1400 rpm to find laboratory measured power, and this power value was factored into the laboratory fuel consumption measurement to find BSFC as shown in Equation 4.1.

$$BSFC = \frac{mdot_{fuel}}{Wdot_{brake}} \tag{4.1}$$

Laboratory engine emissions of nitrogen oxides (NOx) and unburned hydrocarbons (HC) were recorded by the HORIBA exhaust gas analyzer in terms of parts-per-million (PPM) concentration. Soot was recorded by an AVL smoke meter in terms of mg/m^3 concentration. Each was then converted to a brake power specific value. Equation 4.2 shows how brake specific NOx was calculated from laboratory measurements.

$$NOx_{brake\_specific} = M_{NO_2} \cdot concentration_{NOx} \cdot mdot_{fuel} \cdot \left(\left(M_C + \left(\frac{kmol_H}{kmol_C} \right)_{fuel} \cdot M_H \right) \cdot \left(concentration_{CO} + concentration_{CO_2} + concentration_{HC} \right) \cdot \left(Wdot_{brake} \right) \right)^{-1} \quad (4.2)$$

Equation 4.3 shows how brake specific HC was calculated from laboratory measurements.

$$HC_{brake\_specific} = concentration_{HC} \cdot mdot_{fuel} \cdot \left(\left(concentration_{CO} + concentration_{CO_2} + concentration_{HC} \right) \cdot \left(Wdot_{brake} \right) \right)^{-1} \quad (4.3)$$

Equation 4.4 shows how brake specific soot was calculated from laboratory measurement:

$$soot_{brake\_specific} = \frac{concentration_{soot} \cdot Vdot_{exhaust}}{Wdot_{brake}} \quad (4.4)$$

Discrepancies in emissions predicted by the model versus those measured were not corrected by adjusting the model, but rather, by applying

different multipliers to the model's predictions for NOx, HC, and soot. This is detailed later on in this chapter.

Laboratory engine in-cylinder pressure was recorded via pressure transducer fit into the front-most cylinder's glow-plug socket as shown below.

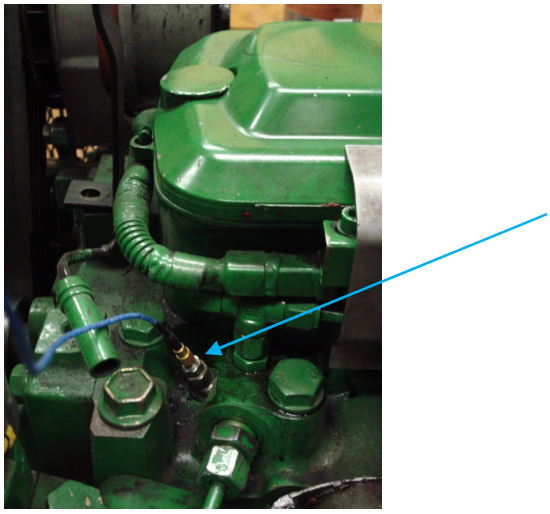

Figure 4.18: Pressure transducer for in-cylinder pressure, fit into glow plug socket of front-most cylinder

This transducer's signal, along with the signal from a device used to measure the engine's crank angle position, were fed into a LabView data acquisition program which then outputted a plot of in-cylinder pressure versus crank angle degrees ATDC.

From here, minor adjustments were made to the GT-Power model until its performance predictions for torque, fuel consumption, and in-cylinder pressure returned values within approximately 10% of those recorded by the laboratory engine. As mentioned, no adjustments were made to the model to correct its emissions predictions, but rather, multipliers were applied to its

outputted results. Figures 4.19 and 4.20 show how the GT-Power model's brake specific fuel consumption (BSFC) predictions compare with those recorded in the laboratory for the 0% EGR condition, for single and double injection cases, respectively.

**Note Figures 4.19 through 4.40 employ the previously used labeling scheme where GT-Power predictions are represented by a solid line with square markers, and corresponding laboratory results are represented by a dashed line with diamond-shaped markers. SOI for double injections refers to the pilot injection SOI, since the main injection for all double injections is fixed at 5 degrees ATDC.

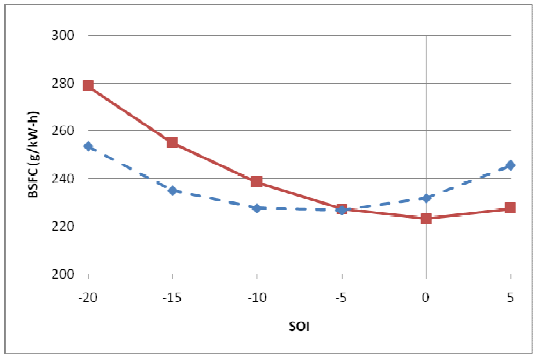

Figure 4.19: BSFC versus SOI for 0% EGR, single injection

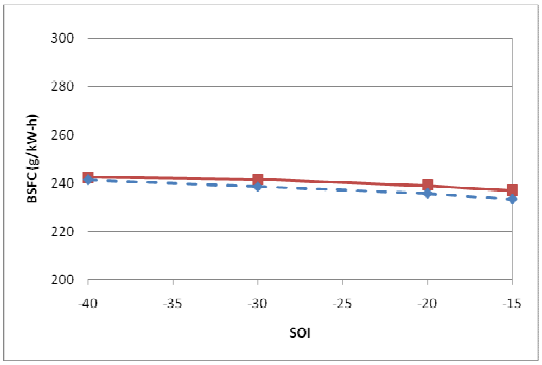

Figure 4.20: BSFC versus SOI for 0% EGR, double injection

Figures 4.21 and 4.22 show how the GT-Power model's BSFC predictions compare with those recorded for the laboratory engine for the 30% EGR condition, for single and double injection cases, respectively.

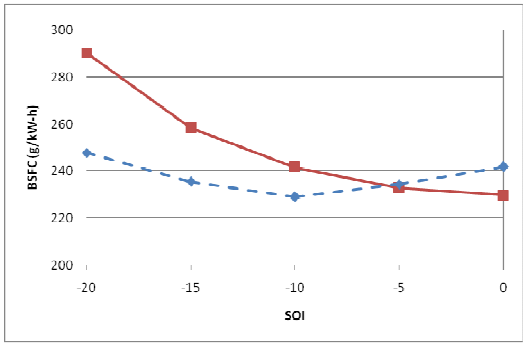

Figure 4.21: BSFC versus SOI for 30% EGR, single injection

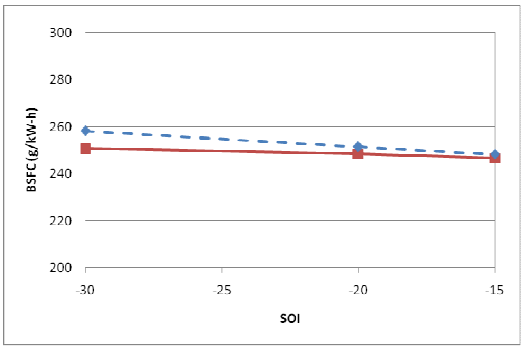

Figure 4.22: BSFC versus SOI for 30% EGR, double injection

Trends in agreement between laboratory and GT-Power BSFC prove similar between both 0% and 30% cases running a single injection. Specifically, early injection timing tended to over-predict BSFC, with the latest injection timing under-predicting. It is suspected that this could have been attributed to discrepancies between the GT-Power model's predictions for in-cylinder pressure and that measured in laboratory, and this is discussed later in this chapter where analysis is performed on figures which show in-cylinder pressure for the 0% and 30% EGR cases.

Figures 4.23, 4.24, and 4.25 show how the GT-Power model's emissions predictions for NOx, HC, and soot, respectively, compare with those recorded on the laboratory engine for the 0% EGR condition for single injection cases. These figures show GT-Power emissions predictions without application of the aforementioned correction multipliers, but instead, show emissions predictions exactly as they are predicted by the GT-Power model. Each figure is meant to provide insight into how the model's predictions differ from laboratory measured trends. In any event, such multipliers were only

calculated for 30% EGR cases since these multipliers would later be used to correct GT-Power emissions predictions for higher EGR cases.

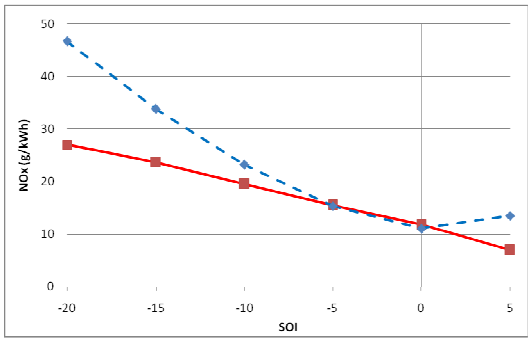

Figure 4.23: NOx versus SOI for 0% EGR, single injection

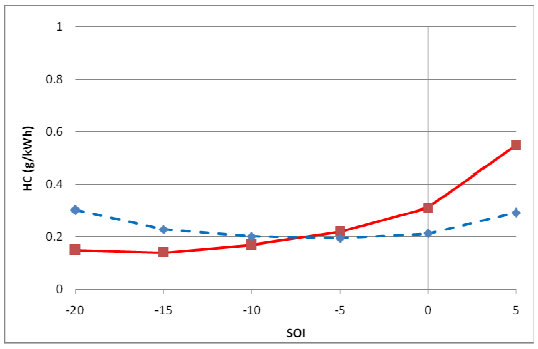

Figure 4.24: HC versus SOI for 0% EGR, single injection

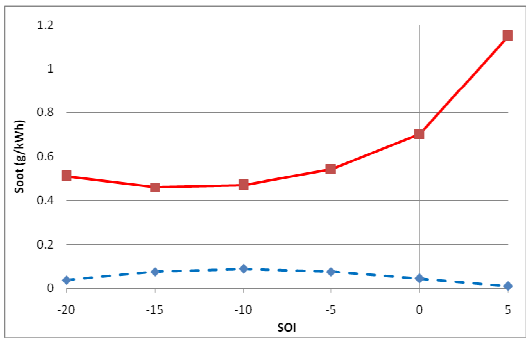

Figure 4.25: Soot versus SOI for 0% EGR, single injection

Figures 4.26, 4.27, and 4.28 show how the GT-Power model's emissions predictions (again, without application of correction multipliers) for NOx, HC, and soot, respectively, compare with those recorded on the laboratory engine for the 0% EGR condition for double injection cases.

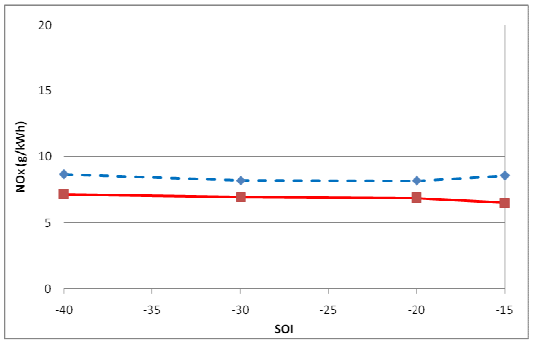

Figure 4.26: NOx versus SOI for 0% EGR, double injection

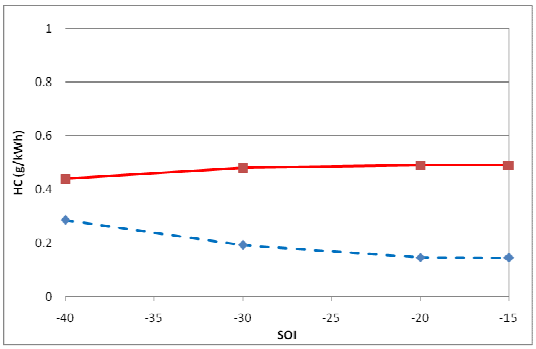

Figure 4.27: HC versus SOI for 0% EGR, double injection

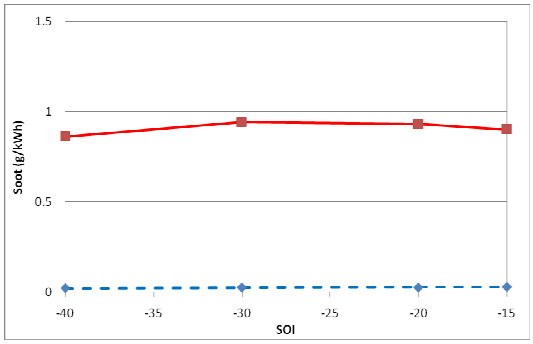

Figure 4.28: Soot versus SOI for 0% EGR, double injection

Among GT-Power's emissions predictions for the 0% EGR condition, greatest discrepancy occurred with the soot predictions, in which GT-Power consistently predicted a good deal too high. This could likely be attributed to GT-Power's employment of an in-cylinder fluid dynamic analysis which is zero-dimensional. Research has shown that soot is best predicted via fluid dynamic analysis which considers at least two dimensions. Predictions for the other emissions of NOx and HC, on the other hand, can still maintain a reasonable level of accuracy when fluid dynamic analysis considers less than two dimensions, but still, zero-dimensional analysis cannot be expected to achieve highest level accuracy in its emissions predictions.

Figures 4.29, 4.31, and 4.33 show how the GT-Power model's emissions predictions for NOx, HC, and soot, respectively, compare with those recorded on the laboratory engine for the 30% EGR condition for single injection cases. Figures 4.29, 4.31, and 4.33 are complemented by Figures 4.30, 4.32, and 4.34, respectively, in which each of these complementary figures shows the GT-Power model's predictions after correction multipliers are applied.

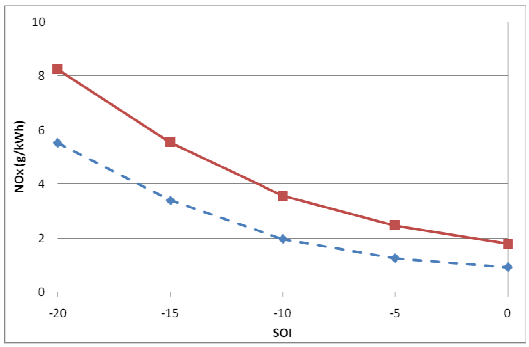

Figure 4.29: NOx versus SOI for 30% EGR, single injection; GT-Power results shown before application of correction multiplier

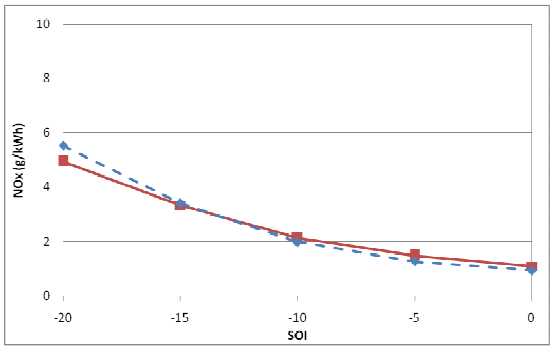

Figure 4.30: NOx versus SOI for 30% EGR, single injection; GT-Power results shown after application of correction multiplier

Figure 4.29 shows that GT-Power predicts NOx consistently too high for the 30% EGR, single injection condition. As such a constant correction multiplier of 0.60 was calculated by dividing the laboratory engine's SOI-average NOx by GT-Power's SOI-average NOx. This multiplier was applied to all SOI cases, the results of which are shown in Figure 4.30.

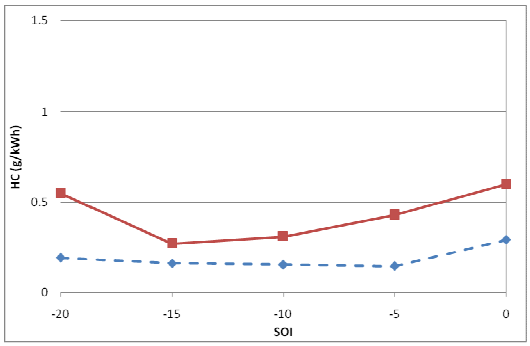

Figure 4.31: HC versus SOI for 30% EGR, single injection; GT-Power results shown before application of correction multiplier

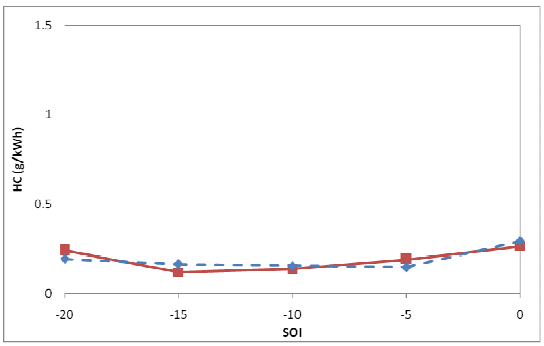

Figure 4.32: HC versus SOI for 30% EGR, single injection; GT-Power results shown after application of correction multiplier

Figure 4.31 shows that GT-Power predicts HC consistently too high for the 30% EGR, single injection condition. As such a constant correction multiplier of 0.44 was calculated by dividing the laboratory engine's SOI-average HC by GT-Power's SOI-average HC, and this multiplier was applied to all SOI cases, the results of which are shown in Figure 4.32.

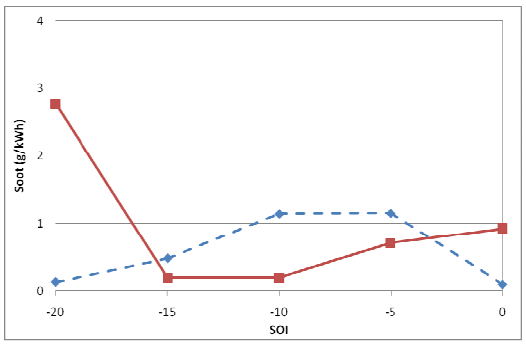

Figure 4.33: Soot versus SOI for 30% EGR, single injection; GT-Power results shown before application of correction multipliers

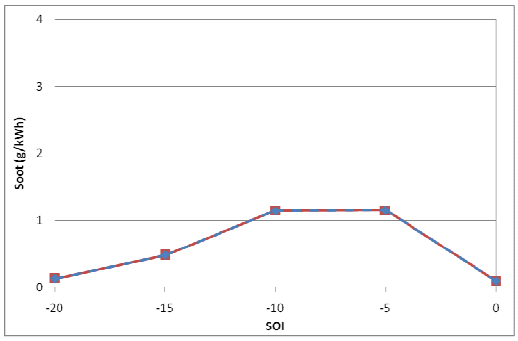

Figure 4.34: Soot versus SOI for 30% EGR, single injection; GT-Power results shown after application of correction multipliers

With soot for single injection cases, no clear trend appeared among varying SOI timings between that predicted by GT-Power and that recorded experimentally, and this is shown in Figure 4.33. As such, a single constant multiplier could not be applied to all SOI cases, but rather, a multiplier needed to be calculated for each SOI case by dividing its experimentally measured soot by its GT-power prediction for soot. This procedure netted results which enabled GT-Power's predicted soot to coincide with experimental results as shown in Figure 4.34, even though such application of a unique multiplier to each SOI case involved a more artificial correction scheme than would be preferred. These SOI case-specific multipliers are shown in Table 4.1.

Table 4.1: Soot correction multipliers versus SOI for single injection

SOI	-20	-15	-10	-5	0
multiplier	0.048	2.51	6.02	1.62	0.106

Figures 4.35, 4.37, and 4.39 show how the GT-Power model's emissions predictions for NOx, HC, and soot, respectively, compare with those recorded on the laboratory engine for the 30% EGR condition for double injection cases. Figures 4.35, 4.37, and 4.39 are complemented by Figures 4.36, 4.38, and 4.40, respectively, in which each of these complementary figures shows the GT-Power model's predictions after correction multipliers are applied.

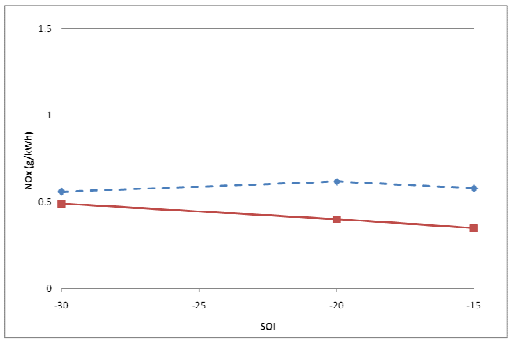

Figure 4.35: NOx versus SOI for 30% EGR, double injection; GT-Power results shown before application of correction multiplier

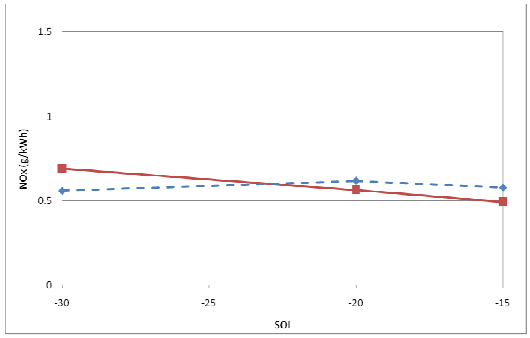

Figure 4.36: NOx versus SOI for 30% EGR, double injection; GT-Power results shown after application of correction multiplier

Figure 4.35 shows that GT-Power's prediction for NOx was consistently too low for the 30% EGR, double injection condition, this being different from the single injection cases in which NOx was predicted too high. A constant correction multiplier of 1.4 was calculated by dividing the laboratory engine's SOI-average NOx by GT-Power's SOI-average NOx, and this multiplier was applied to all SOI cases, the results of this being shown in Figure 4.36.

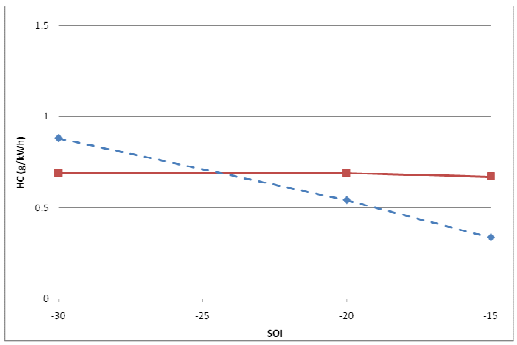

Figure 4.37: HC versus SOI for 30% EGR, double injection; GT-Power results shown before application of correction multipliers

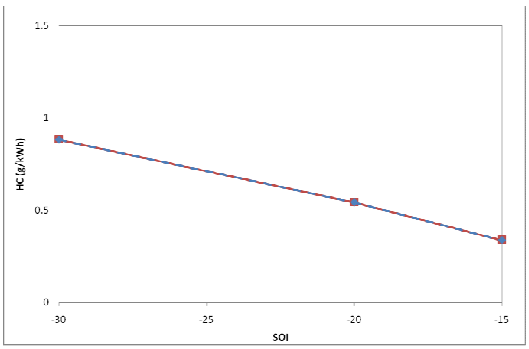

Figure 4.38: HC versus SOI for 30% EGR, double injection; GT-Power results shown after application of correction multipliers

With HC for double injections, no clear trend appeared among varying SOI in predictions by GT-Power versus experimental data, and this is shown in Figure 4.37, so a multiplier was calculated for each SOI case by dividing experimentally measured HC by GT-power's predicted HC. The SOI case-specific multipliers are shown in Table 4.2.

Table 4.2: HC correction multipliers versus SOI for double injection

pilot SOI	-30	-20	-15
multiplier	1.28	0.79	0.50

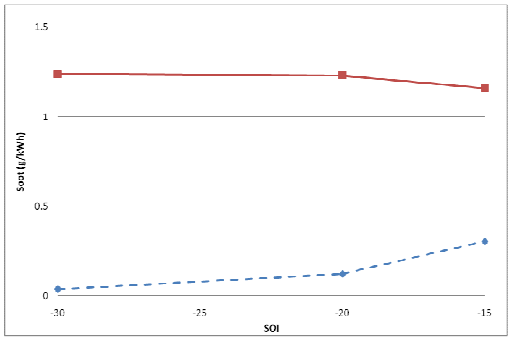

Figure 4.39: Soot versus SOI for 30% EGR, double injection; GT-Power results shown before application of correction multipliers

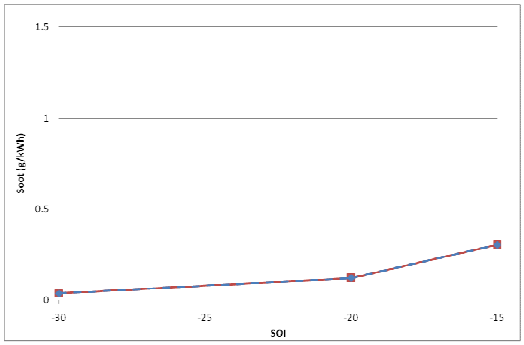

Figure 4.40: Soot versus SOI for 30% EGR, double injection; GT-Power results shown after application of correction multipliers

With soot for double injection cases, GT-Power made sizable over-prediction, as it did with the single injection cases. Due to the unlikeness in shape between the curves for laboratory and GT-Power data for soot, a single constant multiplier could not be applied to all SOI cases, but rather, a multiplier needed to be calculated for each SOI case by dividing

experimentally measured soot by GT-Power's prediction. The SOI case-specific multipliers are shown in Table 4.3.

Table 4.3: Soot correction multipliers versus SOI for double injection

pilot SOI	-30	-20	-15
multiplier	0.0298	0.0993	0.261

Later, when GT-Power was run with higher EGR conditions of 40%, 50%, and 60%, the same emissions multipliers calculated to correct 30% EGR cases for NOx, HC, and soot were used to correct GT-Power predictions for these higher EGR conditions.

Figures 4.41 through 4.46 as follow show how the GT-Power model's predictions for in-cylinder pressure compare with that recorded on the laboratory engine for the 0% EGR condition for single injection cases. Each figure shows results for a specific SOI.

**Note that the labeling scheme where a solid line represents GT-Power prediction and a dashed line represents laboratory results carries on through the remainder of Section 4.1. In addition, certain Section 4.1 plots for in-cylinder pressure also show a dotted line; this represents a second data set taken for laboratory results and is meant to glean insight into the variability that can be expected when taking in-cylinder pressure measurements.

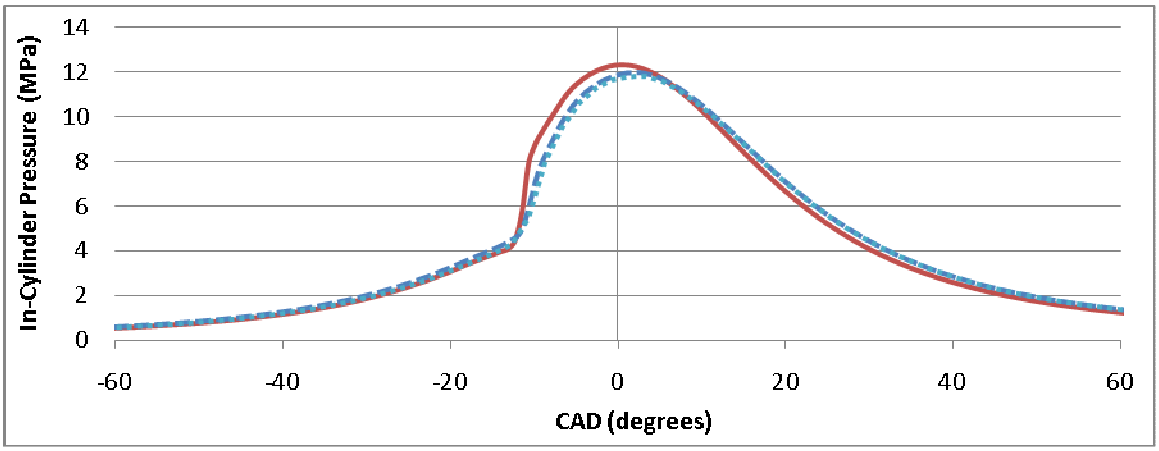

Figure 4.41: In-cylinder pressure versus crank angle degrees ATDC for 0% EGR, single injection at -20 degrees ATDC

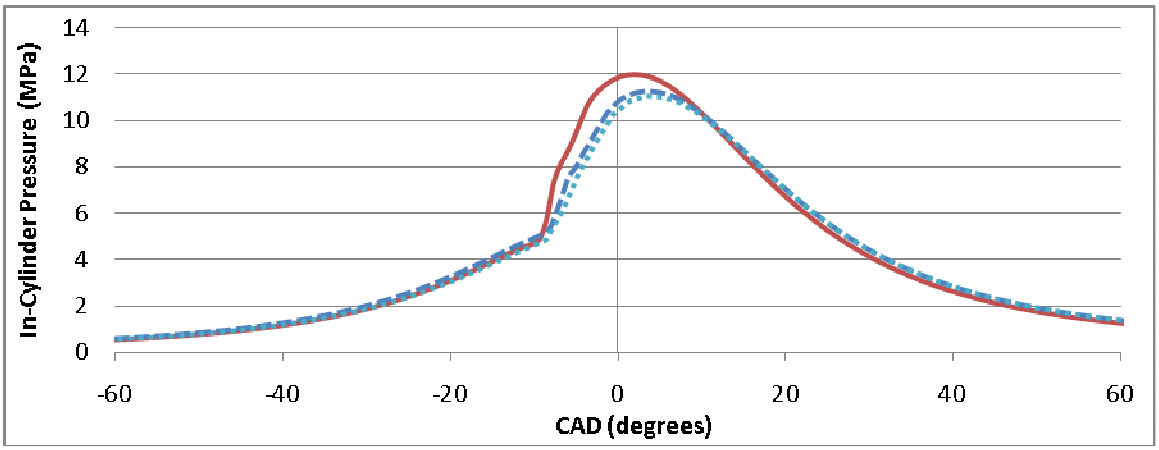

Figure 4.42: In-cylinder pressure versus crank angle degrees ATDC for 0% EGR, single injection at -15 degrees ATDC

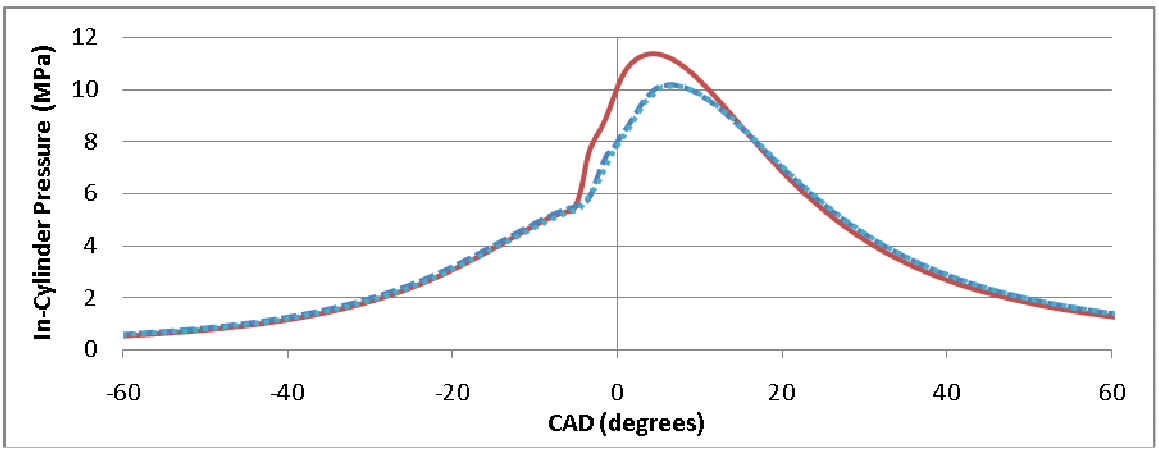

Figure 4.43: In-cylinder pressure versus crank angle degrees ATDC for 0% EGR, single injection at -10 degrees ATDC

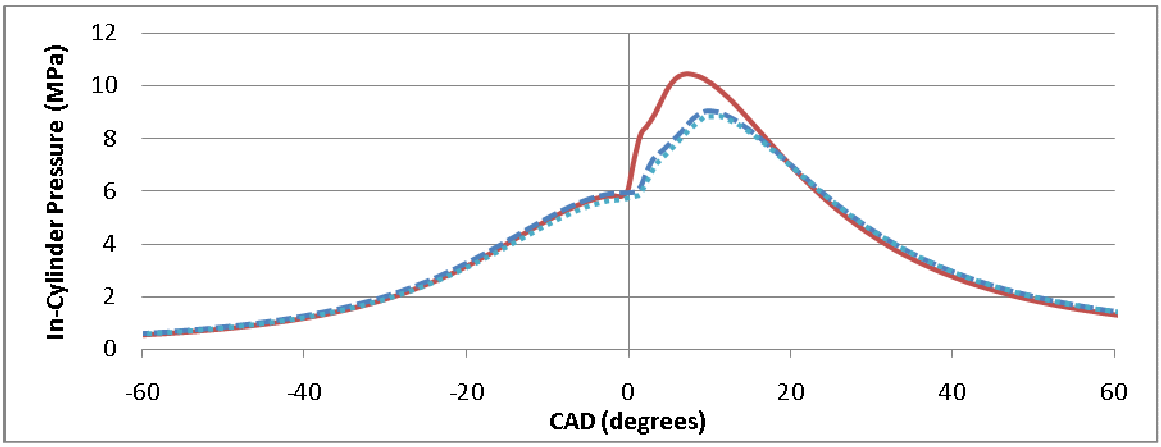

Figure 4.44: In-cylinder pressure versus crank angle degrees ATDC for 0% EGR, single injection at -5 degrees ATDC

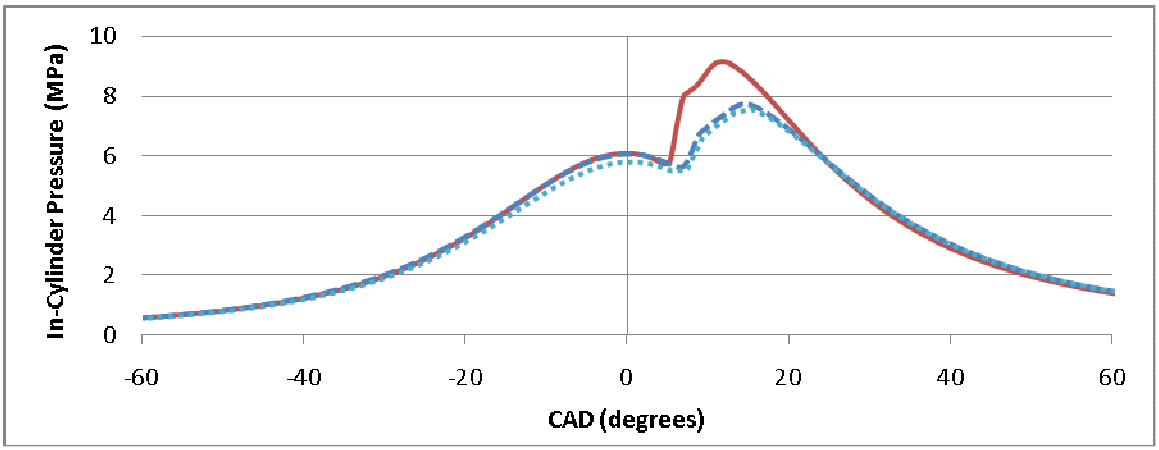

Figure 4.45: In-cylinder pressure versus crank angle degrees ATDC for 0% EGR, single injection at 0 degrees ATDC

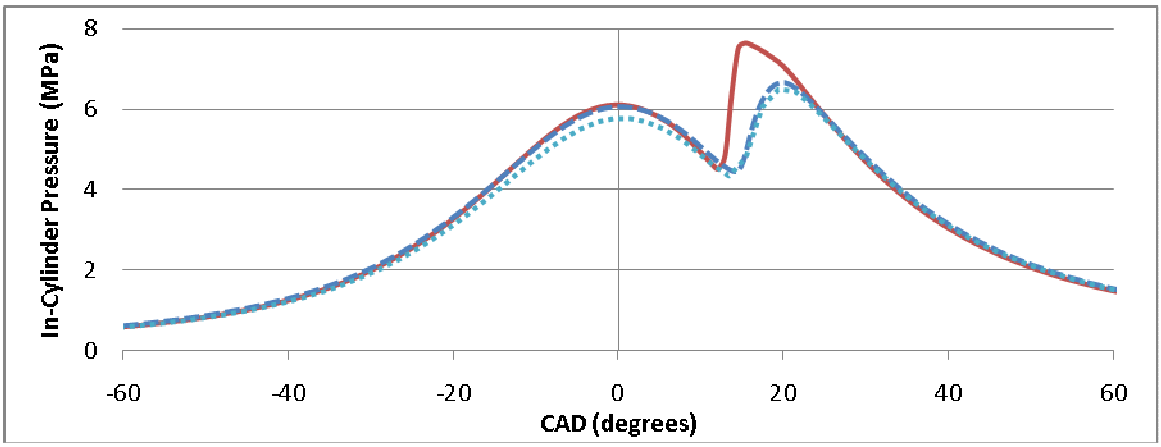

Figure 4.46: In-cylinder pressure versus crank angle degrees ATDC for 0% EGR, single injection at 5 degrees ATDC

For the most part, GT-Power proved itself to predict in-cylinder pressure reasonably well, but not without a few inaccuracies, among which included too early a prediction for start of combustion (SOC) timing. Granted, GT-Power enables input of a multiplier which instructs the program's simulation to delay SOC, but even when this was inputted, GT-Power's simulation still predicted too early an SOC. In any event, the GT-Power predictions illustrated in Figures 4.41 through 4.46 are based on program inputs which utilize such multipliers.

Additionally, GT-Power proved itself to over-predict rate of in-cylinder pressure rise immediately after SOC. It is suspected this may be attributed to the tendency of its zero-dimensional combustion model to oversimplify combustion. As such, this oversimplification may well have caused GT-Power to overly approximate the extent to which heat release occurs instantaneously. Moreover, it is suspected this oversimplification caused the simulation to model too high a combustion efficiency since GT-Power results predict too high of peak in in-cylinder pressures, and also, what appears to be too high of a $\int PdV$ value upon integration of its in-cylinder pressure curves.

It may be reasonable to hypothesize that the tendency of GT-Power to over-predict in-cylinder pressure rise immediately after SOC, and also, to over-predict combustion efficiency, caused GT-Power to inaccurately predict BSFC for certain SOI timings. For early SOI timings, specifically, those at -20, -15, and -10 degrees ATDC, GT-Power's under-prediction of ignition

delay and over-prediction of post-SOC in-cylinder pressure rise caused a greater fraction of the fuel's chemical energy to be liberated as the piston was ascending, thereby performing negative work on the power cycle so as to decrease brake torque and increase BSFC. Any gain in positive work realized through the over-prediction of combustion efficiency would have been offset by this negative work. For the cases of the late injection timings, specifically, those with SOI timings at 0 and 5 degrees ATDC, SOC did not occur until after TDC, so the over-prediction of in-cylinder pressure rise after SOC did not cause increased negative work to be performed. In effect, the gain in positive work done by the model's over-prediction of combustion efficiency would not have been offset, thereby causing GT-Power to over-predict brake torque and under-predict BSFC for these late injection cases.

All the while, the good level of agreement of TCD in-cylinder pressure between GT-Power and laboratory results for 0 and 5 degrees ATDC SOI cases suggested the GT-Power model was well capable of predicting accurate in-cylinder pressures for an engine being motored, and also, confirmed the GT-Power model accurately simulated compression within the cylinder.

Figures 4.47 through 4.50 as follow show how the GT-Power model's predictions for in-cylinder pressure compare with those recorded on the laboratory engine for the 0% EGR condition for double injection cases. Each figure shows results for a specific pilot SOI, the SOI of the main injection always being maintained at 5 degrees ATDC.

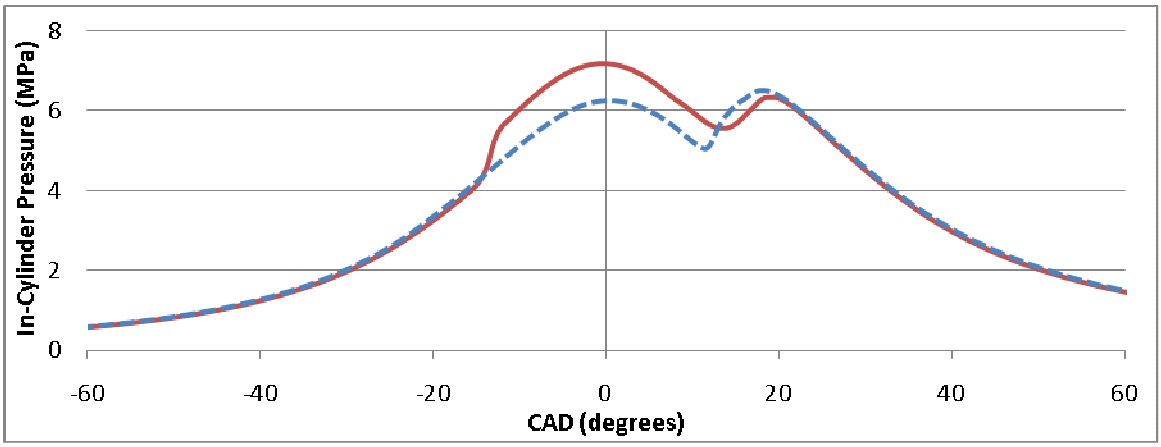

Figure 4.47: In-cylinder pressure versus crank angle degrees ATDC for 0% EGR, double injection pilot SOI at -40 Degrees ATDC

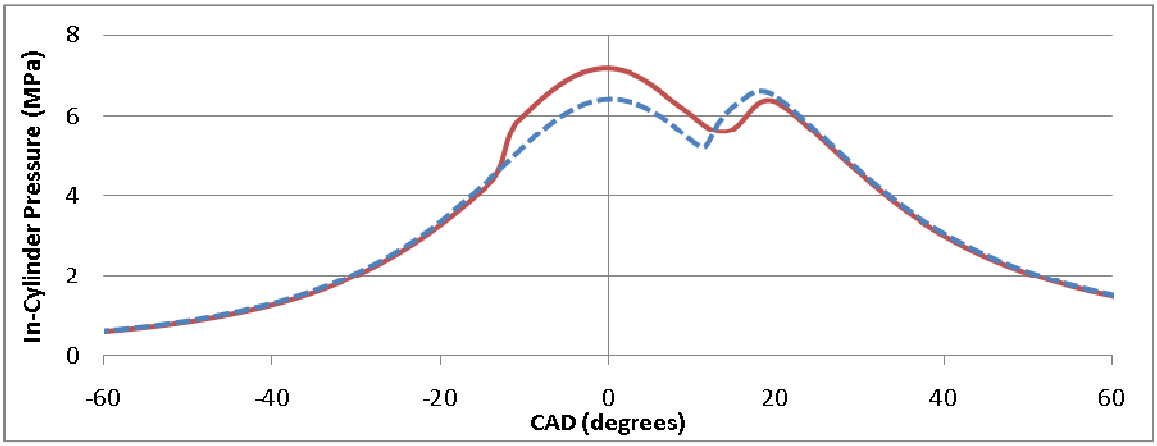

Figure 4.48: In-cylinder pressure versus crank angle degrees ATDC for 0% EGR, double injection pilot SOI at -30 Degrees ATDC

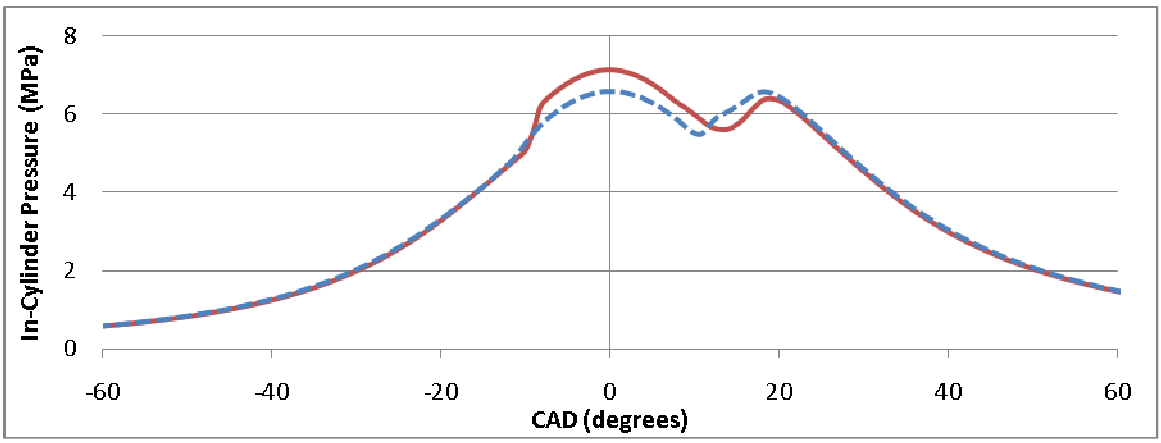

Figure 4.49: In-cylinder pressure versus crank angle degrees ATDC for 0% EGR, double injection pilot SOI at -20 Degrees ATDC

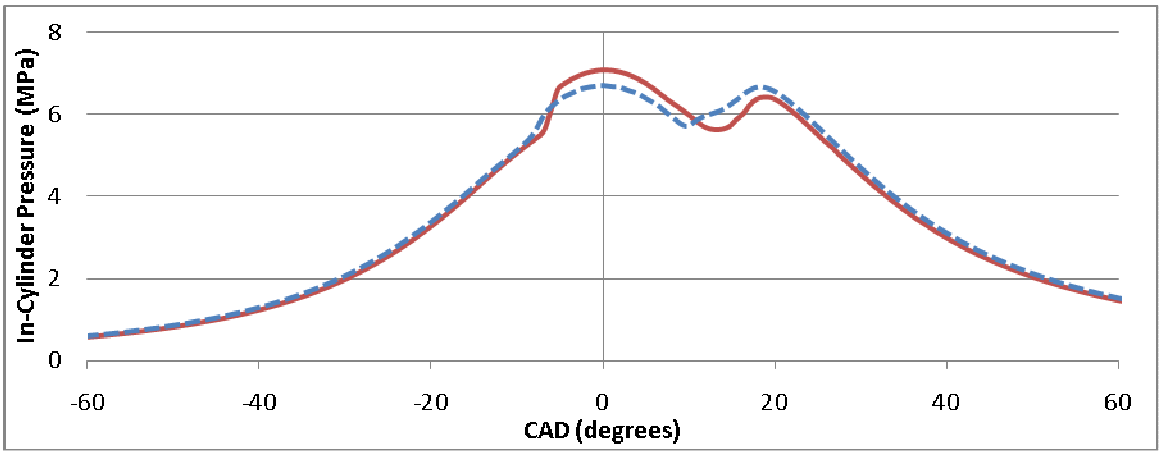

Figure 4.50: In-cylinder pressure versus crank angle degrees ATDC for 0% EGR, double injection pilot SOI at -15 Degrees ATDC

As with the 0% EGR single injection cases, the 0% EGR double injection cases found GT-Power predicting too high of peak in in-cylinder pressures.

Figures 4.51 through 4.55 as follow show how the GT-Power model's predictions for in-cylinder pressure compare with those recorded on the laboratory engine for the 30% EGR condition for single injection cases. Each figure shows results for a specific SOI.

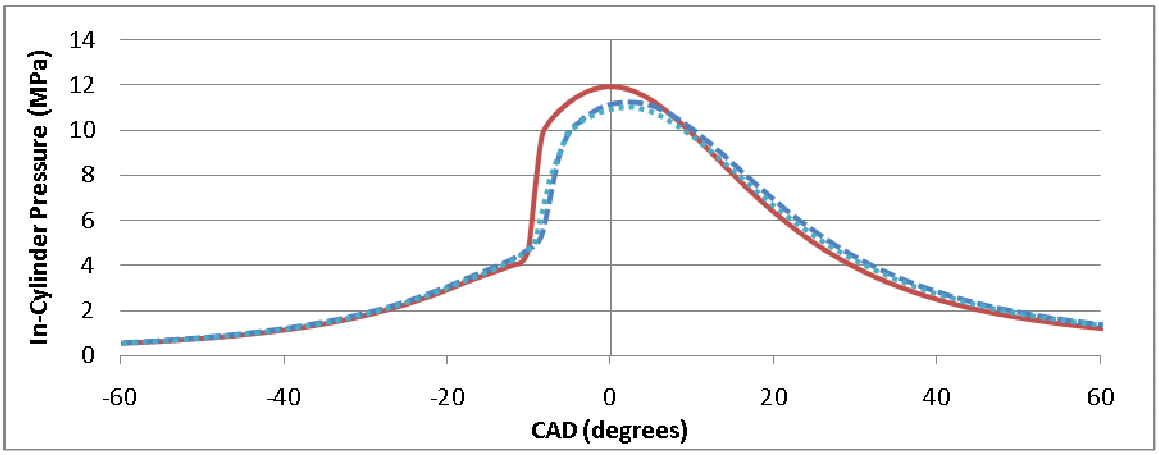

Figure 4.51: In-cylinder pressure versus crank angle degrees ATDC for 30% EGR, single injection at -20 degrees ATDC

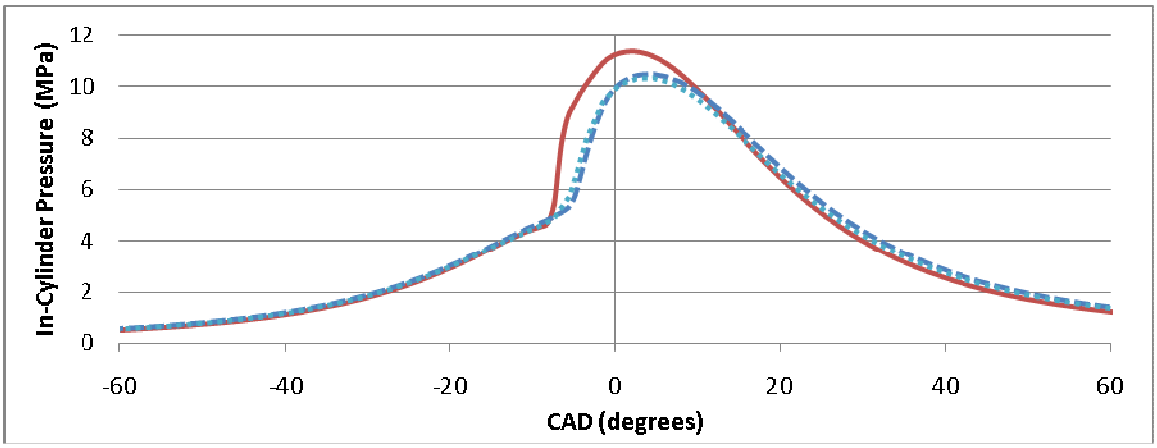

Figure 4.52: In-cylinder pressure versus crank angle degrees ATDC for 30% EGR, single injection at -15 degrees ATDC

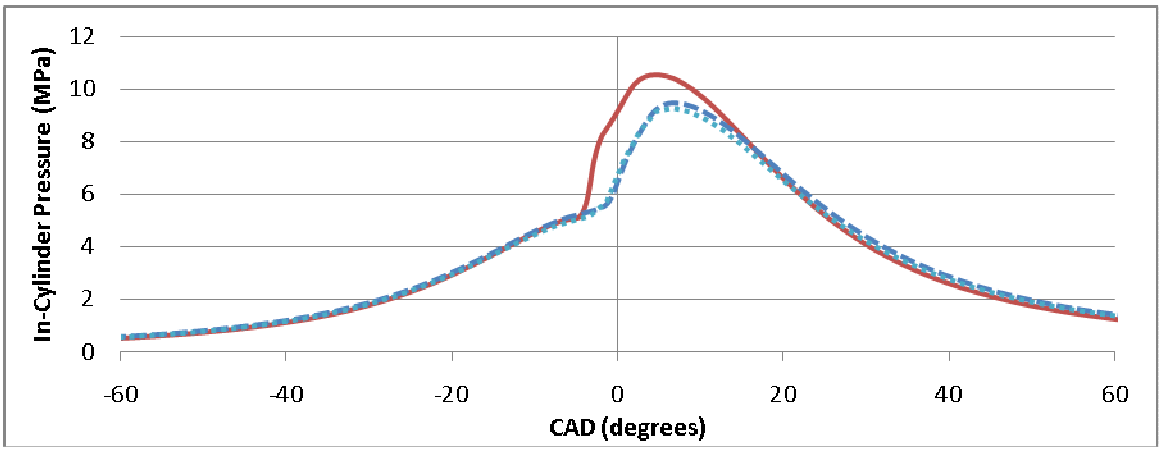

Figure 4.53: In-cylinder pressure versus crank angle degrees ATDC for 30% EGR, single injection at -10 degrees ATDC

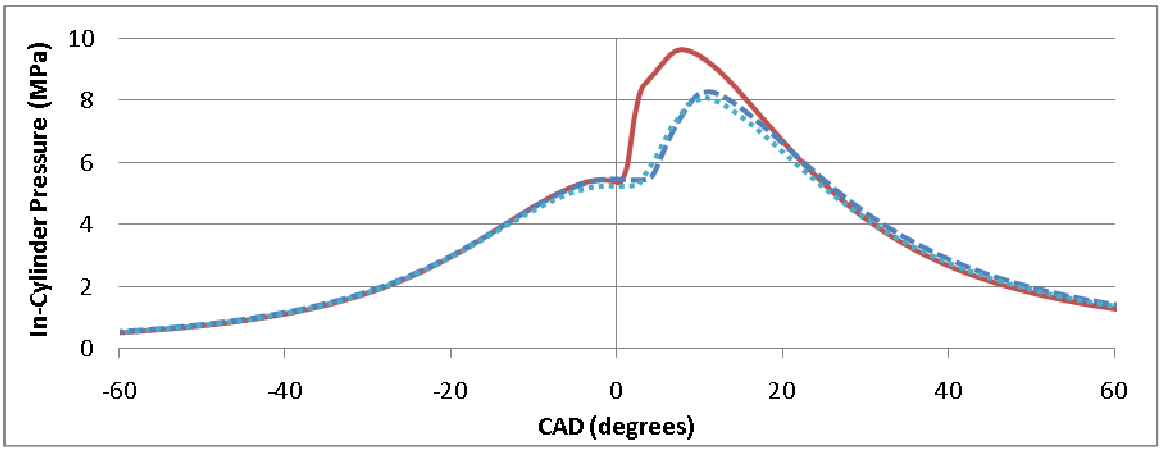

Figure 4.54: In-cylinder pressure versus crank angle degrees ATDC for 30% EGR, single injection at -5 degrees ATDC

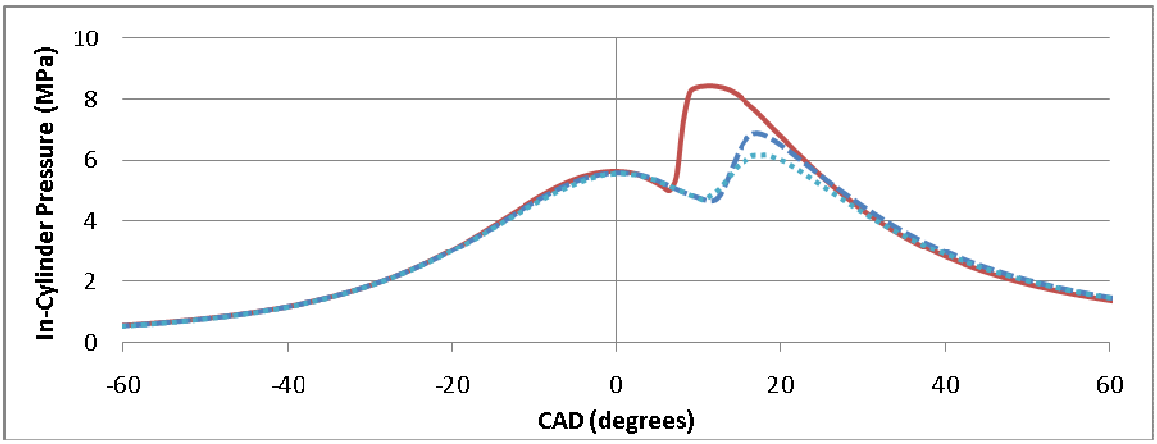

Figure 4.55: In-cylinder pressure versus crank angle degrees ATDC for 30% EGR, single injection at 0 degrees ATDC

As was observed with the 0% EGR single injection cases, GT-Power predicted too early an SOC and too high of peak in in-cylinder pressure for the 30% EGR single injection cases. For the early injection cases of SOI at -20, -15, and -10 degrees ATDC, GT-Power's early predition of SOC is suspected to have increased negative work performed during the power cycle, thereby increasing BSFC and mimicing respective 0% EGR cases in this sense. Moreover, GT-Power's likely over-predicion of combustion efficiency is

hypothesized to have caused it to under-predict BSFC for the late injection case of SOI at 0 degrees ATDC, again mimicing the respective 0% EGR case.

Figures 4.56 through 4.58 as follow show how the GT-Power model's predictions for in-cylinder pressure compare with that recorded on the laboratory engine for the 30% EGR condition for double injection cases. Each figure shows results for a specific pilot SOI.

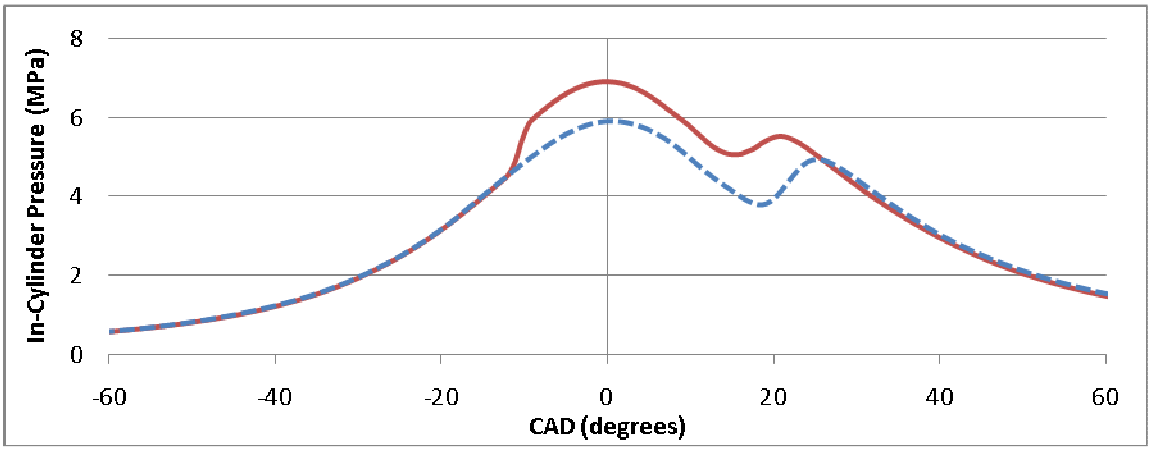

Figure 4.56: In-cylinder pressure versus crank angle degrees ATDC for 30% EGR, double injection pilot SOI at -30 degrees ATDC

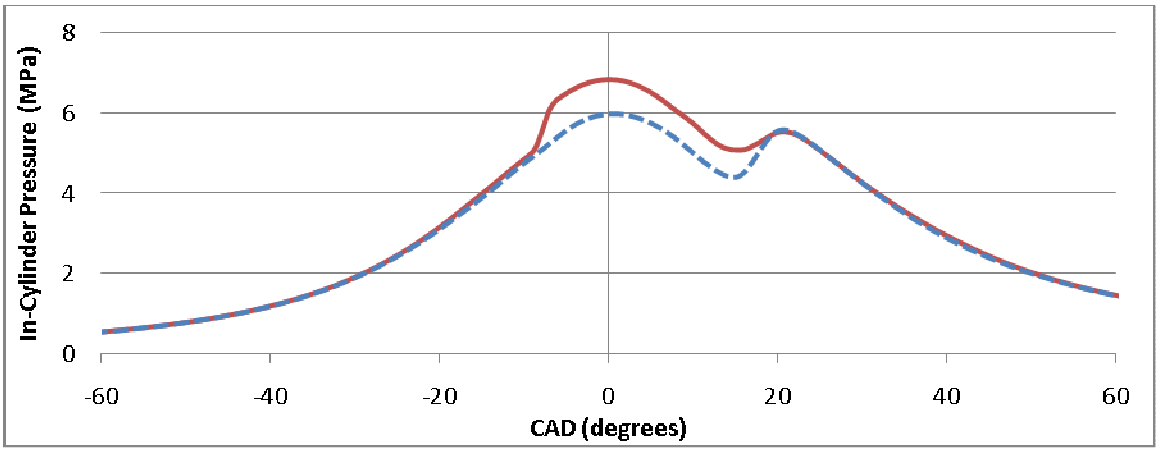

Figure 4.57: In-cylinder pressure versus crank angle degrees ATDC for 30% EGR, double injection pilot SOI at -20 degrees ATDC

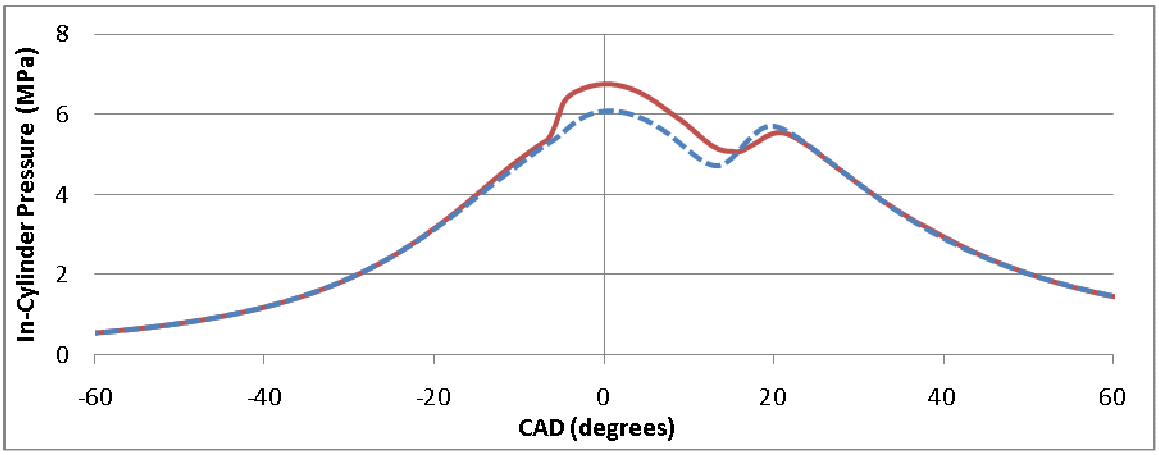

Figure 4.58: In-cylinder pressure versus crank angle degrees ATDC for 30% EGR, double injection pilot SOI at -15 degrees ATDC

4.2 High EGR Modeling

Once adjustments made to the GT-Power model enabled it to accurately predict the laboratory engine's fuel consumption, torque, and in-cylinder pressure for both 0% and 30% EGR conditions, it was decided to increase the EGR level simulated by the model, and then observe how its predictions for 40%, 50%, and 60% EGR compare to those for 30%. Unlike the 0% and 30% EGR conditions, the high EGR conditions of 40% and above were not tested on the laboratory engine. Rather, it was assumed that the agreement between the performance predicted by the model and that recorded on the laboratory engine for both 0% and 30% EGR conditions would suffice to validate the model's predictions for high EGR test conditions.

4.2.1 Single Injection Cases

First, the GT-Power model was run with the single injection operation condition for the EGR levels of 40%, 50%, and 60%. As EGR was increased, so did the model's predictions for ignition delay, a prediction in full agreement with trends known to occur in laboratory setups. As such, late injection timing tended to introduce misfiring into high EGR runs. Specifically, the 50% EGR condition proved incapable of sustaining combustion for the 0 degrees ATDC SOI case, and the 60% EGR condition for both the -5 and 0 degrees ATDC SOI cases. For this reason, this study will not consider GT-Power results for the single injection cases of 50% EGR / 0 degrees ATDC SOI, 60% EGR / 0 degrees ATDC SOI, and 60% EGR / -5 degrees ATDC SOI.

Figures 4.59 through 4.61 show the model's predictions for the engine's dependent operation conditions of intake manifold temperature, intake manifold pressure, and air-to-fuel ratio, all for high EGR cases using single injection. As a baseline reference, these figures also show the model's 30% EGR predictions as shown in Section 4.1.

**Note the labeling convention for Figures 4.59 through 4.79, which continues for all of Section 4.2, is as follows: 30% EGR cases are represented by a solid line; 40% EGR cases are represented by a line with short dashes; 50% EGR cases are represented by a dotted line, and 60% EGR cases are represented by a line with long dashes.

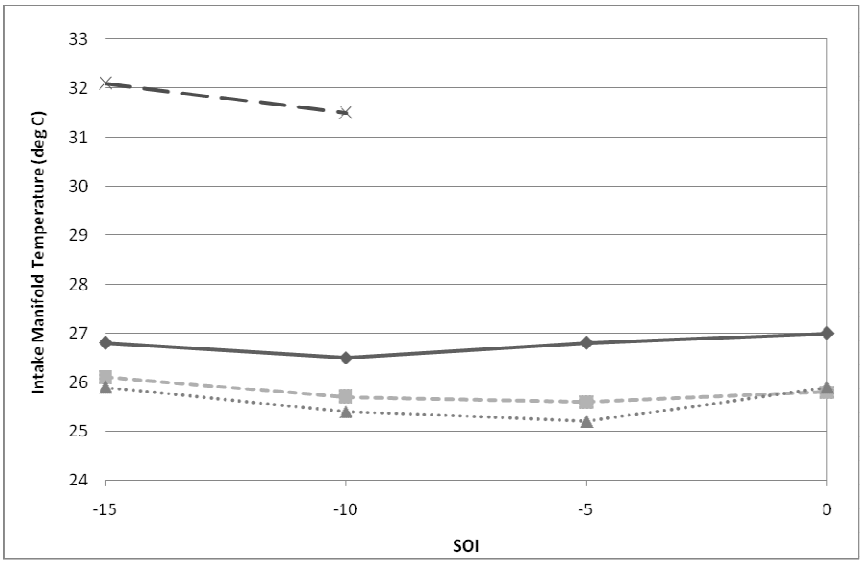

Figure 4.59: GT-Power intake manifold temperature versus SOI for 30% (solid line), 40% (line with short dashes), 50% (dotted line), 60% EGR (line with long dashes); single injection

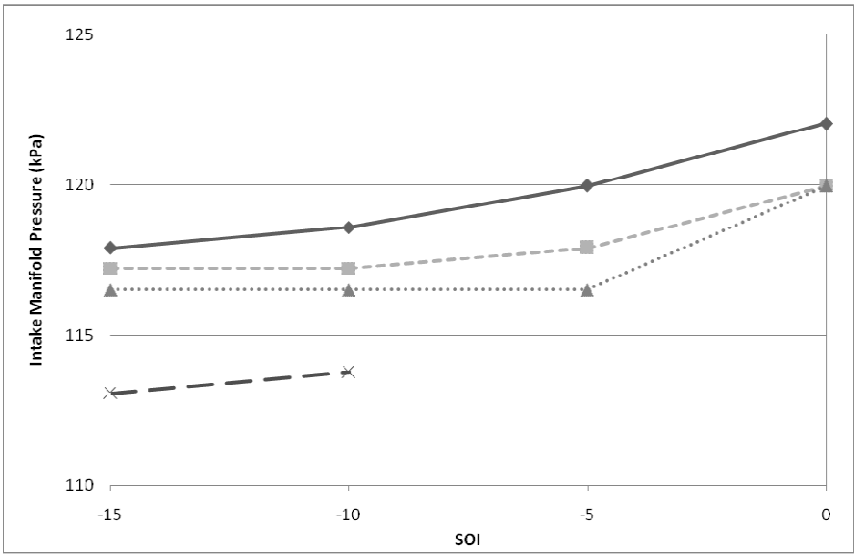

Figure 4.60: GT-Power intake manifold pressure versus SOI for 30% (solid line), 40% (line with short dashes), 50% (dotted line), 60% EGR (line with long dashes); single injection

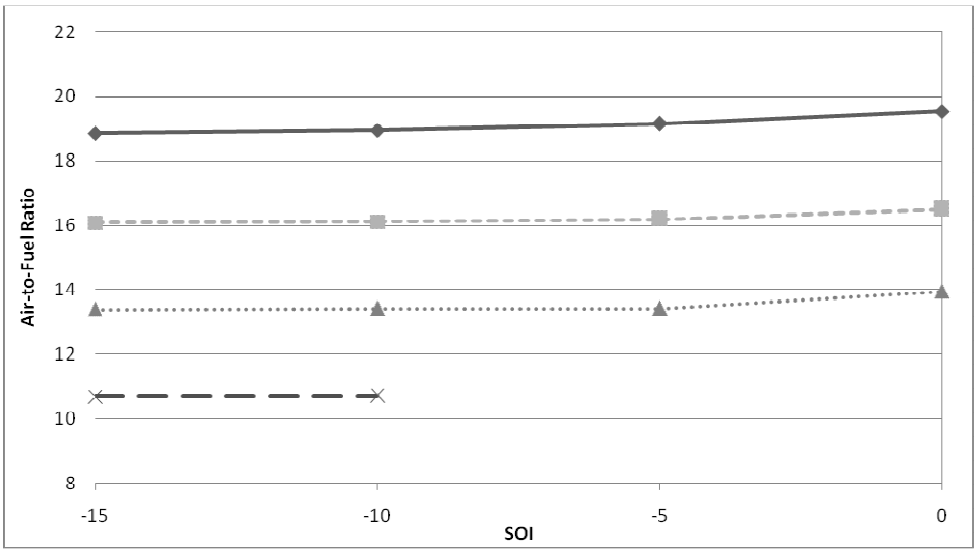

Figure 4.61: GT-Power air-to-fuel ratio versus SOI for 30% (solid line), 40% (line with short dashes), 50% (dotted line), 60% EGR (line with long dashes); single injection

As expected, for higher EGR rates, air-to-fuel ratio decreased. In fact, for cases of 50% and 60% EGR, air-to-fuel ratio dropped below stoichiometric for diesel, thereby ensuring a greater level of incomplete combustion. It is suspected that for the 60% EGR case, the increase in incomplete combustion amply decreased thermal energy in the exhaust gases sent to the turbocharger turbine, thereby adversely impacting turbocharger performance. This is evidenced by Figure 4.60 which shows that the 60% EGR case produced the lowest intake manifold pressure.

Figure 4.62 shows the model's predictions for the engine's BSFC for high EGR cases using single injection. Again, the model's predictions for the 30% EGR / single injection condition are shown as baseline reference.

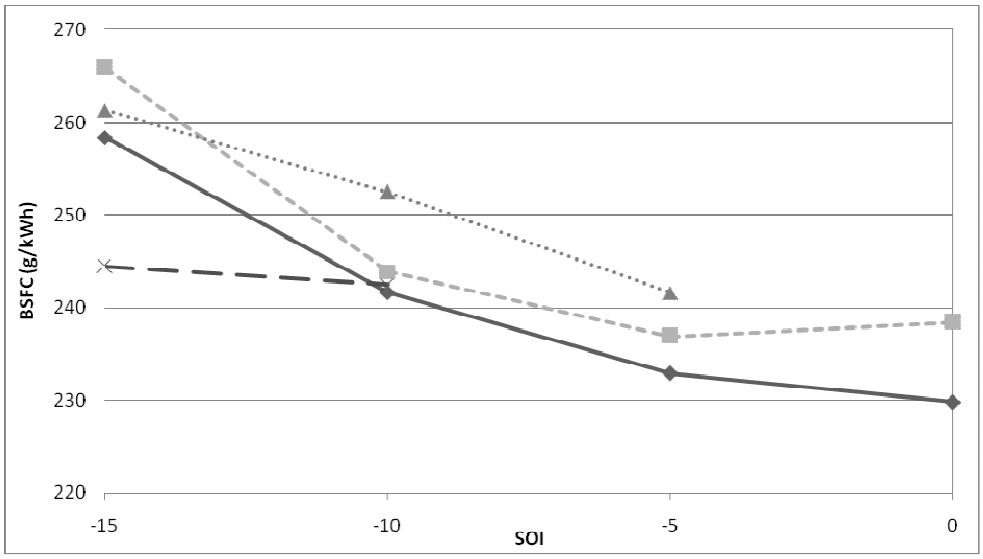

Figure 4.62: GT-Power BSFC versus SOI for 30% (solid line), 40% (line with short dashes), 50% (dotted line), 60% EGR (line with long dashes); single injection

As expected, the model predicted higher BSFC for higher levels of EGR, except for the 60% EGR condition, where operation at this EGR level managed to predict the lowest BSFC for the -15 degrees ATDC SOI condition. This may be attributed to the tendency of high EGR to increase ignition delay, which (especially for early injection timings) ensured that a greater fraction of the combustion heat release performed work after TDC, thereby lowering negative work performed and increasing brake torque.

Among all cases utilizing EGR, including double injection cases discussed later in this section, the case of 30% EGR / single injection SOI at 0 degrees ATDC produced the lowest BSFC, 229.3 g/kWh. As is shown in GT-Power's emissions level predictions next, this case also produced a low soot level, in fact, the best among the single injection cases running EGR.

However, for this case, GT-Power predicted a NOx level of 1.07 g/kWh, which was above the Tier 4 required limit of 0.40 g/kWh.

Figures 4.63 through 4.65 show GT-Power's predictions for NOx, HC, and soot, for high EGR cases using single injection. Predictions displayed below do not represent results directly outputted by GT-Power, but rather, take into account the correction multipliers discussed in Section 4.1. As a reference, these figures also show GT-Power's multiplier-corrected predictions for 30% EGR.

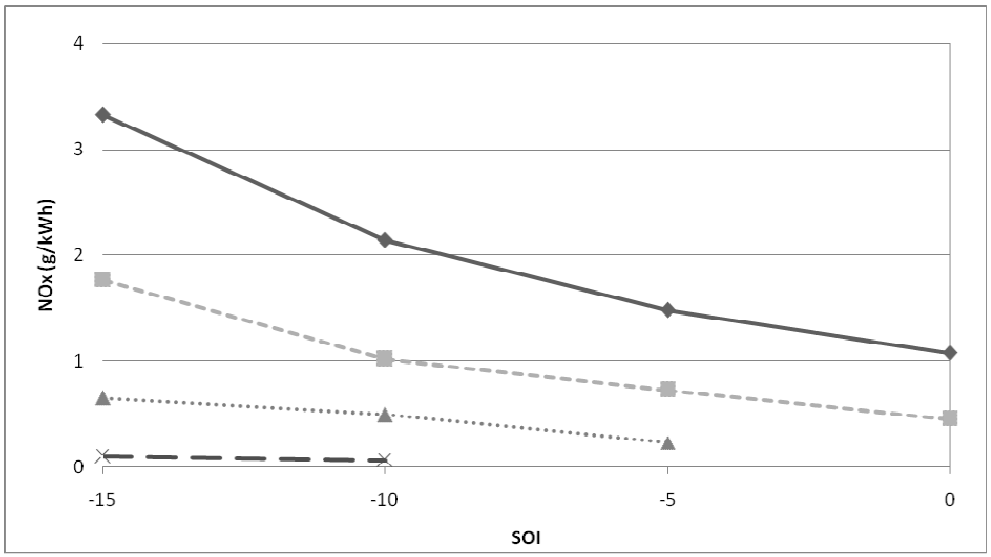

Figure 4.63: GT-Power NOx versus SOI for 30% (solid line), 40% (line with short dashes), 50% (dotted line), 60% EGR (line with long dashes); single injection

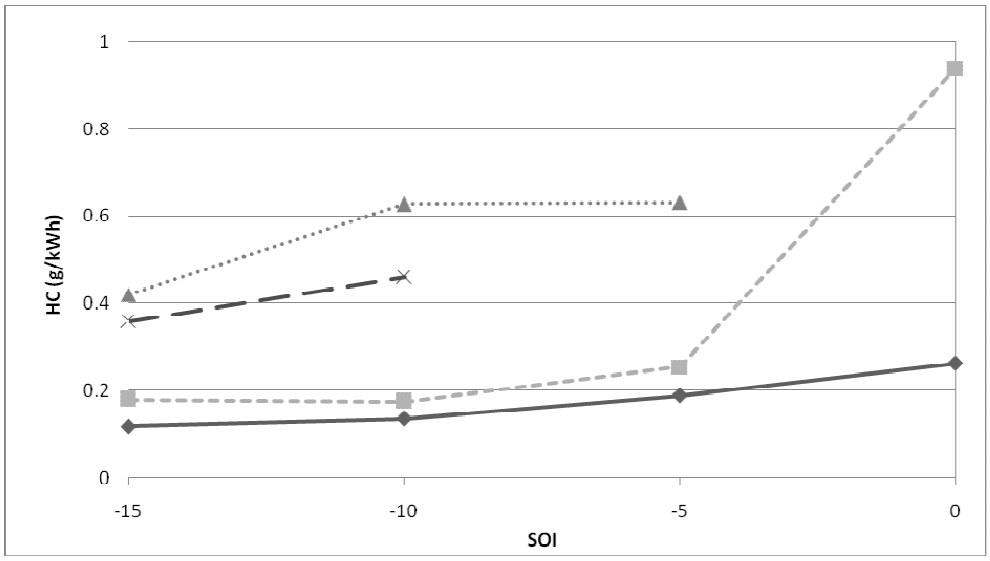

Figure 4.64: GT-Power HC versus SOI for 30% (solid line), 40% (line with short dashes), 50% (dotted line), 60% EGR (line with long dashes); single injection

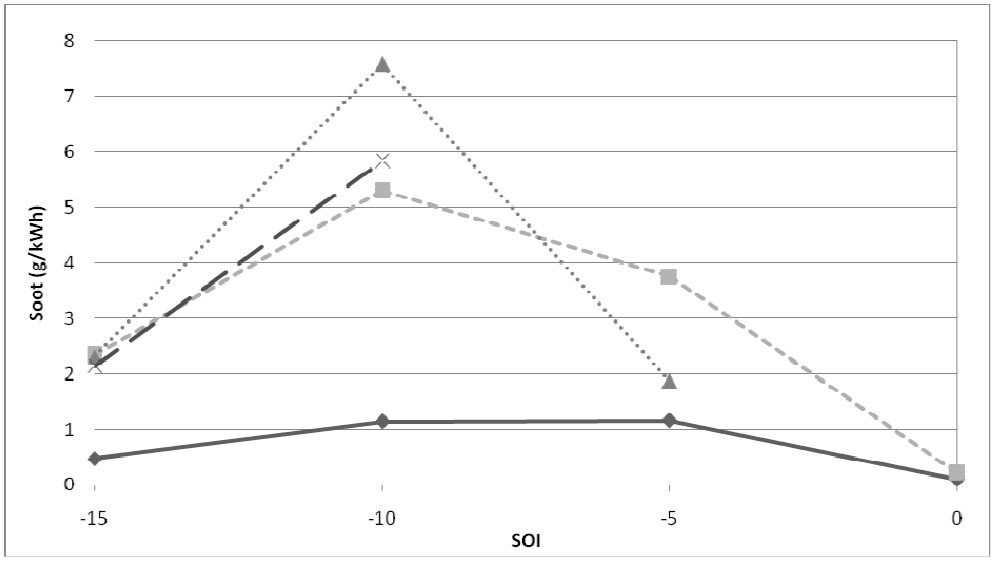

Figure 4.65: GT-Power soot versus SOI for 30% (solid line), 40% (line with short dashes), 50% (dotted line), 60% EGR (line with long dashes); single injection

GT-Power's predictions for NOx versus EGR level agreed well with what can be expected to be observed experimentally, where increased EGR progessively lowers NOx. It is also worth noting that only the 60% EGR

condition consistently reached NOx levels below that of the Tier 4 standard of 0.40 g/kWh; the 50% EGR condition managed to do so for its latest injection case, SOI -5 degrees ATDC. No other cases met the Tier 4 standard for NOx, even though the 40% EGR condition nearly reached the Tier 4 limit for its latest injection timing of 0 degrees ATDC, achieving 0.45 g/kWh NOx.

Conversely, only the 30% EGR condition came close to meeting the Tier 4 standard of 0.02 g/kWh for soot, and only for the 0 degrees ATDC SOI condition in which GT-Power predicted 0.10 g/kWh soot. In any event, these trends provide insight into why it is presently common practice in industry to fit high EGR diesel engines with soot after-treatment devices such as diesel particulate filtration (DPF) and diesel oxidation catalyst (DOC).

GT-Power's predictions for emissions illustrate how meeting Tier 4 standards for both NOx and soot will likely require some type of after-treatment. Laboratory results show that the actual 4.5L engine was able to produce less than the 0.02 g/kWh soot emissions standard when running 0% EGR, but this was achieved at the cost of well exceeding Tier 4 NOx standards. As such, the addition of NOx after-treatment such as urea injection would be needed to make the engine Tier 4 compliant if running 0% EGR. Increasing EGR level on the laboratory engine of course decreased NOx, but increased the likelihood the engine would need soot after-treatment to achieve emissions compliance. Note these constaints apply to engines employing a single injection and don't necessarily apply to double injections.

Figures 4.66 through 4.69 show the model's predictions for in-cylinder pressure for high EGR cases using single injection at specified SOI.

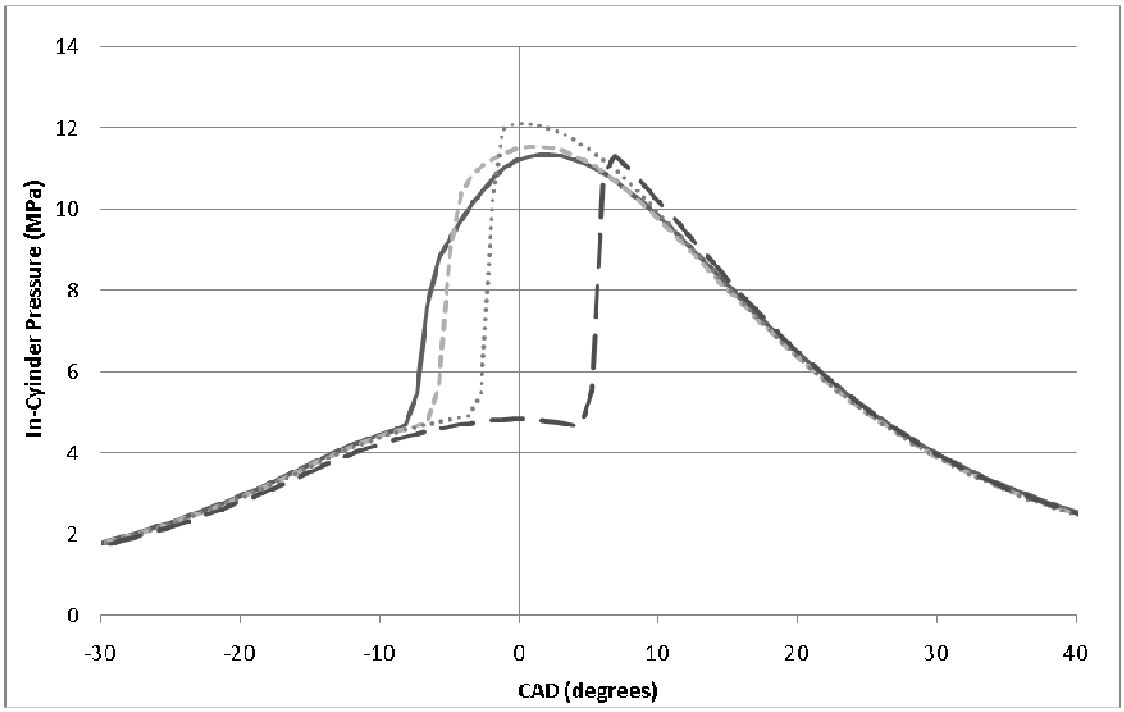

Figure 4.66: In-cylinder pressure versus crank angle degrees ATDC for 30% (solid line), 40% (line with short dashes), 50% (dotted line), 60% EGR (line with long dashes); single injection at -15 degrees ATDC

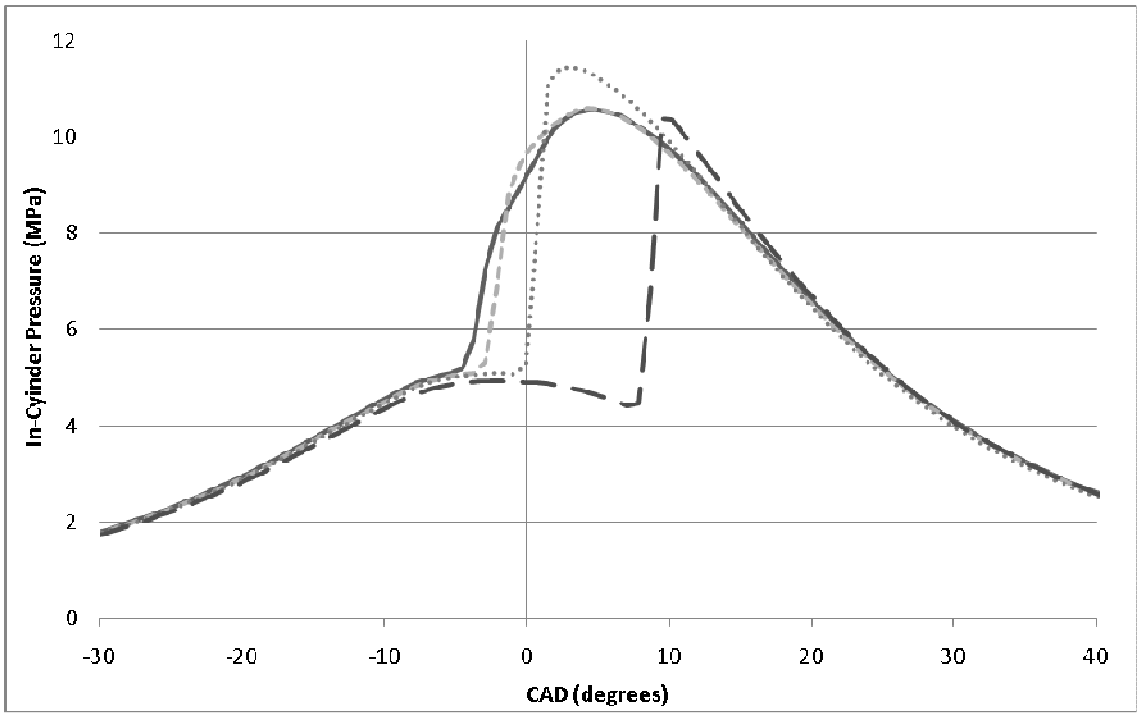

Figure 4.67: In-cylinder pressure versus crank angle degrees ATDC for 30% (solid line), 40% (line with short dashes), 50% (dotted line), 60% EGR (line with long dashes); single injection at -10 degrees ATDC

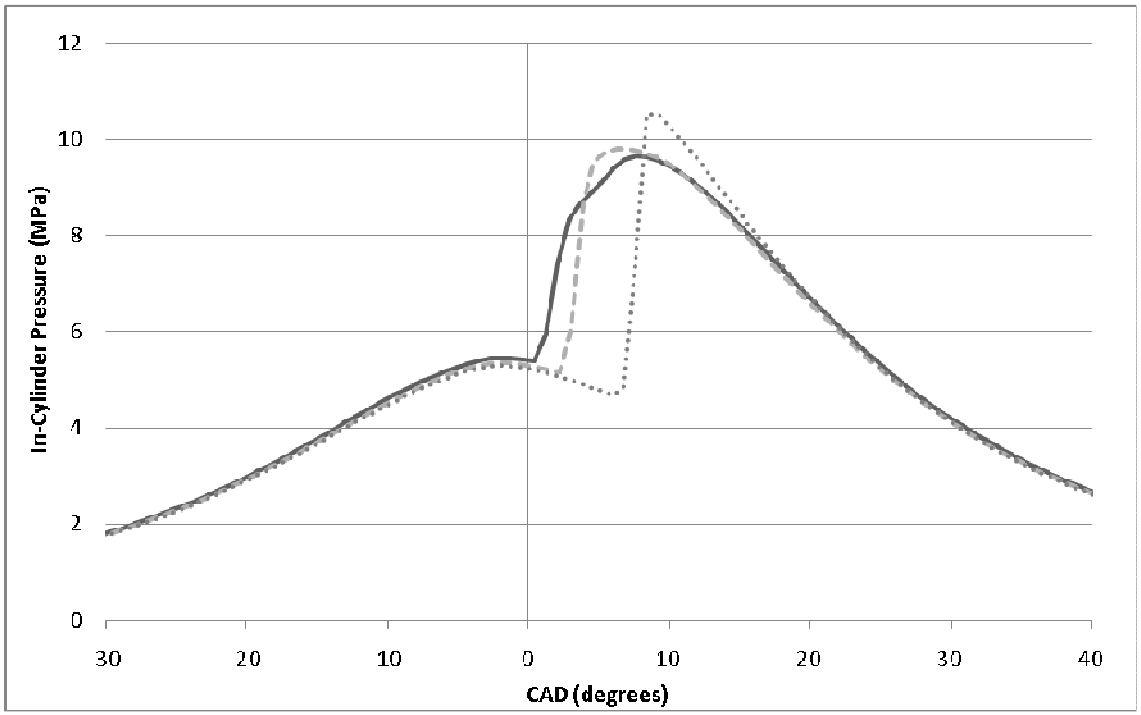

Figure 4.68: In-cylinder pressure versus crank angle degrees ATDC for 30% (solid line), 40% (line with short dashes), 50% EGR (dotted line); single injection at -5 degrees ATDC

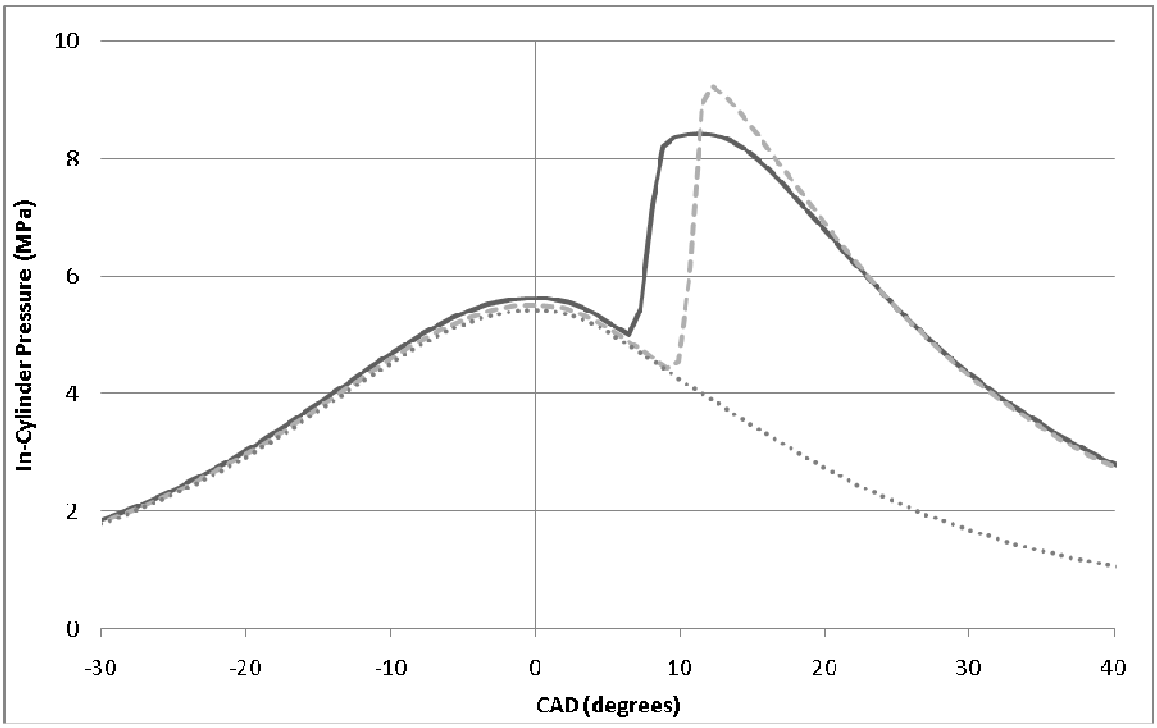

Figure 4.69: In-cylinder pressure versus crank angle degrees ATDC for 30% (solid line), 40% (line with short dashes), 50% EGR (dotted line); single injection at 0 degrees ATDC

As was expected, higher EGR levels increased ignition delay, so much so, in fact, that late injection with SOI 0 degrees ATDC was unable to produce combustion for both 50% and 60% EGR conditions; SOI -5 degrees ATDC was unable to produce combustion for the 60% EGR condition. Moreover, as high EGR levels delayed SOC timing, they also increased the fraction of premixed (as opposed to diffusion) combustion, and this is evidenced by the higher rate of in-cylinder pressure rise after SOC for higher EGR cases. Since GT-Power predicted increasingly lower NOx levels for increased EGR, it may be concluded that the increase in NOx usually generated by increased heat release rate was not enough to offset the decrease in NOx provided by the greater heat capacity of the EGR gases.

4.2.2 Double Injection Cases

Next, the GT-Power model was run with double injection operation conditions for 40%, 50%, and 60% EGR. Even though increasing EGR conditions proved to increase ignition delay for the single injection condition, no double injection test conditions produced misfiring as observed for the high EGR cases employing a single, late injection. Granted, each double injection employed a very late main injection, i.e., 5 degrees ATDC, but the pilot injection enabled a fraction of total fuel injected to be heated sufficiently to commence combustion, and this ignited the remainder of the fuel which was then injected at 5 degrees ATDC. As such, each double injection pilot SOI of -30, -20, and -15 degrees ATDC proved able to sustain combustion for even the highest EGR level of 60%.

Figures 4.70 through 4.72 show the model's predictions for the engine's dependent operation conditions of intake manifold temperature, intake manifold pressure, and air-to-fuel ratio, all for high EGR cases using double injection. As a reference, these figures also show GT-Power's 30% EGR predictions.

**Note that figures which identify SOI for double injections refer to the pilot injection SOI, since the main injection for all double injections is fixed at 5 degrees ATDC.

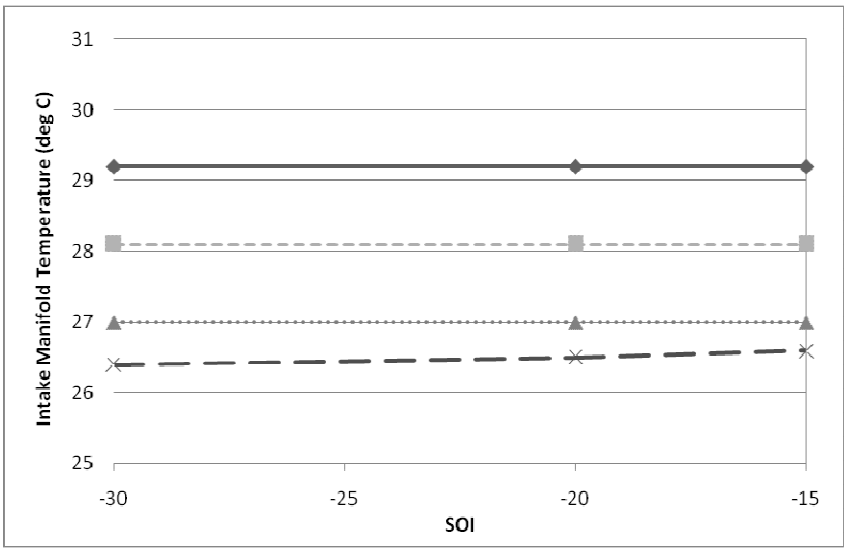

Figure 4.70: GT-Power intake manifold temperature versus SOI for 30% (solid line), 40% (line with short dashes), 50% (dotted line), 60% EGR (line with long dashes); double injection

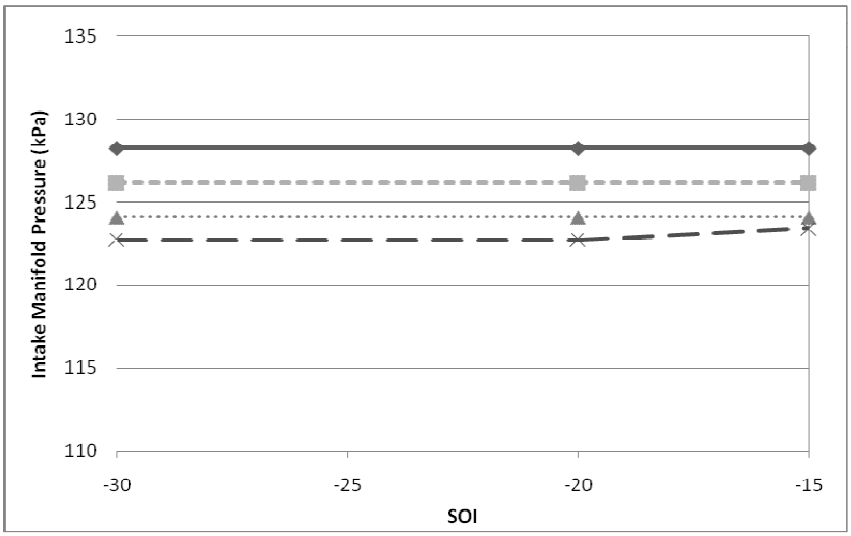

Figure 4.71: GT-Power intake manifold pressure versus SOI for 30% (solid line), 40% (line with short dashes), 50% (dotted line), 60% EGR (line with long dashes); double injection

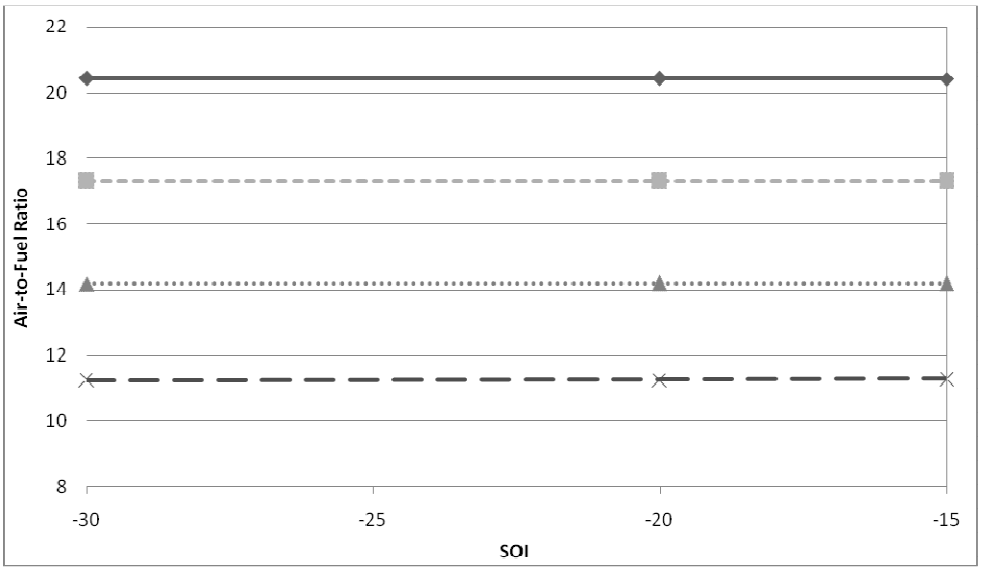

Figure 4.72: GT-Power air-to-fuel ratio versus SOI for 30% (solid line), 40% (line with short dashes), 50% (dotted line), 60% EGR (line with long dashes); double injection

As is consistent with expectation, increased levels of EGR for the double injection condition caused both intake manifold pressure and air-to-fuel ratio to drop

Figure 4.73 shows the model's predictions for the engine's BSFC for high EGR cases using double injection.

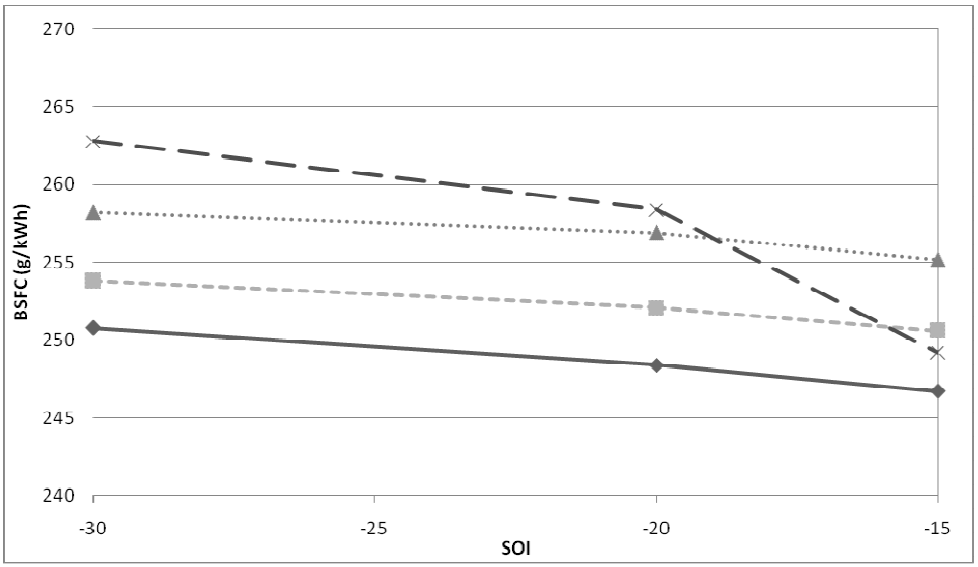

Figure 4.73: GT-Power BSFC versus SOI for 30% (solid line), 40% (line with short dashes), 50% (dotted line), 60% EGR (line with long dashes); double injection

With exception to the 60% EGR double injection case using pilot SOI -15 degrees ATDC, Figure 4.73 consistently shows that GT-Power predicted higher BSFC for cases running higher EGR levels. This can perhaps be explained, in part, to the increase in incomplete combustion caused by higher EGR rates which displace fresh air with recirculated exhaust gases and effectually decrease air-to-fuel ratio, below stoichiometric for the 50% and 60% EGR conditions, as shown previously in Figure 4.72.

Figures 4.74 through 4.76 show the model's predictions for NOx, HC, and soot, for high EGR cases using double injections. As a reference, these figures also show the model's 30% EGR predictions as first shown in the previous section.

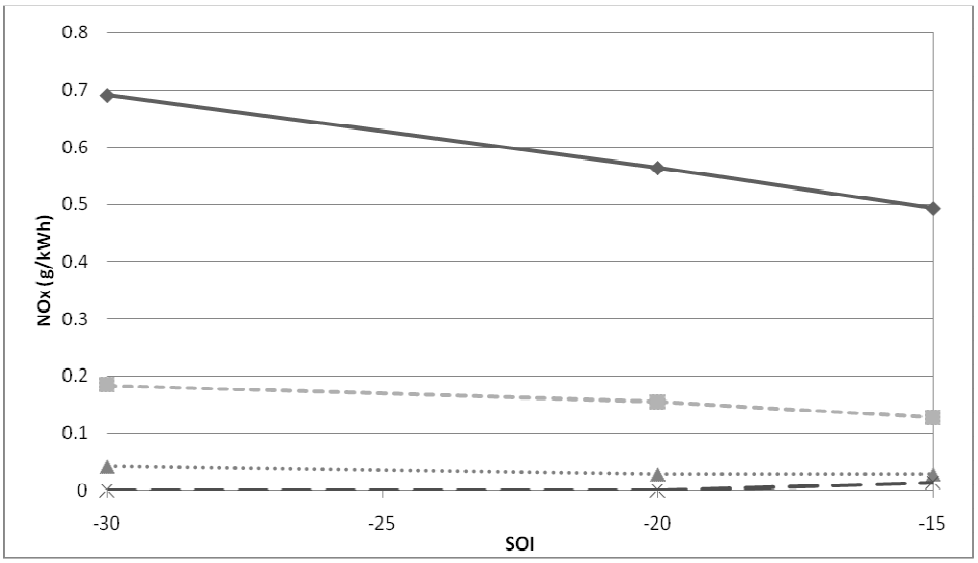

Figure 4.74: GT-Power NOx versus SOI for 30% (solid line), 40% (line with short dashes), 50% (dotted line), 60% EGR (line with long dashes); double injection

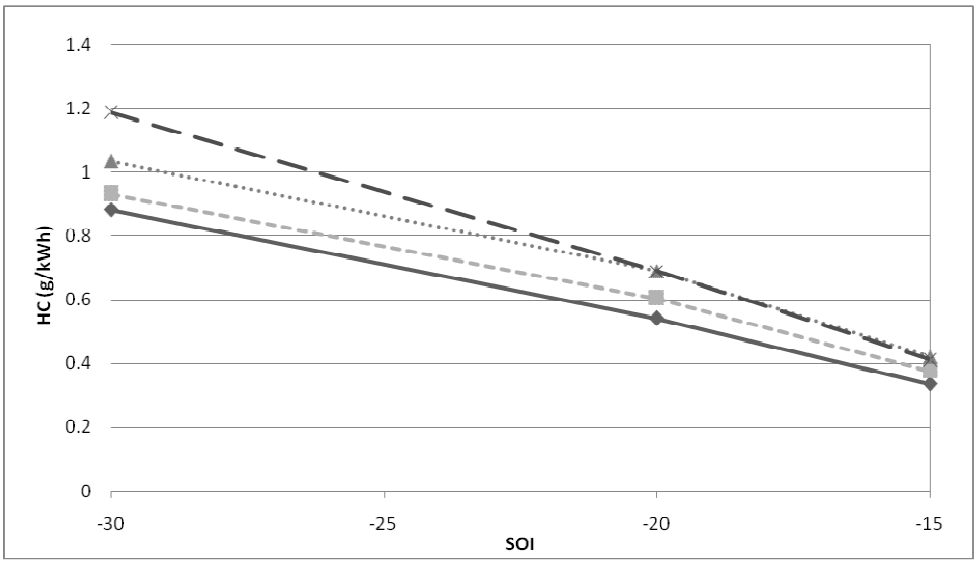

Figure 4.75: GT-Power HC versus SOI for 30% (solid line), 40% (line with short dashes), 50% (dotted line), 60% EGR (line with long dashes); double injection

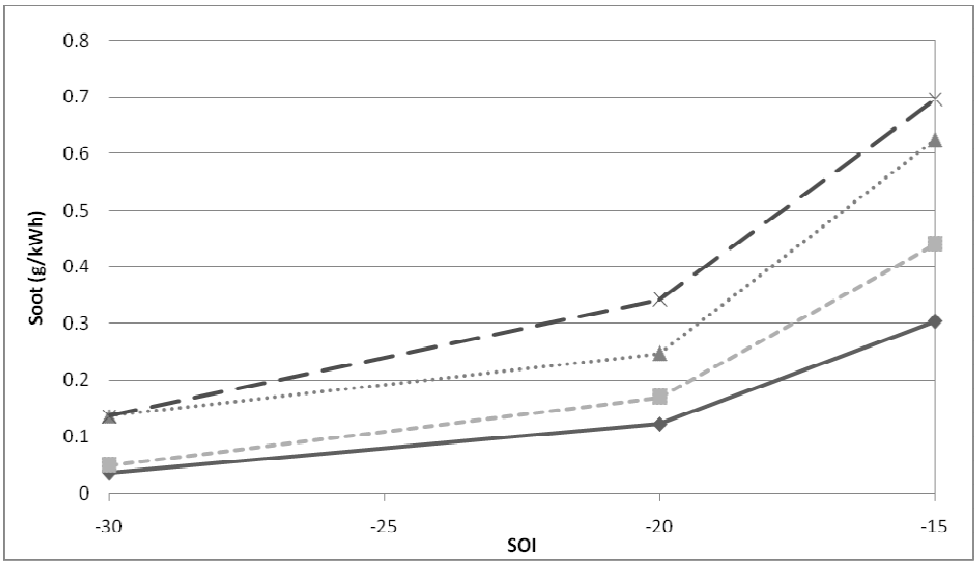

Figure 4.76: GT-Power soot versus SOI for 30% (solid line), 40% (line with short dashes), 50% (dotted line), 60% EGR (line with long dashes); double injection

Figures 4.74 through 4.76 show that GT-Power predicted trends of emissions levels versus EGR percentages which were consistent with those expected, that is, NOx decreased with increased EGR, and both soot and HC increased.

These figures show one of the attractive features of double injection fuel delivery coupled with high EGR: it manages to produce low emissions levels for both NOx and soot. NOx is low for the primary reason that high EGR levels are employed, whereas soot is low for the primary reason that double injection unsually enables a greater degree of premixed combustion to take place.

Among all cases run using GT-Power, the case using 40% EGR and double injection with pilot SOI -30 degrees ATDC proved the most attractive in terms of its total emissions. Not only did this case achieve a NOx level of

0.18 g/kWh, less than half that of the Tier 4 required limit of 0.40 g/kWh, but also achieved a low soot level of 0.05 g/kWh, not far above the Tier 4 required limit of 0.02 g/kWh. While still not able to meet Tier 4 requirements for both NOx and soot emissions, this case could allow the engine to run without NOx after-treatment while using only miminal soot after-treatment. In any event, as with all double injection cases, these low emission levels were achieved at the cost of increased BSFC, which was 254 g/kWh for the case of 40% EGR with double injection pilot SOI -30 degrees ATDC, as shown in Figure 4.73. In comparison, the best BSFC predicted by GT-Power among all cases was 223.3 g/kWh, which was achieved for the case of 0% EGR with single injection at 0 degrees ATDC.

Figures 4.77 through 4.79 show the model's predictions for in-cylinder pressure for high EGR cases using double injections at specified pilot SOI.

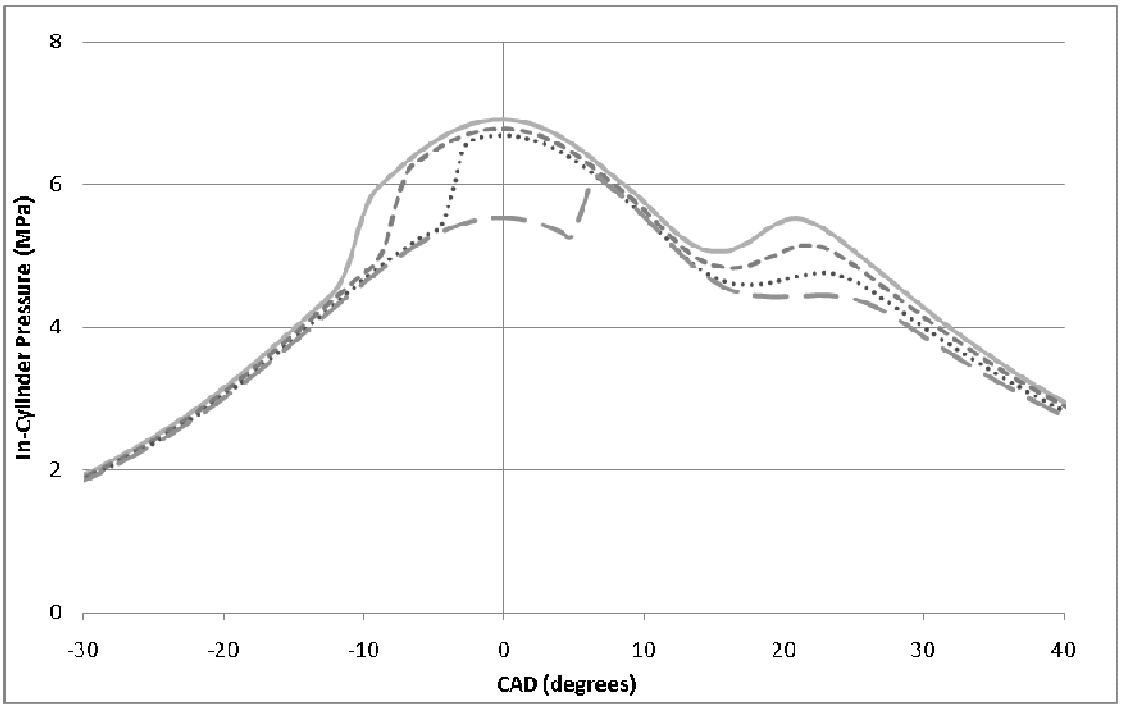

Figure 4.77: In-cylinder pressure versus crank angle degrees ATDC for 30% (solid line), 40% (line with short dashes), 50% (dotted line), 60% EGR (line with long dashes); double injection pilot SOI at -30 degrees ATDC

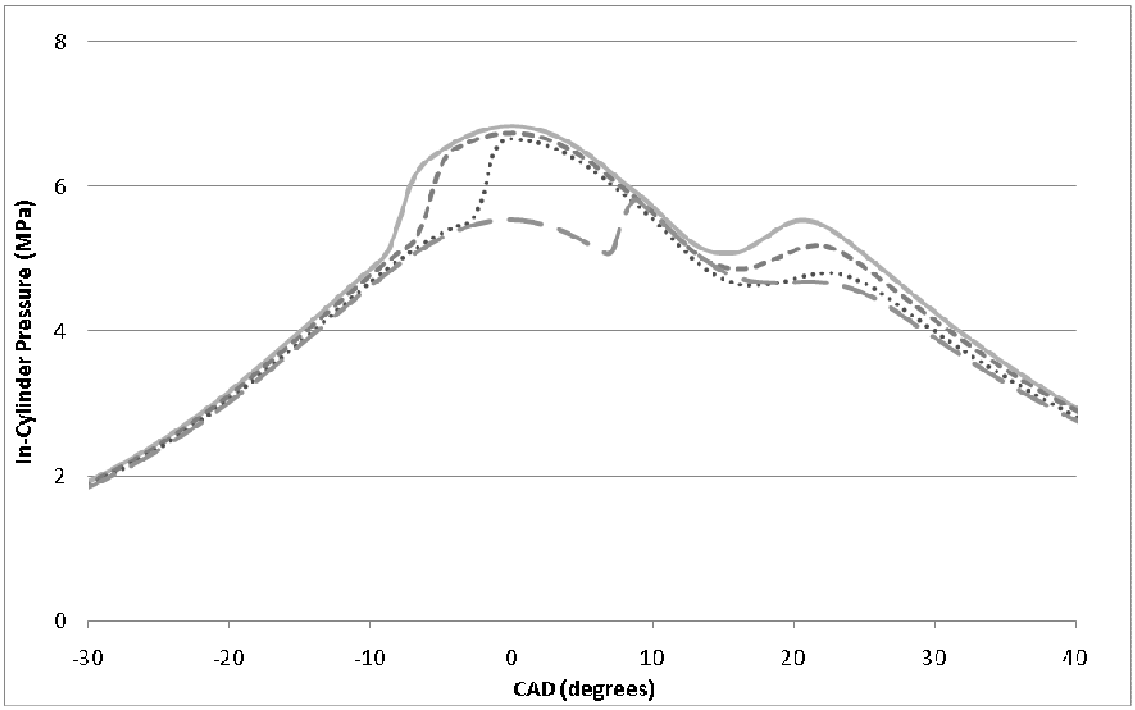

Figure 4.78: In-cylinder pressure versus crank angle degrees ATDC for 30% (solid line), 40% (line with short dashes), 50% (dotted line), 60% EGR (line with long dashes); double injection pilot SOI at -20 degrees ATDC

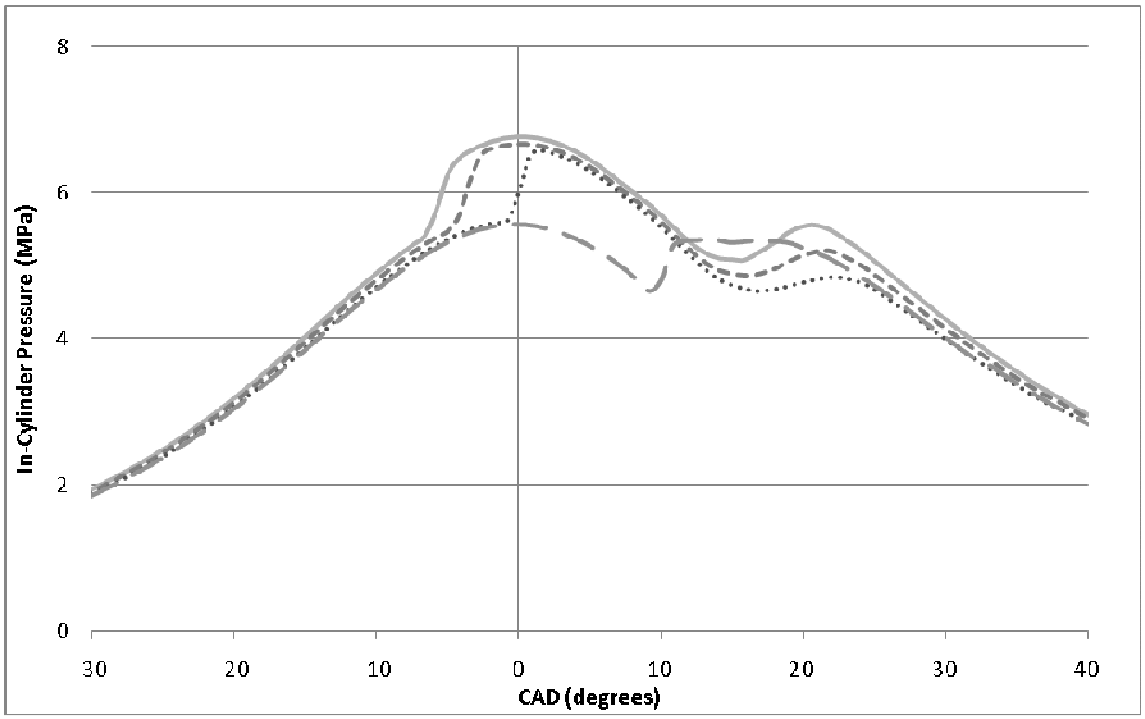

Figure 4.79: In-cylinder pressure versus crank angle degrees ATDC for 30% (solid line), 40% (line with short dashes), 50% (dotted line), 60% EGR (line with long dashes); double injection pilot SOI at -15 degrees ATDC

As expected, GT-Power predicted greater delay between SOI and SOC as EGR levels increased. In fact, delay was increased to such a great extent for the 60% EGR condition that the usually observed two spikes in in-cylinder pressure nearly merged into one spike for the case using a pilot injection with SOI -15 degrees ATDC, thereby making for a pressure versus crank angle degree curve which more closely resembles that of a case utilizing a single injection at late SOI.

CHAPTER 5. ENERGY RECOVERY STRATEGY

5.1 Cooling EGR Gases

To reduce both fuel usage and emissions, it is desirable to maximize the efficiency with which an engine converts a fuel's chemical energy into kinetic energy. An inherent problem with the internal combustion engine, however, is that a good deal of the energy bound within its fuel's chemical bonds is ultimately wasted as heat. Specifically, most heat is either dissipated to the engine's cooling system or expelled to the exhaust stream. Since the temperature of the working fluid within the cooling system is on the order of only 100 K above ambient, this fluid does not offer much potential to perform work. Exhaust gases, however, leave the combustion chamber at temperatures a good deal higher and offer more exergetic potential.

5.1.1 Present Methods for Cooling EGR Gases

High EGR engines provide a unique opportunity to recover energy from exhaust gases, since any recirculated exhaust gas which is introduced

into the intake stream must be cooled in order to minimize the temperature of the intake gases entering into the combustion chamber, and in effect, minimize peak in-cylinder temperatures and NOx emissions.

Most present EGR setups cool EGR gas by routing it through a heat exchanger which transfers the exhaust's thermal energy to EGR coolant, i.e., water or some other working fluid with high heat capacity. The present laboratory John Deere 4045HF475 engine in study employs this cooling approach, and a picture of its heat exchanger, an EGR cooler from a John Deere Tier 3 13.5L diesel engine, is shown as follows.

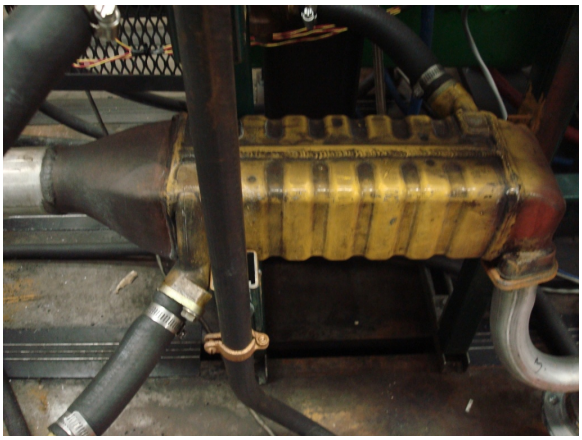

Figure 5.1: Water cooled heat exchanger used to cool EGR gases in laboratory engine setup

In most setups, once EGR coolant absorbs heat from the EGR exhaust gases, the coolant is sent to another heat exchanger where it is cooled using fan-blown air or some other fluid, often at ambient temperature, so as to discharge to the environment the thermal energy first taken from the EGR exhaust gases. In the case of the laboratory engine, tap water was used as

EGR coolant. Once this tap water absorbed heat from EGR exhaust gases, it was discharged to the city drain system.

An alternative method for cooling EGR exhaust gases is to transfer the thermal energy from these gases into an energy recovery system which utilizes a thermodynamic cycle to convert this thermal energy into shaft power. From here, this shaft power could be used to perform mechanical work by coupling the energy recovery system's power output shaft to the engine crankshaft via infinite variable transmission (IVT), or to power a generator and charge a battery.

5.1.2 Exploring Alternative Methods for Cooling EGR Gases

Before using GT-Power to model ideas for exhaust energy recovery systems, estimation was made as to whether an energy recovery system could produce enough shaft power to render the system worth designing and testing. To make this estimation, it was first assumed an EGR system would need to cool 30% or so of the engine's spent exhaust gas from 600 K to approximately 400 K. Additional assumptions were made as follow: EGR mass flow rate equals 0.025 kg/s; the energy recovery system will only cool the exhaust gas by 100 K, meaning another heat exchanger downstream (not part of the energy recovery system) will be needed to cool the exhaust gas yet further to make it cool enough for recirculation; the energy recover system will be 25% efficient at converting exhaust gas thermal energy to kinetic

energy; and the exhaust gas has a constant heat capacity of 1.1 $kJ/kg \cdot K$. As such, the following calculation can be made:

$$mdot_{exhaust-gas} \cdot Cp_{exhaust-gas} \cdot \Delta T_{exhaust-gas} \cdot \eta_{system} = Wdot \tag{5.1}$$

$$\left(0.025\frac{kg}{s}\right) \cdot \left(1.1\frac{kJ}{kg \cdot K}\right) \cdot (100K) \cdot (0.25) = 0.69kW$$

If an engine running at operation conditions of 50 mg per injection for fueling and 1400 rpm speed could generate 40 kW and produce a BSFC of 240 g/kWh, the generation of this extra 0.69 kW would effectually reduce this BSFC figure to 236 g/kWh. Since 50 mg per injection and 1400 rpm corresponds to a low-load/low-speed operation condition, a high-load/high-speed condition would likely offer even more potential for energy recovery since more EGR gases would be flowing, and also, exhaust gas expelled from the exhaust ports would be hotter.

The aforementioned GT-Power model of the present John Deere 4045HF475 diesel engine was used to test viability of potential energy recovery systems. Two versions of this model were then utilized, one being the same version discussed in Chapter 4, the model which incorporated a low pressure EGR loop. A second version was then created by slightly modifying the first, that is, by replacing its low pressure EGR loop with a high pressure EGR loop. For comparison, Figure 5.2 below shows the EGR loop portion of

the GT-Power model of the engine incorporating a low pressure EGR loop, the same model shown in Figure 3.11. Figure 5.3 below shows the EGR loop portion of the GT-Power model of the engine incorporating a high pressure EGR loop. Again, note the GT-Power schematic convention in which solid lines with arrows are used to show how air and/or exhaust flow from one engine component to the next.

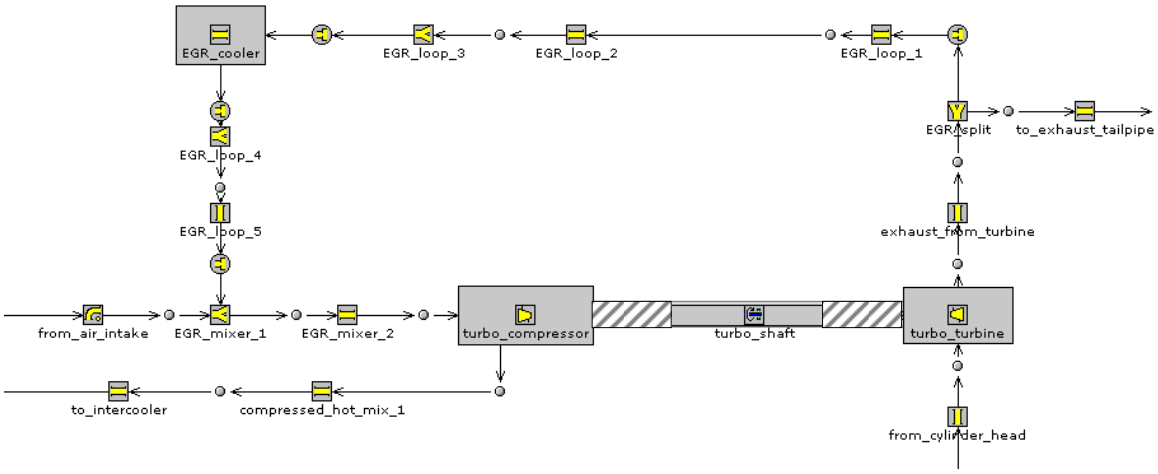

Figure 5.2: Low pressure EGR loop

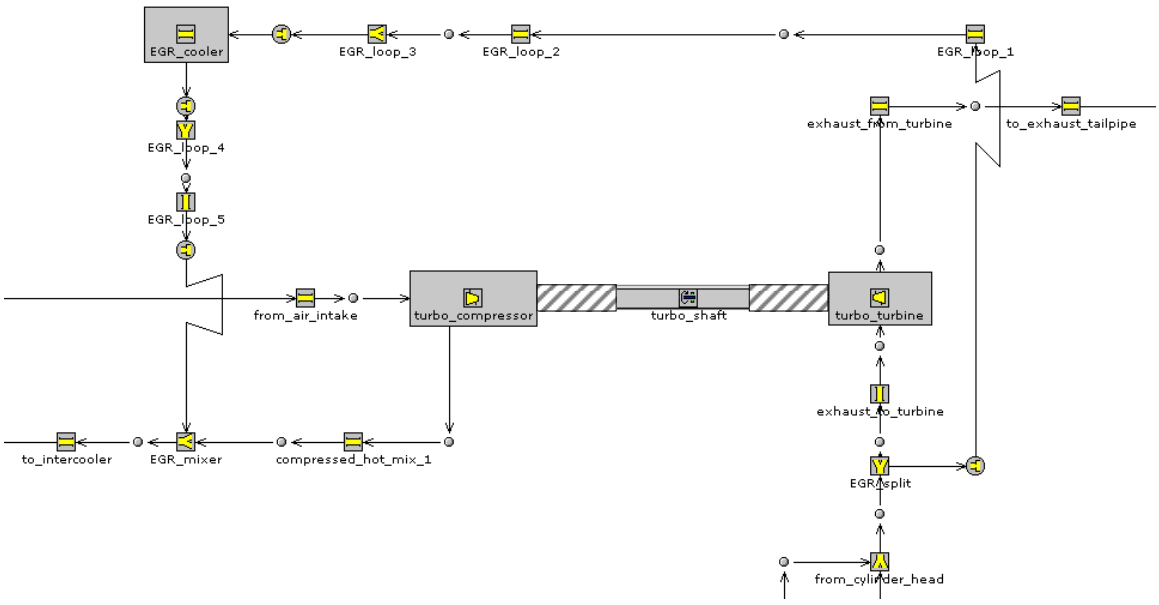

Figure 5.3: High pressure EGR loop

As is shown in Figure 5.3, the high pressure EGR loop pulls exhaust gas from upstream of the turbocharger's turbine, that is, before it would otherwise undergo expansion through the turbine. Current John Deere Tier 3 production engines actually incorporate this high pressure design, and do so in part because it enables the vane position of the Variable-Geometry Turbine (VGT) to control the pressure upstream of the turbine, and in effect, how much EGR flows through the EGR loop, thereby allowing the engine's EGR valve to run at a fairly constant position.

5.2 Designs for Energy Recovery System

In considering the criteria of power, complexity, cost, and also, which working fluid to use, it was concluded that either a Brayton or Rankine cycle

would be best to incorporate into the proposed energy recovery system.

In review, the Brayton cycle is that which is used to model gas turbines, and involves the following processes [28]:

1) Compression of gaseous working fluid by compressor
2) Constant pressure heat addition
3) Expansion of gaseous working fluid through turbine
4) Constant pressure heat rejection to environment

In comparison, the Rankine cycle is that which is used to model steam power plants, and involves the following processes [28]:

1) Compression of condensed liquid working fluid by pump
2) Vaporization of and heat addition to working fluid
3) Expansion of gaseous working fluid through turbine from vapor to the condenser pressure
4) Condensation of working fluid in condenser and heat rejection to environment

In comparing the two different cycles for integration into an engine, the Brayton cycle could operate via open-loop thermo-circuit and use air as its working fluid, thereby reducing system complexity. The Rankine cycle, however, could feasibly offer performance advantages over the Brayton cycle since it would not need to perform work on compressing a gaseous working

fluid before sending it to a heat exchanger for heat addition.

Regardless as to which cycle would be employed, a non-recovery EGR cooler would need to be fit into the EGR loop near the loop's exit, the purpose of which would be to provide additional cooling of the EGR gas beyond that alone provided by the energy recovery heat exchanger.

5.2.1 Energy Recovery for High versus Low Pressure EGR

It was decided that a recovery system integrated into a low pressure loop would utilize one heat exchanger to both cool EGR exhaust gases and provide heat addition to the recovery system. This heat exchanger would be placed immediately downstream of the turbocharger's turbine and upstream of the EGR loop, thereby extracting thermal energy from the entirety of the exhaust gas expelled by the engine, regardless of amount of EGR gas being recirculated. This single heat exchanger is labeled in Figure 5.4 as follows:

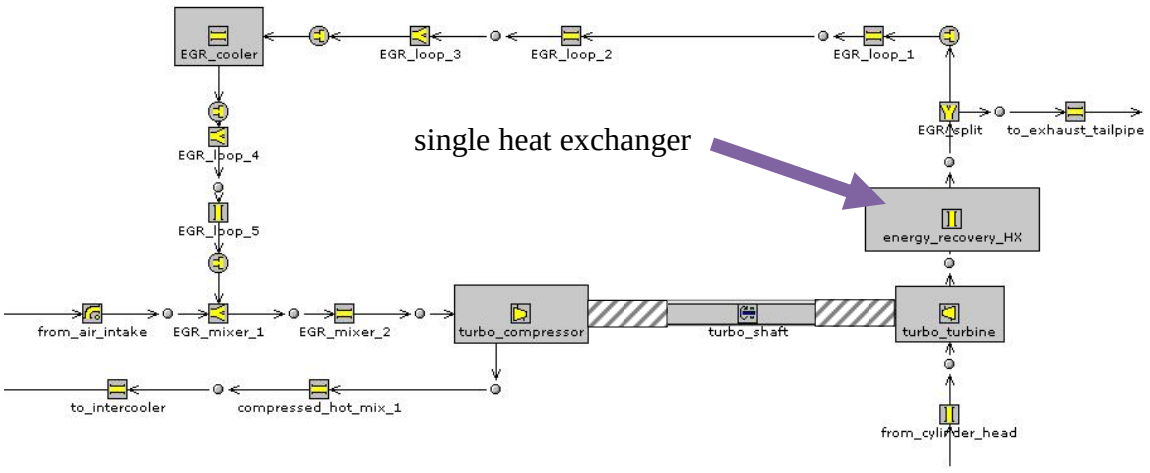

Figure 5.4: Low pressure EGR loop with energy recovery heat exchanger

It was decided that a recovery system integrated into a high pressure EGR loop would differ by using two heat exchangers (placed in series) instead of one. The first would be placed downstream of the turbocharger's turbine and extract thermal energy from all exhaust not diverted to the EGR loop. This heat exchanger would contribute the first stage of thermal energy transfer to the recovery system's working fluid. A second heat exchanger would be placed in the high pressure EGR loop and contribute a second stage of thermal energy transfer to the working fluid already heated by the first stage heat exchanger.

The high pressure EGR loop would lend itself well to using two heat exchangers in series since the exhaust gas within its EGR loop would not have undergone expansion and consequential cooling as it would have otherwise upon passing through the turbocharger's turbine. The placement of both heat exchangers relative to the high pressure EGR loop is shown in Figure 5.5 as follows:

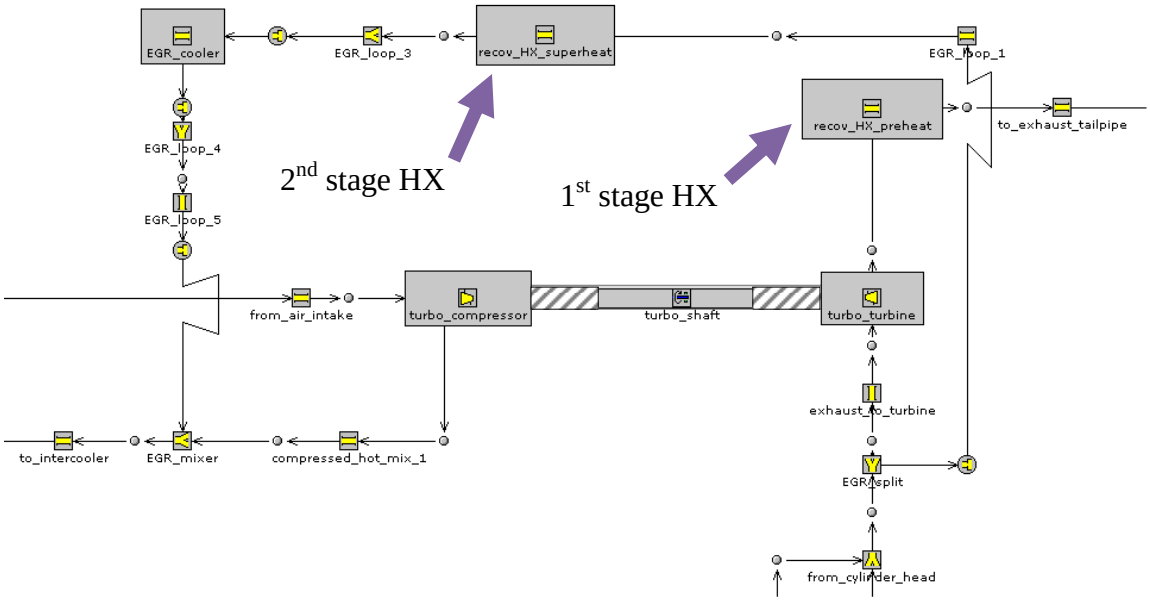

Figure 5.5: High pressure EGR loop with both energy recovery heat exchangers (HX)

5.2.2 Brayton Cycle Designs

It was eventually decided to use three different designs of recovery system for each of the two types of EGR loops (high and low pressure). Specifically, two different designs for the Brayton cycle, and one for the Rankine cycle resulted.

Design 1 was selected to employ a Brayton cycle and produce power in the following steps:

1) Ambient air at approximately 1 atm is drawn in and then compressed using a centrifugal compressor, which is powered by the exhaust energy recovery system's turbine.

2) Next, the compressed air is passed into the heat addition heat

exchanger(s) which pull(s) thermal energy from exhaust gas, specifically, one heat exchanger for the low pressure EGR loop, and two for the high pressure EGR loop.

3) The heated, compressed air is sent to a centrifugal turbine to undergo expansion and drive the turbine, after which the air is discharged to the ambient. The turbine's generated power is used to both drive the energy recovery system's compressor and provide recovered energy as shaft power.

Design 2 works the same way as Design 1, but employs a slight modification. Instead of using power from the exhaust energy recovery system's turbine to drive the compressor, a drive turbine is placed downstream of the turbocharger's turbine, and this is used to drive the recovery system's compressor. This is similar to the technology of exhaust turbocompounding, which places a turbine downstream of the turbocharger turbine(s) to produce shaft power from exhaust gas enthalpy.

Design 2 has the advantage of not needing to expend some of the power it generates to recycle back into its system to perform compression work on its working fluid. In effect, Design 2 has the potential to generate more power.

Both Designs 1 and 2 were modeled using GT-Power to observe if either could produce sufficient and reliable power. First, each design was

tested using a low pressure EGR loop since this proved less complicated than doing so using a high pressure EGR loop. To perform this test, two additional copies were made of the GT-Power model utilizing low pressure EGR and an EGR rate of 40%. The Design 1 recovery system was attached to the EGR loop of one copy; a GT-Power schematic of this is shown in Figure 5.6 below. Note that solid lines with unfilled arrows show direction of flow for engine air and/or exhaust between adjacent engine components. Additionally, dotted lines with filled arrows show direction of flow for the energy recovery system working fluid.

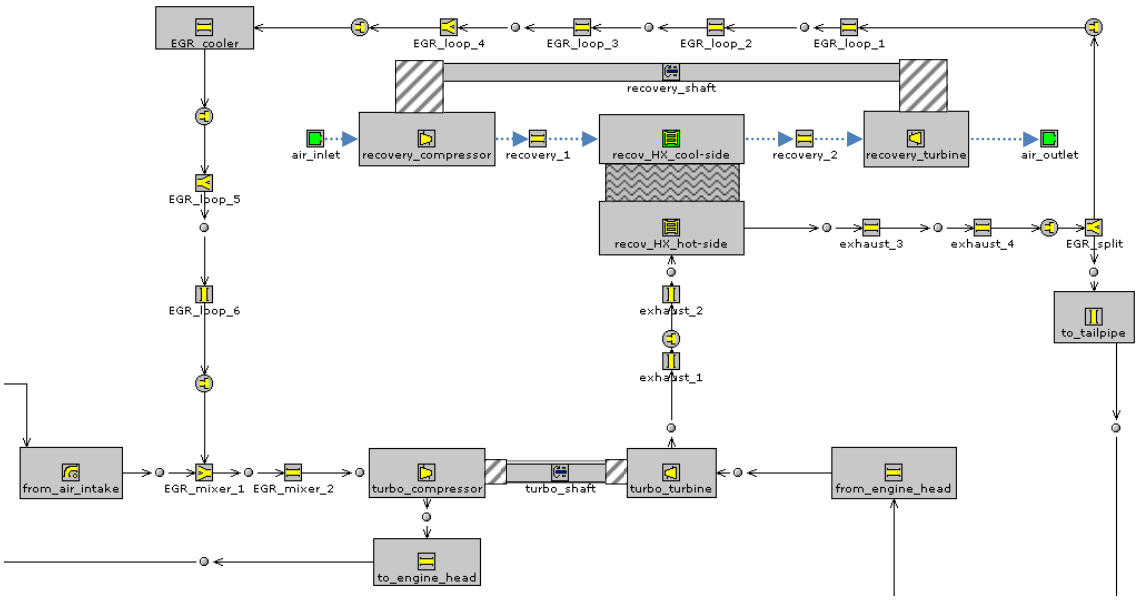

Figure 5.6: Design 1 for energy recovery system

Then, the Design 2 system was attached to the second copy. A GT-Power schematic of this is shown in Figure 5.7 below.

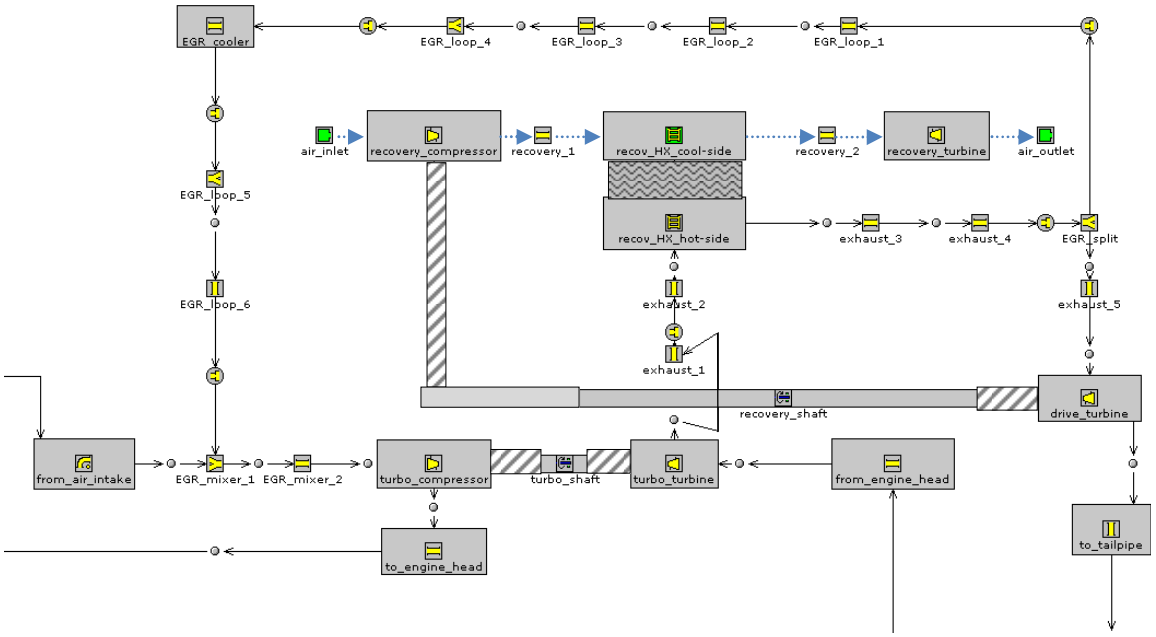

Figure 5.7: Design 2 for energy recovery system

Next appropriate specifications were loaded into both exhaust energy recovery system Design 1 and Design 2 copies of the GT-Power model. Each model was run, and it was discovered that neither system could produce much over 0.5 kW with the engine operating at 50 mg per injection for fueling, 1400 rpm speed, and 40% EGR. Granted, optimization of the recovery system's compressor, turbine, and heat exchanger could have feasibly brought this above 1 kW, but these initial results suggested consideration of the Rankine cycle.

As for Design 1, certain combinations of energy recovery system compressor, turbine, and heat exchanger could sustain power generation of slightly under 0.5 kW, but most combinations yielded a design in which the turbine did not produce enough power to both drive the recovery system's

compressor and provide shaft power.

Design 2 fared better at power generation and could sustain power of slightly more than 0.5 kW. Also, it could sustain power generation for a wider range of compressor, turbine, and heat exchanger combinations. A significant drawback to Design 2, however, was that it adversely affected turbocharger turbine performance since it required placement of a drive turbine downstream of the turbocharger turbine. The addition of this restriction downstream of the turbocharger turbine decreased the extent to which pressurized exhaust gases leaving the engine's exhaust ports could expand across the turbocharger turbine. This effectually hampered turbocharger performance and increased engine BSFC, often times to 300 g/kWh or so. Whatever potential Design 2 could offer to lower BSFC through energy recovery appeared to be offset by its adverse affect on turbocharger performance. It is worth noting, however, that optimization of both turbocharger turbine and drive turbine, as is done in exhaust turbocompounding setups, could make this design a good deal more viable.

5.2.3 Rankine Cycle Design

With neither Design 1 nor Design 2 providing desirable performance, attention was next turned to Design 3, which was selected to employ a Rankine cycle. It was designed to produce power in the following steps:

1) The working fluid (refrigerant or water), while in the liquid phase, is preheated by sending it to a heat-exchanger which draws heat from the engine's coolant.
2) The liquid phase working fluid is pressurized using a pump.
3) The compressed liquid is passed into the heat addition heat exchanger which evaporates the liquid and heats the resulting vapor. This heat exchanger pulls thermal energy from exhaust gas. For the low pressure EGR loop, a single heat exchanger is used to both evaporate and superheat the working fluid. For the high pressure EGR loop, two heat exchangers placed in series are used to accomplish this.
4) The vaporized superheated working fluid is sent to the energy recovery system's turbine where it undergoes expansion and drives the turbine. All shaft power produced at this turbine is then directed to the engine's crankshaft via variable-speed transmission, or is used to generate electricity.
5) The low pressure vapor discharged by the turbine is sent to a condensing heat exchanger which is mounted near the engine's other heat exchangers through which the engine's fan blows ambient air for cooling.
6) Finally, the condensed working fluid is recycled back into the energy recovery system.

Design 3 was modeled using GT-Power to observe if it could produce sufficient and reliable power. To do this, an additional copy was made of the GT-Power model which utilized low pressure EGR and a usage rate of 40% EGR. The Design 3 recovery system was attached to this copy's EGR loop, and GT-Power was run. A GT-Power schematic of this setup is shown as follows.

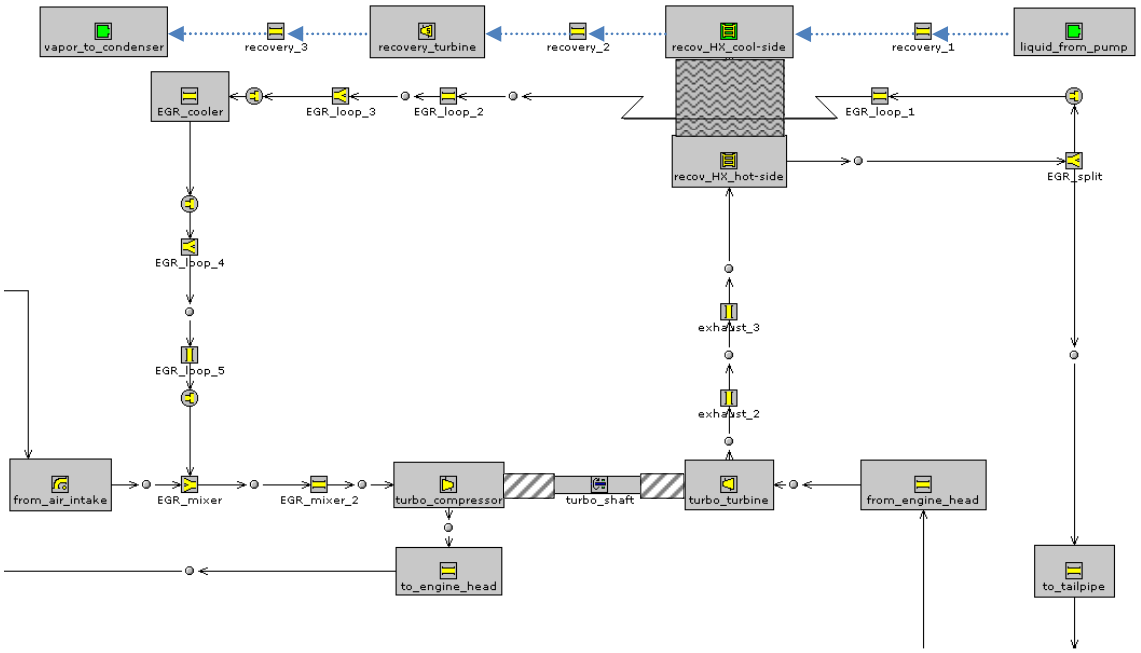

Figure 5.8: Design 3 coupled to low pressure EGR loop

Initial GT-Power runs which tested Design 3 incorporated into a low pressure EGR loop suggested this design could produce enough power to make it viable for further consideration, so a copy was made of the GT-Power model which utilized high pressure EGR and a usage rate of 40% EGR. The

Design 3 recovery system was then fit with two heat exchangers in series and attached to the GT-Power high pressure EGR loop, and the model was run. A GT-Power schematic of this setup is shown as follows:

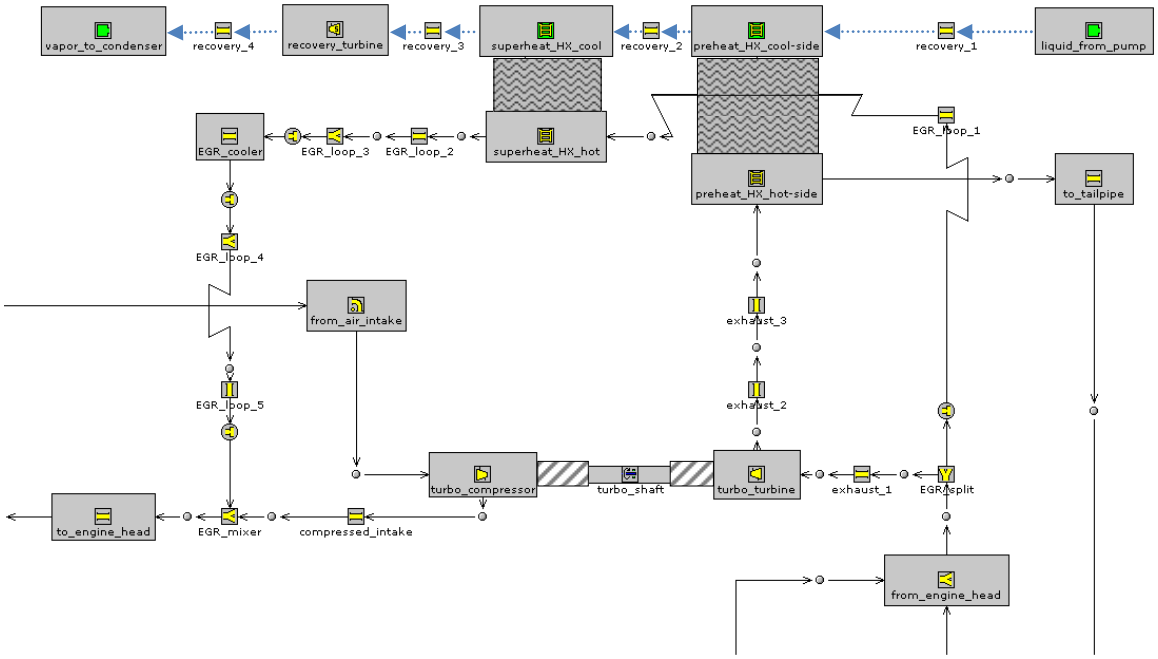

Figure 5.9: Design 3 coupled to high pressure EGR loop

As for Design 3, most combinations of pump, turbine, and heat exchanger proved able to produce power levels of at least 0.5 kW, and in many cases, around 1 kW. Despite its increased complexity over Designs 1 and 2, the ability of Design 3 to produce these levels of shaft power without optimization of its pump, turbine, and heat exchanger rendered it the most viable for further study, which is discussed in Section 5.3.

5.3 Energy Recovery System Performance

To calculate energy recovery system performance, specifically that for Design 3, four versions of the GT-Power model of the John Deere 4.5L diesel engine were prepared. Each version was created by starting with the GT-Power model discussed in Chapter 4, and then inputting unique sets of operation conditions into each version. These conditions are listed as follows.

Table 5.1: Operation conditions inputted into each GT-Power model version

Model Version	**1**	**2**	**3**	**4**
Fuel per Injection (mg)	50	50	95	95
Engine Speed (RPM)	1400	1400	1400	2400
Single Injection SOI (deg. ATDC)	0	0	-10	-10
Nominal EGR Level	30%	30%	30%	30%
EGR Loop Type	low-pressure	high-pressure	low-pressure	low-pressure

Note that Model Version 1 represented that which was discussed in Chapter 4. Version 2 differed from Version 1 in that it replaced the low pressure EGR loop of Version 1 with a high pressure EGR loop. Version 3 differed by replacing the 50 mg injection of Version 1 with a 95 mg injection; also, Version 3 advanced SOI by 10 degrees since the duration of the 95 mg injection was about twice as great as that for the 50 mg injection. Version 4 was the same as Version 3, only it replaced the 1400 rpm engine speed with 2400 rpm.

Each of these four sets of operation conditions was selected for assignment to one of the four model versions because each set could provide insight into what diesel engine applications could benefit most from the

energy recovery system. As such, Versions 1 and 2 modeled low-load/low-speed application. Version 3 modeled high-load/low-speed, specifically the condition for which the factory engine achieved its peak torque rating of 645 N-m at 1400 rpm. Version 4 modeled high-load/high-speed, specifically the condition for which the factory engine achieved its peak power rating of 129 kW at 2400 rpm.

The relatively late injection timings indicated in Table 5.1 were used for two reasons: 1) present diesel engine technology favors the use of later injection timings to reduce NOx emissions; 2) later timing decreases the amount of heat transferred to the cylinder walls over the duration of the expansion stoke, thereby increasing the temperature of the exhaust gas expelled into the exhaust manifold, aiding recovery system performance.

From here, it was decided that the best method for estimating power output from a theoretically optimized model of the Design 3 recovery system would be to record GT-Power's predictions for mass flow rate of exhaust gas through the energy recovery system's heat exchanger(s), temperature of the exhaust gas going into the inlet of the same heat exchanger(s), and average heat capacity of the exhaust gas within the heat exchanger(s). Next it would be assumed the Design 3 energy recovery system would be 25% efficient at converting exhaust gas thermal energy into shaft power. This information would then be used in the following equation, which would be used once for each heat exchanger incorporated into the exhaust energy recovery system.

$$mdot_{exhaust-gas} \cdot Cp_{exhaust-gas} \cdot \Delta T_{exhaust-gas} \cdot \eta_{system} = Wdot_{shaft} \quad (5.2)$$

One of the main reasons for deciding to use Equation 5.2 for finding power output was because the GT-Power models for each energy recovery system would have required a good deal of adjustment for optimization, more than would have been fitting for the intended scope of this study. Each model, including that for Design 3, would have required a very specific combination of compressor/pump, turbine, and heat exchanger specifications to produce optimal power.

Next, each of the four sets of GT-Power operation conditions was run, making sure to input into GT-Power non-varying specifications for both the compressed air intercooler and EGR cooler. EGR levels were noted, and EGR valve position was adjusted for each set until EGR rate maintained steady near 30%. In any event, this EGR rate was selected instead of 40% EGR because performance of the laboratory engine running the 30% EGR condition was a good deal more studied than for higher EGR conditions. Table 5.2 shows engine performance as predicted by GT-Power for the four sets of GT-Power operation conditions.

Table 5.2: Operation conditions inputted into each GT-Power model version and resulting performance predictions for each

Model Version	**1**	**2**	**3**	**4**
Fuel per Injection (mg)	50	50	95	95
Engine Speed (RPM)	1400	1400	1400	2400
EGR Loop Type	low-pressure	high-pressure	low-pressure	low-pressure
Intake Manifold Temperature (deg C)	29.5	29.3	39.0	58.4
Intake Manifold Pressure (kPa)	127	129	184	299
Air-to-Fuel Ratio	20.03	21.08	14.84	20.64
EGR (%)	28.1	28.2	29.9	30.0
Power (kW)	36.7	37.8	71.4	120.4
Torque (N-m)	250.3	258.1	486.9	479.1
BSFC (g/kWh)	229.3	222.2	224.2	227.4

From here, data necessary to use Equation 5.2 was taken from the GT-Power results for each model version / operation conditions set. For Model Versions 1, 3, and 4, that is, the model versions utilizing low pressure EGR, mass flow rate and temperature leaving the turbocharger turbine were recorded, and these were used as mass flow rate of exhaust gas through and inlet temperature of exhaust gas to, respectively, the recovery heat exchanger. Moreover, heat capacity of the exhaust gas en route from the turbocharger turbine outlet to the EGR mixer was recorded at different points along this path, and a heat capacity versus temperature curve was fit to this data so that average heat capacity of the exhaust gas in the recovery heat exchanger could be found later.

For Model Version 2, that is, the only model version utilizing high pressure EGR, mass flow rate and temperature entering the EGR loop were recorded, and these were used as mass flow rate of exhaust gas through and

inlet temperature of exhaust gas to, respectively, the second stage heat exchanger. Additionally, mass flow rate and temperature exiting the turbocharger turbine were recorded, and these were used as mass flow rate of exhaust gas through and inlet temperature of exhaust gas to, respectively, the first stage heat exchanger. Average heat capacity of the exhaust gas inside each heat exchanger was found using a curve fit method similar to that employed for the low pressure EGR loop model versions / operation conditions sets.

To find temperature change of exhaust gas before and after traversing through a recovery heat exchanger, it was assumed the heat exchanger would cool the exhaust gas down to 525 K. This temperature was chosen because the GT-Power model (case of 50 mg fuel per injection, 1400 rpm speed, 40% EGR, low pressure EGR loop) for the Design 3 recovery system proved able to cool exhaust gas down to this temperature for runs which produced useful shaft power levels for the recovery system; this was the same GT-Power model discussed in subsection 5.2.3.

From here, it was assumed the Design 3 energy recovery system's pump would adjust flow rate of the working fluid within this system as necessary to maintain the energy recovery heat exchanger's outlet temperature at 525 K for the heat exchanger's exhaust gas side, and would adjust for varying levels of exhaust gas inlet temperature and flow rate.

Table 5.3: GT-Power predictions for exhaust gas properties used to calculate energy recovery system performance; for Model Versions 1, 3, and 4, HX 1 denotes each version's single heat exchanger; for Model Version 2, HX 1 denotes the first stage heat exchanger, and HX 2 denotes the second stage heat exchanger

Model Version	**1**	**2**	**3**	**4**
Fuel per Injection (mg)	50	50	95	95
Engine Speed (RPM)	1400	1400	1400	2400
EGR Loop Type	low-pressure	high-pressure	low-pressure	low-pressure
Inlet Temperature to HX 1 (K)	614	615	633	568
HX 1 Temperature Change (K)	89	90	108	43
HX 1 Mass Flow Rate (kg/s)	0.06845	0.05183	0.1009	0.2264
*Average Cp in HX 1 (J/kg*K)*	1119	1116	1142	1113
Inlet Temperature to HX 2 (K)	-	636	-	-
HX 2 Temperature Change (K)	-	111	-	-
HX 2 Mass Flow Rate (kg/s)	-	0.01982	-	-
*Average Cp in HX 2 (J/kg*K)*	-	1119	-	-

Using Equation 5.2, calculations were made for energy recovery system power output, and these results are shown in the following tables.

Table 5.4: Energy recovery system shaft power output

Model Version	**1**	**2**	**3**	**4**
Fuel per Injection (mg)	50	50	95	95
Engine Speed (RPM)	1400	1400	1400	2400
EGR Loop Type	low-pressure	high-pressure	low-pressure	low-pressure
Energy Recovery System Power (kW)	1.70	1.92	3.12	2.71

Table 5.5: Impact of energy recovery system on decreasing engine fuel consumption

Model Version	**1**	**2**	**3**	**4**
BSFC without Recovery (g/kWh)	229.3	222.2	224.2	227.4
BSFC with Recovery (g/kWh)	219.1	211.5	214.8	222.4
BSFC Reduction (g/kWh)	10.2	10.7	9.4	5.0
Percent Change in BSFC	-4.4%	-4.8%	-4.2%	-2.2%

This calculated improvement in BSFC merits the Design 3 recovery system a viable means to reduce fuel consumption and increase engine power. Assuming integration of this system into a factory John Deere 4045HF475 could lower this engine's optimal BSFC of 203 g/kWh by 4.2% (Table 5.5), a net BSFC of 194 g/kWh would be achieved.

CHAPTER 6. CONCLUSION

As deadlines to meet Tier 4 emissions standards approach, it is expected that diesel engine manufactures will likely need to employ some type of after-treatment to meet regulations. However, results from this study suggest certain operation conditions provide ample in-cylinder control so that after-treatment would only be required for soot or for NOx, depending upon the operation conditions.

Among this study's two primary intentions, one was to investigate what combinations of EGR levels and fuel injection strategies enable a diesel engine running low-load/low-speed operation conditions to meet Tier 4 emissions levels with little to no use of after-treatment, and all the while, achieve low fuel consumption. Among the various categories of cases tested for the low-load/low-speed condition of 50 mg fueling per injection / 1400 rpm engine speed, those which proved able to meet Tier 4 emissions standards for soot (but would still require NOx after-treatment) included:

1) 0% EGR, single injection, late injection (SOI at 0 degrees ATDC or later)
2) 0% EGR, double injection

Between these two categories of cases, GT-Power found that 0% EGR with double injection produced slightly better BSFC, an average of 237 g/kWh among its cases in which pilot injection timing was varied.

Categories of cases which proved able to meet Tier 4 emissions for NOx (but would still require soot after-treatment) included:

1) above 30% EGR, single injection, late injection (SOI at 0 degrees ATDC or later)
2) 30% EGR, double injection
3) above 30% EGR, double injection

Among these three categories, above 30% EGR with single injection / late injection achieved, by an ample margin, the best BSFC, 240 g/kWh on average.

In terms of lowest overall emissions, including for both NOx and soot, the case category of above 30% EGR with double injection achieved the best results. The 40% EGR case running a double injection with pilot SOI at -30 degrees ATDC surpassed Tier 4 NOx limits by achieving 0.18 g/kWh NOx, and nearly reached Tier 4 soot limits by achieving 0.05 g/kWh soot. As such, this condition would only require minimal soot after-treatment to achieve Tier 4 compliance for both NOx and soot. However, this case produced a fairly high BSFC of 254 g/kWh.

The second of this study's primary intentions was to investigate exhaust energy recovery systems and for what engine load/speed conditions

such a system could reduce BSFC enough to justify further consideration for design and manufacture.

For low-speed / 30% EGR conditions employing a single injection with SOI at 0 degrees ATDC, and using either 50 mg or 95 mg fuel delivery per injection, integration of a Rankine cycle exhaust energy recovery system was calculated to decrease BSFC by 4% to 5%. The magnitude of this decrease was lowered to 2.2% for the high-speed / 30% EGR condition using 95 mg fuel per injection. Assuming the integration of this system into a John Deere 4.5L 4045HF475 diesel engine could decrease this engine's optimal BSFC of 203 g/kWh by 4.2%, a net BSFC of 194 g/kWh would be achieved.

Using a Rankine cycle recovery system on a high pressure EGR loop was shown to generate 13% more power than its low pressure counterpart. When the engine was fitted with a high pressure EGR loop coupled with a Rankine cycle recovery system, it was shown to produce exceptionally low BSFC, 211.5 g/kWh as observed for the low-load / low-speed / 30% EGR test condition. For this test condition the GT-Power model predicted a BSFC of 222.2 g/kWh when the recovery system was not integrated into the engine while employing the same high pressure EGR. When the engine employed low pressure EGR and did not integrate the recovery system, GT-Power predicted a BSFC of 229.3 g/kWh, which represents an increase of 8% over the aforementioned 211.5 g/kWh prediction.

If the Rankine cycle energy recovery system had been integrated into

the GT-Power model which operated the engine with 40% EGR and double injection with pilot SOI at -30 degrees ATDC, this operation condition, which produced exceptionally low overall emissions, would have been able to achieve a respectable BSFC of around 240 g/kWh, assuming the recovery system could decrease BSFC by 4% to 5%. The net result would be a low-load/low-speed operation condition which achieves decently good BSFC, achieves Tier 4 limits for NOx without employment of after-treatment, and only requires minimal soot after-treatment to meet Tier 4.

An idea worth investigating would be whether a vehicle's air conditioning system could be modified to serve as the proposed Rankine cycle energy recovery system when not used to condition air. This would enable present vehicles, whether powered by diesel or gasoline engine, to easily adopt the energy recover system.

REFERENCES

1. Environmental Protection Agency. *Control of Emissions of Air Pollution from Nonroad Diesel Engines and Fuel; Final Rule*. 2004; Available from: http://www.epa.gov/fedrgstr/EPA-AIR/2004/June/Day-29/a11293a.pdf.

2. Costlow, T. *Tackling Tier 3*. 2004. SAE Paper No. 11-12-6-33.

3. Cohen, A.J. and M.W.P. Higgins. *Diesel Exhaust: A Critical Analysis of Emissions, Exposure, and Health Effects*. 1995. Health Effects Institute.

4. Bhatia, R.P., P. Lopipero, and A.H. Smith. *Diesel Exhaust Exposure and Lung Cancer*. 1998. Epidemiology, 9(1): pp 84-91.

5. Needham, J.R., D.M. Doyle, and A.J. Nicol. *The Low NOx Truck Engine*. 1991. SAE Paper No. 910731.

6. Arrowsmith, D. and A. Bott. *Development of a Compact Urea-SCR+CRT System for Heavy-Duty Diesel using a Design of Experiments Approach*. 2006. SAE Paper No. 2006-01-0636.

7. Miles, P.C., et al. *Rate-Limiting Processes in Late-Injection, Low-Temperature Diesel Combustion Regimes*. Proc. *THIESEL 2004 Conference*. 2004. pp 429-447.

8. Erickson, P.A. and M.P.B Musculus. *In Cylinder and Exhaust Soot in Low-Temperature Combustion Using a Wide-Range of EGR in a Heavy-Duty Diesel Engine*. 2007. SAE Paper No. 2007-01-4017.

9. Tomazic, T. and A. Pfeifer. *Cooled EGR – A Must or an Option for 2002/04*. 2002. SAE Paper No. 2002-01-0962.

10. John Deere Power Systems. Personal Interviews. August 2008.

11. Helmantel, A. *Reduction of NOx Emissions from a Light Duty DI Diesel Engine in Medium Load Conditions with High EGR Rates*. 2008. SAE Paper No. 2008-01-0643.

12. Ladommatos, N., et al. *Effects of EGR on Heat Release in Diesel Combustion*. 1998. SAE Paper No. 980184.

13. Incropera, F.P., et al. *Fundamentals of Heat and Mass Transfer*. 2007: John Wiley & Sons, Inc.

14. Heywood, J.B. *Internal Combustion Engine Fundamentals*. 1998: McGraw-Hill.

15. Jacobs, J.J., D.N. Assanis, and Z.S. Filipi. *The Impact of Exhaust Gas Recirculation on Performance and Emissions of a Heavy-Duty Diesel Engine*. 2003. SAE Paper No. 2003-01-1068.

16. Pieter, R., et al. *Reducing Engine-Out Emissions for Medium High Speed Diesel Engines: Influence of Injection Parameters*. 2009. SAE Paper No. 2009-01-1437.

17. Klingbeil, A.E. *Particulate and NOx Reduction in a Heavy-Duty Diesel Engine Using High Levels of EGR and Very Early or Very Late Start of Injection*. 2002. *Mechanical Engineering*, University of Wisconsin-Madison: Madison.

18. Senecal, P.K. and R.D. Reitz. *Simultaneous Reduction of Engine Emissions and Fuel Consumption Using Genetic Algorithms and Multi-Dimensional Spray and Combustion Modeling*. 2000. SAE Paper No. 2000-01-1890.

19. Ferguson, C.R. and A.T. Kirkpatrick. *Internal Combustion Engines*. 2001: John Wiley & Sons, Inc.

20. Borman, G.L. and K.W. Ragland. *Combustion Engineering*. 1998: McGraw-Hill.

21. Hountalas, D.T., C. Katsanos, and V. Lamaris. *Recovering Energy from a Diesel Engine Using Mechanical and Electrical Turbocompounding*. 2007. SAE Paper No. 2007-01-1563.

22. Leising, C.J., et al. *Waste Heat Recovery in Truck Engines*. 1978. SAE Paper No. 780686.

23. Ecker, H.J., D. Gill, and M. Schwaderlapp. *Downsizing of Diesel Engines: 3-Cylinder/4-Cylinder*. 2000. SAE Paper No. 2000-01-0990.

24. Updike, Ken. *International Harvester Tractors, 1955-1985*. 2000: MBI.

25. University of Nebraska-Lincoln. *Nebraska Tractor Test Laboratory Reports*. 1962-2006. Test Report No. 828, 947, 1100, 1263, 1461, 1622, 1691, 1777, 1801, 1873; Available from: http://digitalcommons.unl.edu/tractormuseumlit/.

26. Deere & Company. *4045H Diesel Engine*. 2008; Available from: http://www.deere.com/en_US/rg/ESC/SpecSheet/Ind/4045HF475_A_S0_R0.html.

27. Gamma Technologies. *GT-Power*. 2009; Available from: http://www.gtisoft.com/img/broch/broch_gtpower.pdf.

28. Moran, M.J. and H.N. Shapiro. *Fundamentals of Engineering Thermodynamics*. 2004: John Wiley & Sons, Inc.